



Exploration of Electrospinning Methods for Fabricating Synthetic Human Knee Ligaments

Aleksia Pilja

Supervised by Dr Saulo Martelli

**Submitted to Flinders University
College of Science and Engineering
Master of Engineering (Biomedical)**

October 2019

Abstract

The ligaments of the knee are crucial in providing particular movement limitations and overall stability to the joint. Cruciate ligaments maintain anteroposterior, rotational and one-plane medial or lateral stability in conjunction with the collateral structures [41]. Rupture to any of the supportive structures disrupts the kinematics of the femoral-tibial joint, causing functional impairment in the initial trauma [39]. In the majority of cases, surgical intervention is required to repair the initial function, however replacement grafts often lack the mechanical properties of the original ligament. Disruption in the stability of the knee eventually causes long-term effects, many associated with early onset osteoarthritis [39]. Investigations into developing a more suitable replacement graft is on the incline, with aims to reduce the occurrence of long-term effects. This study focuses on the development of synthetic ligaments through electrospinning means, with key objectives in replicating the elastic modulus of native knee ligaments. For the anterior cruciate ligament (ACL), the elastic modulus was found to be between 65 and 128 MPa [13,14].

The process of electrospinning involves the development and collection of small-scale fibres, with aims to replicate the fibrous nature of native ligaments. Fibre formation was achieved in the electrospinning device by passing a polymer solution through a high electric field and onto a rotating drum collector. The solutions tested consisted of numerous concentrations of polycaprolactone (PCL) in ratios of chloroform and dimethylformamide (DMF). The fibre stream formed in the process is highly governed by the electrospinning parameters used during experiments. Although influenced by all contributing factors, the fibre morphology was highly dependent on the flow rate of the solution, the applied voltage and the rotational speed of the collecting drum. The solution flow rate was typically set to 1.5 mL/h, while the applied voltage and rotational speed of the collector varied between 20-30 kV and 1000 to 1500 rpm, respectively. After the two-hour test duration, fibre sheets were rolled into a cylindrical bundle structures for mechanical testing. Tensile testing of samples was conducted at a 30% per second strain rate, where resultant data was used to produce stress-strain curves and calculate the elastic modulus of the samples. The unrolled fibres were viewed using a scanning electron microscope (SEM), in order to determine the resulting fibre morphology from the test conditions.

Upon testing, it was found that the 13% w/v PCL concentration solutions produced synthetic ligament samples with desirable mechanical properties. The elastic modulus for these samples was found to be between 69 and 106 MPa (n=8). Although exact fibre alignment was not achieved, an eventual recruitment of fibres under increasing tension was displayed in the stress-strain curves for particular samples. The smallest fibres were seen in the 10% solutions (198 – 366 nm), with diameters within the fibril range of a native ligament. The 13% solutions however, produced larger fibres (0.4 – 2 μm), placing them in the collagen fibre range of native ligaments [23]. Results indicate that a desirable elastic modulus can be achieved in the synthetic electrospun ligaments with the use of 13% w/v PCL solutions and the correct combination of electrospinning parameters.

Declaration

I certify that this thesis:

1. Does not incorporate without acknowledgement any material previously submitted for a degree or diploma in any university; and
2. To the best of my knowledge and belief, does not contain any material previously published or written by another person except where due reference is made in the text.

Aleksia Pilja, 13/2/2020

Acknowledgements

A great expression of gratitude to Dr Saulo Martelli for the structure and the ongoing guidance throughout the duration of the project. Many thanks also go to Dr Youhong Tang and Samaneh Mirzaei for laboratory and electrospinning inductions. Much appreciation would also like to be given to Michael Russo for assistance in mechanical testing. Also, many thanks to Aoife McFadden for SEM imaging training and the assistance in sample preparation.

Contents

Abstract	2
Declaration.....	3
Acknowledgements	4
List of Figures.....	7
List of Tables	8
List of Equations	8
1. Introduction.....	9
2. Literature Review	10
2.1 Description of the Problem.....	10
2.2 Current Solutions and Limitations	11
2.3 Synthetic Electrospun Ligaments	12
2.4 Electrospinning Background.....	13
2.5 Parameter Impact on Fibres.....	14
2.6 Mechanical Properties.....	16
2.7 Research Variations.....	17
2.8 Overview of Proposed Study.....	21
2.8.1 Aim.....	21
2.8.2 Objectives	22
2.8.3 Justifications of Decisions	22
2.8.4 Overview of Experimental Method.....	22
3. Methodology	23
3.1 Solution Preparation.....	23
3.2 Electrospinning Procedure.....	24
3.3 Mechanical Testing.....	30
3.4 Normalising Data	33
3.5 SEM Imaging Method.....	34
4. Results	36
4.1 Electrospinning Outcomes.....	36
4.2 Material Properties of Ligament Samples.....	37
4.3 Fibre Morphology	45
5. Discussion	54
5.1 Key Findings	54
5.1 Polymer Concentrations and Solution Preparation.....	54

5.2 Electrospinning Procedure and Outcome	55
5.3 Potential Sources of Error	55
5.4 Mechanical Testing.....	57
5.5 SEM Imaging.....	58
5.6 Future Studies	58
5.6.1 Project Continuation.....	58
5.6.2 Further Research	58
6. Conclusion	59
7. References.....	59
8. Appendices.....	62
Appendix A – Round One Stress-Strain Graphs.....	62
Appendix B - Round Two Stress-Strain Graph	68
Appendix C - Round Three Stress-Strain Graphs.....	73
Appendix D – MATLAB Code for Graph Generation	76
Appendix E – MATLAB Code for Correlation Graphs.....	76

List of Figures

FIGURE 1 - LIGAMENTS OF THE KNEE [26]	9
FIGURE 2 - ACL RECONSTRUCTION WITH PATELLAR TENDON REPLACEMENT [37]	9
FIGURE 3- HIERARCHICAL STRUCTURE OF TENDON/LIGAMENT [23]	11
FIGURE 4 - TYPICAL STRESS-STRAIN RESPONSE FOR COLLAGEN FIBRES IN LIGAMENTS [20]	12
FIGURE 5 - SOLUTION IMPACT WITH INCREASE IN VOLTAGE, TAYLOR CONE FORMATION AT C [24]	13
FIGURE 6 - TYPICAL ELECTROSPINNING SETUP [25]	13
FIGURE 7 - METHOD FOR ALIGNED FIBRE BUNDLE COLLECTION [27]	15
FIGURE 8 - SYRINGE PUMP AND FLOW RATE CONTROL	24
FIGURE 9 - ROTATING MANDREL COLLECTOR COVERED IN BAKING PAPER	25
FIGURE 10 – NEU-PRO ELECTROSPINNING UNIT	25
FIGURE 11 - A) SHORT FIBRE STREAM B) LONG FIBRE JET	26
FIGURE 12 - A) LONG FIBRE STREAM B) SHORTER, FINER FIBRE JET	27
FIGURE 13 - REMOVED BAKING PAPER WITH FIBRE SHEET	28
FIGURE 14 - ROLLED-UP FIBRE SHEET INTO LIGAMENT SAMPLE	28
FIGURE 15 - TEST RESOURCES DEVICE FOR TENSILE TESTING	30
FIGURE 16 - A) INCREASED STRAIN PRIOR TO B) INCREMENTAL BREAKING C) INCREASED STRAIN PRIOR TO D) CLAMP BREAKING	31
FIGURE 17 – A) LOOPED END SAMPLE PRIOR TO TESTING B) LOOPED END SAMPLES DURING TESTING	32
FIGURE 18 - SAMPLES POST SPUTTER COATING	34
FIGURE 19 - A) SEM WITH OPEN CHAMBER B) SAMPLES PLACED ON CHAMBER STAGE PRIOR TO IMAGING	34
FIGURE 20 - STRESS-STRAIN GRAPH OF SAMPLE L6	36
FIGURE 21 - STRESS-STRAIN CURVE FOR SAMPLE L12	37
FIGURE 22 - STRESS-STRAIN CURVE FOR SAMPLE L9	37
FIGURE 23 - STRESS-STRAIN CURVE OF SAMPLE L32	38
FIGURE 24 - STRESS-STRAIN CURVE OF SAMPLE L34	39
FIGURE 25 - RELATIONSHIP BETWEEN PCL CONCENTRATION IN SOLUTIONS AND ELASTIC MODULUS	40
FIGURE 26 - STRESS-STRAIN CURVE FOR SAMPLE L26	41
FIGURE 27 - STRESS-STRAIN CURVE FOR SAMPLE L33	43
FIGURE 28 - A) SAMPLE L19/L20 AT 2000X MAGNIFICATION B) SAMPLE L29/30 AT 1000X MAGNIFICATION	44
FIGURE 29 - A) SAMPLE L19/20 B) SAMPLE L21/22 C) SAMPLE L23/24 D) SAMPLE L25/26 E) SAMPLE L27/28 F) SAMPLE L29/30	45
FIGURE 30 - CORRELATION GRAPHS FOR 10% SOLUTION FIBRE DIAMETERS AGAINST VOLTAGE AND FINAL RPM	47
FIGURE 31 - SAMPLE L31/32 AT A) 1500 MAGNIFICATION AND B) 600X MAGNIFICATION	48
FIGURE 32 - SAMPLE L33/34 AT A) 2500X MAGNIFICATION AND B) 600X MAGNIFICATION	48
FIGURE 33 - SAMPLE L35/36 AT A) 1300X MAGNIFICATION AND B) 700X MAGNIFICATION	49
FIGURE 34 - SAMPLE L37/38 AT A) 2500X MAGNIFICATION AND B) 600X MAGNIFICATION	49
FIGURE 35 - A) L31/32 B) L33/34 C) L35/36 D) L37/38	50
FIGURE 36 - CORRELATION GRAPHS FOR 13% SOLUTION FIBRE DIAMETERS AGAINST VOLTAGE AND FINAL RPM	51

List of Tables

TABLE 1 - STIFFNESS AND ELASTIC MODULUS RANGE OF NATIVE ACL	15
TABLE 2 - STIFFNESS RANGES FOR NATIVE PCL, MCL, LCL	16
TABLE 3 - STIFFNESS RANGE SUMMARY OF ALL KNEE LIGAMENTS	16
TABLE 4 - ELECTROSPINNING EXPERIMENTS WITH KEY PARAMETERS	18
TABLE 5 - ELECTROSPINNING EXPERIMENTS RESULT SUMMARY	19
TABLE 6 - TOP SELECTION ELECTROSPINNING EXPERIMENTS	20
TABLE 7 - SOLVENT RATIOS	23
TABLE 8 - ROUND ONE ELECTROSPINNING TEST PARAMETERS	35
TABLE 9 - ROUND TWO ELECTROSPINNING TEST PARAMETERS	35
TABLE 10 - ROUND THREE ELECTROSPINNING TEST PARAMETERS	36
TABLE 11 - ROUND ONE LIGAMENT SAMPLE MEASUREMENTS AND PROPERTIES	40
TABLE 12 - ROUND TWO LIGAMENT SAMPLE MEASUREMENTS AND PROPERTIES	41
TABLE 13 - ROUND THREE LIGAMENT SAMPLES MEASUREMENTS AND PROPERTIES	42
TABLE 14 - SUMMARY OF VOLTAGE AND COLLECTOR RPM IN COMPARISON TO AVERAGE FIBRE DIAMETER AND PORE SIZE FOR 10% SOLUTIONS	46
TABLE 15 - SUMMARY OF VOLTAGE AND COLLECTOR RPM IN COMPARISON TO AVERAGE FIBRE DIAMETER AND PORE SIZE FOR 13% SOLUTIONS	50

List of Equations

<i>Equation 1– Volume Fraction</i>	32
<i>Equation 2– Stress</i>	33
<i>Equation 3– Strain</i>	33
<i>Equation 4– Young's Modulus</i>	33
<i>Equation 5– Scaling Force</i>	43

1. Introduction

The progressive nature of the biomedical field can be seen in the ever-evolving research and development of synthetic biological replacements. With focus on synthetic knee ligament replacements, it has been recognised that improvement in surgical substitutions is required in order to limit variation from the original ligament of concern. Surgical intervention is recommended in the case of ligament rupture, particularly for anterior cruciate ligaments (ACL), in order to regain knee function [34]. Even with surgical reconstruction of the ACL, 10 to 25% of patients experience unsatisfactory results 7 to 10 years following the procedure, indicating further investigation regarding ligament function and replacement is required [35].

Current autograft and allograft replacements offer a sound biocompatibility, yet the material and structural behaviour in comparison to the original native ligament is often misaligned [30]. There is value in ensuring the replacement graft has a better suited stiffness. The mismatch in desired replacement properties can often lead to negative long-term effects due to abnormal knee kinematics, potentially causing early onset osteoarthritis [32]. This issue can arise as a result of the replacement altering the overall mechanics of the knee, inducing uneven force distribution across the articular cartilage [33]. Existing synthetic replacements are not often recommended due to high patient failure rates and potential of re-rupture [36].

An emerging method for synthetic ligament developing is electrospinning through the production and collection of nanofibers. Manipulation of a polymer solution can be done in a high electric field in order to achieve high-speed fibre jet production. The concept of fibre development is highly desirable in this application since ligaments exhibit a hierarchical structure made of fibril, fibre and fascicle layers [23]. Much research is being conducted to determine which materials, electrospinning parameter combinations and collection methods are best suited for efficient and desirable synthetic ligament development. There is however, a variation in key aims and what aspect deems the synthetic ligaments as suitable for replacement.

While many studies take part in mechanical testing, few place objectives on replicating the elastic modulus of the synthetic models to the range seen in native ligaments. This study however, sets the primary objective as developing electrospun fibre bundles which match the desired elastic modulus range (65 – 128 MPa), for the anterior cruciate ligament [13,14]. This mechanical evaluation is achieved through tensile testing of the synthetic ligament fibre bundles, assessing the material properties and response under increased load and strain. Calculating the stress and strain experienced by each sample allows for corresponding graphs to be drawn, interpreting and determining the elastic response within the linear region of the graphs.

Furthering material evaluation, the fibres are viewed using a scanning electron microscope (SEM). This imaging technique allows for the analysis of fibre diameters due to great deals of magnification. The fibre diameters are valuable to correlate which electrospinning parameters impact the fibre production and the overall nature of the fibre material. There is also benefit is determining which segment of the ligament hierarchical structure matches to the sizes of the synthetic samples produced.

2. Literature Review

2.1 Description of the Problem

Knee ligament injuries have become an increased issue, with an estimation of 2 in every 1000 people per year experiencing this issue [35], with a particular occurrence in athletes. These injuries primary involve the anterior cruciate ligament (ACL) and the medial collateral ligament (MCL), accounting for 90% of all sport-related injuries [35]. There have also been studies surrounding the greater risk females experience in regards to ACL injures, with occurrence at 2 to 8 times greater than their male counterparts [35]. Although the ACL and MCL account for the greatest amount of this injury type, the lateral collateral ligament (LCL) and the posterior cruciate ligament (PCL) are also capable of rupture. Traditionally, knee ligament reconstruction surgeries involve the complete removal of the ruptured ligament and a replacement achieved from the use of an autograft, allograft or synthetic graft. For ACL reconstruction surgery, holes are drilled through the femur and the tibia, in which the replacement is inserted (Figure 2). Screws, wires or sutures are used for fixation of the replacement [37].

Image removed due to copyright restriction.

Figure 1 - Ligaments of the Knee [26]

Image removed due to copyright restriction.

Figure 2 - ACL Reconstruction with Patellar Tendon Replacement [37]

2.2 Current Solutions and Limitations

Autografts are achieved by harvesting a section of ligament or tendon from the patient undergoing surgery. ACL replacement surgeries most commonly involve the removal of a section of the patellar tendon or semitendinosus hamstring and using it as the replacement ligament [16]. Alternative autograft options still involve invasive measures which create an additional aspect to the procedure. The harvesting of the graft also raises concerns in regards to donor site morbidity, with potential issues in patellar fracture, muscle weakness, decreased range of motion and chronic knee pain [45]. These issues may be reduced with the use of an allograft replacement, which is a graft obtained from the ligament or tendon of a deceased donor. However, issues regarding pathogen transmission and prolonged inflammatory response become more of a risk [5]. Despite the surrounding risks of both autografts and allografts, if the replacement is sourced from a different location in the body, it is likely the fibre orientation is not best suited for the ligament replacement, immediately creating variation in what the microarchitecture should be.

Synthetic replacements, such as the LARS™ developed product, is made from terephthalic polyethylene polyester fibres, where the fibres are woven in a way to prevent fibre breakdown and promote cell ingrowth [17]. The success rates are very dependent on each patient's case, with some athletes making full short-term recoveries and others experiencing secondary ruptures. The lack of consistency makes it difficult to determine whether this type of replacement is suitable for all patients. In the case of another ligament replacement other than the ACL, the same orientation of fibres is used, meaning this option is more of a 'one size fits all' solution rather than a customised one. Each of the knee ligaments perform according to their fibre alignment and their positioning in the knee, so the same type of replacement may not be the best suited for all positions in the knee. The fixation methods of the LARS™ products vary for each case, meaning surgeons need to alter methods according to each patient's situation [18]. A ten-year post-surgery study was conducted with LARS replacements to investigate outcomes from a cohort of 26 [46]. It was found that 56% percent of patients experiencing some type of complication and 63% showed signs of early onset osteoarthritis [46]. Another synthetic replacement is the JewelACL™. This product focuses on achieving the tensile strength of the semitendinosus hamstring tendon, which is typically 1200 N [40]. The hamstring tendon can be used as an autograft in reconstructive surgery, however the product should aim to have a tensile strength similar to an ACL, which is typically 2160 N [39]. For both cases there is strong emphasis on the force the synthetic replacement can withstand, rather than highlighting the stiffness of the material. Although related, it would be beneficial to understand whether the synthetic graft stiffness is within the range of a native human ligament, ensuring the overall knee movement does not experience compromise post-surgery.

Despite the replacement method used, even with the large amount of surgeries occurring each year, there are tendencies in knee having abnormal kinematics after surgery [35]. These abnormalities include; increases in anterior translation, axial tibial rotation and valgus rotation which can cause progressive damage to other aspects of the knee [35]. Although the vast majority are considered successful surgeries, there is also a high occurrence of osteoarthritis post-surgery [16]. This drawback is not fully understood, however there is a likelihood that this is being induced by the graft limitations or the joint trauma during surgery. In the case of the graft limitation, the microstructure of the replacement rarely is identical to the microarchitecture of the original ligament. This also relates to a variation in the replacement graft stiffness, where the overall knee movement can be altered if the new ligament exhibits a stiffness well above or below the desired range. Although these impacts may seem minute, alteration to the overall knee mechanics

postsurgery can mean the joint force distribution and orientation also becomes altered. If this in fact does induce early onset osteoarthritis, it is presumed that a replacement with the correct microarchitecture and stiffness would reduce the potential of this occurring.

2.3 Synthetic Electrospun Ligaments

A method which can be used to replicate the ligament more closely is electrospinning. This process enables the production of nanofibers, which can be collected in a way to similarly replicate the hierarchical structure of a native ligament (Figure 3). Provided that the electrospun fibres have diameters within the fibril range, and are collected in aligned fibre bundles, a more desirable microarchitecture can be achieved in comparison to the current replacement grafts.

Image removed due to copyright restriction.

Figure 3- Hierarchical Structure of Tendon/Ligament [23]

The matrix of the ligament follows a sinusoidal type wave, referred to as 'crimp'. The crimp pattern straightens out during low loads of tensile stretching without causing damage to the fibrils. Under larger loads, the fibrils are elongated, with more fibril elongation as the load increases [19]. This type of non-linear response can be represented in a force-displacement or stress-strain curve (Figure 4). As all fibrils are recruited with increasing load, the gradual increase in stiffness can also be interpreted. Beyond the toe region into the linear region is where the elastic modulus of the fibres can be determined. It will be most desirable for electrospun fibre bundles to exhibit this type of behaviour and the correct stiffness range when subject to tensile loads.

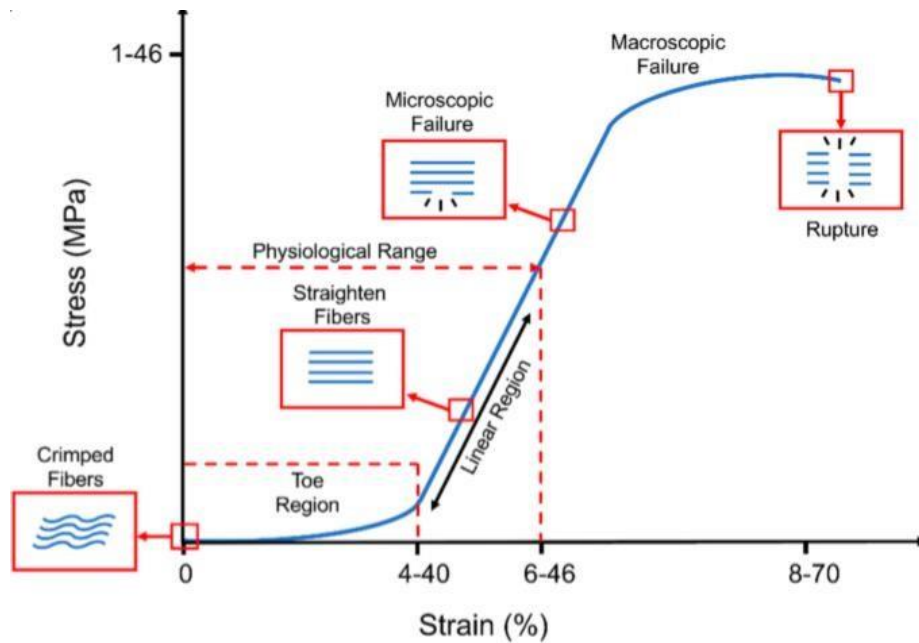


Figure 4 - Typical Stress-Strain Response for Collagen Fibres in Ligaments [20]

2.4 Electrospinning Background

Electrospinning is a widely used method for fibre development in many aspects of tissue engineering and medicinal applications. Its ability to vary parameters and collection methods make the process adjustable to meet desired needs. The application of concern is to develop fibre bundles which more closely replicate native knee ligaments, meaning parameters should be altered to suit this aim.

Electrospun fibres are formed when a suitable polymer solution is placed in a syringe with a needle attachment. When subject to a high voltage and a consistent flow rate through the needle, the solution is subject to elongation and potentially fibre formation. A strong electric field is applied between the positive needle electrode and negative collector electrode. The collector electrode can vary based on the desired collection type. When the voltage is increased to a particular level, enough positive charges in the solution are collected on the needle tip, forming a Taylor cone and a fibre stream (Figure 5). The Taylor cone is formed at 49.3° angle and is achieved when the critical potential is reached and the equilibrium at the needle is disturbed [29]. The voltage at which this occurs is dependent on the combination of all electrospinning parameters. It is vital that the solution used is electrically conductive so that this response occurs, overcoming the solution's dielectric constant and the surface tension within the needle. In some cases, the combination of electrospinning parameters can elicit a fibre cone (Figure 6). Other cases elicit an electrospaying type response which is less fibre orientated with more solution droplet formation. For the current application creating uniform fibre production is highly desirable.

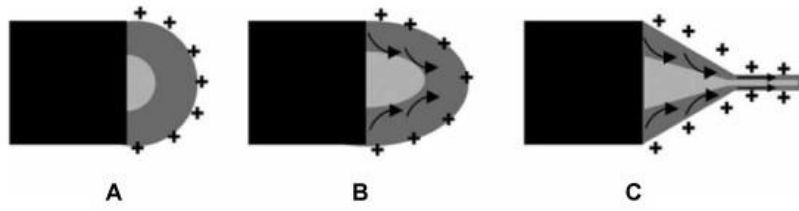


Figure 5 - Solution Impact with Increase in Voltage, Taylor Cone Formation at C [24]

Image removed due to copyright restriction.

Figure 6 - Typical Electrospinning Setup [25]

The type of collection most desirable for synthetic ligament applications is the use of a rotating mandrel. By employing a high-speed rotating collector, the fibres can be collected with some stretch and over a large surface area. This collection method would be most beneficial in replicating the natural fibre structure of ligaments, allowing for bundling of the fibres after collection. There are limitations in aligned fibre production since the high electric field in a short distance induced whipping in the fibre jet, potentially widening the cone before it lands on the collector. It is worth ensuring the electric field can be controlled by the applied voltage and the distance between the electrodes. In cases where the distance is too small, the solution may not have sufficient opportunity to dry and for the solvent to evaporate, leaving wet fibres or solution droplets on the collector. There are also limitations with knowing what type of fibres are being produced during testing as they are nanoscale structures. Although the type of jet can be indicative of the fibre production, the use of a nanoscale imaging device will provide conformation of the fibre size and orientation.

2.5 Parameter Impact on Fibres

The characteristics of the fibres that are formed are dependent on the electrospinning parameters set during the process. The polymer's concentration and molecular weight in the solution used, directly impacts the fibre diameter. In cases where all electrospinning parameters are kept constant

and only concentration is altered, it is expected higher concentrations result in thicker fibre diameters. Based on the given experimental findings, the higher the molecular weight, the higher tensile loads the specimen is capable of withstanding. Again, with consistency in all other parameters, increasing voltage, electrode distance and mandrel rotational speed independently, the fibre diameters will be decreased [21]. All these factors need to be considered when developing fibres for this particular application.

Due to the specific microstructure of each knee ligament, it is vital to collect the electrospun fibres in a way which replicates or closely matches the ligament structure. Ideally, the synthetic samples should have aligned bundles of fibres which exhibit some crimping. A worthwhile method in order to achieve this is to use a rotating mandrel as the negative electrode. Fibres can be collected in an aligned state when the mandrel is rotated at high speeds. Rolling the fibres off of the mandrel is a suggested method for having both aligned and bundled fibres [20] (Figure 7). Perfecting the collection method will be pivotal in achieving similarity of the native ligaments on a microstructural point of view.

The production of electrospun fibres are also subject to variation based on ambient conditions. The surrounding temperature and humidity of the testing conditions will influence the extent the solvents will be evaporate in the fibre formation and collection [29]. The temperature also has the ability to affect the conductivity of the solution. This is due to the weakening or strengthening of the intramolecular forces, which in turn affects the polarity of the solvent. Once the polarity is affected, the applied voltage may need to be altered accordingly to still produce a desired response.

Image removed due to copyright restriction.

2.6 Mechanical Properties

A key aspect of developing synthetic knee ligaments is that the mechanical properties are within the same range of a native ligament. A common ACL replacement procedure is the use of a sectioned patellar tendon. While the biocompatibility is high if sourced from the patient, the elastic modulus is found to range between 597 to 843 MPa [30]. This range indicates that the patellar tendon is too elastic and not stiff enough to be used as a replacement for any of the knee ligaments, highlighting the importance of producing a replacement with a more desirable elastic modulus.

A series of papers were investigated to determine the stiffness range of the electrospun ligament should lie in (Table 1). There were many exclusions as comparisons were made to animal models rather than human. The animal models may be regarded as outliers and give an inaccurate representation of the stiffness range, and hence were excluded. The majority of studies also put a focus on the ACL without consideration for the other ligaments.

Table 1 - Stiffness and Elastic Modulus Range of Native ACL

Source	Native Ligament	Specimen no.	Stiffness (N/mm)	Elastic Mod. (MPa)
13	ACL (48-86 yrs)	20	129±39	65.3±24
	ACL (16-26 yrs)	6	182±56	111±26
14	ACL (male 2650 yrs)	8	308±89	128±35
	ACL (female 17-50 yrs)	9	199±88	99±50

Table 2 - Stiffness Ranges for Native PCL, MCL, LCL

Ligament	Stiffness Range (N/mm)	Elastic Modulus (MPa)
ACL	129 – 308	65.3 – 128
PCL	64 – 107	
MCL	53 – 86	
LCL	68 - 84	

Table 3 - Stiffness Range Summary of all Knee Ligaments

Source	Native Ligament	Specimen no.	Stiffness (N/mm)
22 (L141432)	PCL	1	107
	MCL	1	83

	LCL	1	84
22 (S142395L)	PCL	1	86
	MCL	1	53 – 57
	LCL	1	68
22 (S142444L)	PCL	1	64
	MCL	1	61
	LCL	1	75
22 (142444)	PCL	1	64
	MCL	1	68
	LCL	1	73

Even though a stiffness summary was made based on the four key knee ligaments, the ACL was the focus in most studies, so the stiffness range was established with the values from ACL findings. There is difficulty making a direct comparison across all studies as all used different mechanical tests and procedures. However, all four ligament ranges will be useful when developing electrospun samples to determine whether the specimen stiffness's match a particular ligament.

As studies varied based on method and testing, only those which provided a stiffness or elastic modulus value could be considered. Even with this normalisation, the samples were made up of different shapes and pore sizes, hence affecting the cross-sectional area of the synthetic ligament. This of course is a factor that needs to be considered in determining the elastic modulus.

2.7 Research Variations

The span of the electrospinning synthetic ligament research is quite broad with a great deal of variation in the research aims. Although most papers place a specific aim to replicate the ACL in some way, be it through fibre diameters or mechanical properties, materials used, electrospinning parameters and methods, all have significant variance.

The properties of the fibres produced have a high dependence on the materials used in the solution. The polymers, solvents and concentrations used was the first aspect to separate the studies. Although some experiments have overlaps in the materials used, the parameters overall methods vary too drastically to make a direct comparison. The key electrospinning parameters are outlined so that a suggested range for each aspect could be established (Table 4).

As all studies had various aims, the results and outcomes of each are fairly varied. Some place emphasis on the fibre diameter, while other studies focus on mechanical properties. There were some papers which have aims surrounding pore size, cell attachments and in vivo testing, which is beyond the scope of this study. Based on all results, a summary of outcomes has been outlined (Table

5), however those that provide information about stiffness or the elastic modulus can be considered further for experimental guidelines.

The considerations which need to be made when mechanically testing the samples relates to the porosity, size and shape. While some cases follow a desired porosity percentage, others intentionally aim to eliminate pores within the samples for more accurate mechanical testing. This is because the closely packed fibres provide a cross-sectional area not compromised by spaces between the fibres and therefore more accurate calculations of stress. Some studies laser cut pores to result in a 15% porosity and a specific pore diameter suitable for cell ingrowth [5, 10, 11]. These cases are tested post-implantation, where the cells make contributions to the sample's mechanics. Some studies employ specific mechanical testing techniques where the samples are subject to some weight which flattens the overall structure, condensing the fibres [2]. The porosity remains higher than a native ACL, however more accurate mechanical testing can take place with a more condensed structure.

The previously mentioned differences in testing method means that a caution when testing will need to be taken for result accuracy. The degree of porosity is likely to vary with the fibre thickness, the collection method and its rotational speed. Ideally, consistency should be aimed for through each test, however it is likely that variation in parameters will be required to have consistent fibres.

Table 4 - Electrospinning Experiments with Key Parameters

	Polymer	Solvent	Voltage (kV)	Distance (cm)	Flow rate (mL/h)	Needle	Mandrel RPM	Additional Info.
1	20% polyurethane	DMF	14	20		18G	620.7	
2	10% PCL (80,000 mw) and oleic acid sodium salt 97:3	3 chloroform : 1 methanol	15	10	2.5	18G flat tip	3000	
3	5% P(LLA-CL)	3:1 DCM/DMF	15	15	0.3mL/min	21G blunt tip	1000	Additional heating for crimping
4	13% PLLA (84,000 mw)	65:35 DCM/DMF	18	20	1.2	2-40mm apart 18G	2900	

5	10 % PCL (110,000 Mw)	1,1,1,3,3,3hexafluoro2-propanol	20		2.5		3450	Pores were laser cut Bathed in EtOH and collagen
6	20 % PLGA (153,000 mw)	(60:40) acetone/DMF	21	20	3	18G flat tip	612.1	Fibres land in water bath, rotating mandrel next to it
7	7, 12, 20% PEUUR (146 kDa mw)	1,1,1,3,3,3hexafluoro2-propanol	15	15	3	22G	9.5m/s	
8	15% poly(Llactic-co-e-caprolactone) (PLCL (LA/CL 70/30))	(90/10) chloroform/DMF)	6-9	15	2	19G	1500	Scaffolds were knitted after electrospinning
9	20 – 35% poly(L-lactide-co-acryloyl carbonate) (P(LLA-AC))	3:1 dichloromethane/DMF	15	15	1.8	21G	1000	Crimping in 37 degree C phosphate buffered saline
10	10% UHMWPCl (500kDa)	1,1,1,3,3,3hexafluoro2-propanol	25		0.7		1725	Laser cut stacked mats – bathed in 70% EtOH
	10% PCL (80kDa)	1,1,1,3,3,3hexafluoro2-propanol	20		2.5		3450	
11	10% PCL in chloroform (140k g/mol)	1,1,1,3,3,3hexafluoro2-propanol	20		2.5		3450	
12	5,11, 16% PLGA	1,1,1,3,3,3hexafluoro2-propanol	15	15, 12	5	22G Teflon tip	Stationary, 580,1010 1450	
15	18% PLGA	70/30 (THF:DMF)	20	15	1	0.8 mm diam.	3000	

Table 5 - Electrospinning Experiments Result Summary

Source	Fibre Diameter	Specimen size	Pore size	Pore area %	Young's Modulus (MPa)	Ultimate Strength (MPa)	Yield Stress	Stiffness (N/mm)
1	657±183 nm	10 X 40 X 1 mm ³	0.0032 – 366.7 µm (diameters)	82.72	3.55	3.52		

2	474±57µm	3.17 mm W 4cm L	5µm		154 ± 28			
3	0.88 ± 0.002 µm				0.349		193±44 kPa	
4	550-600 µm bundle 0.59±0.14 µm	100mm L 6.5mm diameter			156.2±36 7		15.8±2.8 MPa	
5		1.5mm X 35mm X 900µm (stacked sheets)	150µm (laser cut)	15%				1.95±0.3 5
6	2.15 ± 0.55 µm (parallel fib.)	32 × 5 mm ² (rectangle)			775 ± 35			
7	(7) 0.50± 0.11mm							
	(12) 1.08± 0.22mm							
	(20) 2.08± 0.57mm							
8	2.6 ± 0.3 µm (aligned)				202±12	46±4		
9	(12% AC) 0.85 ± 0.10 µm				26±1.4			
10		1.5mm X 35mm X 150 µm	150 µm Laser cut	15%				
11		1.5mm X 35mm X 150 µm		15%				6.2±3.9
12	(Stat.) 0.014±0.07 µm 0.076±0.36 µm 3.6±0.6 µm							
15	900 nm				129.07±2 0.22			

Those studies which provided a stiffness or elastic modulus within or close to the range previously found for the native ligaments were further summarised with comparison to the electrospinning parameters used (Table 6). As desirable outcomes were achieved in these cases, this gives a good indication on the test parameters and materials which can be used to produce the synthetic electrospun ligaments.

Table 6 - Top Selection Electrospinning Experiments

	Polymer	Solvent	Voltage (kV)	Dist. (cm)	Electric field (kV/cm)	Flow rate (mL/h)	Needle	Rpm	E (MPa)
2	10% PCL (80,000mw) and oleic acid sodium salt 97:3	3 chloroform : 1 methanol	15	10	1.5	2.5	18-G flat tip	3000	154 ± 28
4	13% PLLA (84,000 mw)	65:35 DCM/DMF	18	20	0.9	1.2	2 syringes (40mm apart) 18G	2900	156.2 ±36.7
8	15% poly(Llactic-co-e-caprolactone)(PLCL (LA/CL 70/30))	(90/10) chloroform/ DMF	6-9	15	0.4-0.6	2	19G	1500	202±12
15	18% PLGA	70/30 (THF:DMF)	20	15	1.33	1	18G	3000	129.07±20.22

2.8 Overview of Proposed Study

2.8.1 Aim

To develop an electrospun ligament replacement which closely mimics the elastic modulus and microarchitecture of a native human ligament. Achieving this would mean development towards a graft which is most similarly matched to the original ligament without compromise to the overall mechanics of the knee.

2.8.2 Objectives

The aim will be achieved through explorative testing of polycaprolactone (PCL) in various combinations of dimethylformamide (DMF) and chloroform. Collection method will also be tested so that efficient fibre collection can take place while achieving the desired alignment. The microarchitecture of the samples will be viewed on SEM imaging techniques, while the elastic modulus will be determined through tensile testing.

Many studies aim to create a replacement using electrospinning methods, but then further the study with cell seeding and in vivo testing prior to perfecting these two key aspects. There was no study found to simply develop a synthetic ligament, not only limited to the ACL, and provide information on both its microarchitecture and its stiffness. The explorative nature of this study aims to do so, potentially progressing the development of synthetic knee ligaments.

2.8.3 Justifications of Decisions

Various combinations of polymers and solvents can be used in electrospinning, yet the materials should reflect the desired outcome. An overview of polymers with potential applications were assessed in order to give conformation to decisions made [20]. Although there would be value in testing a number of materials, limitations are placed on the polymer and solvent option due to both budget and timeframe limitations. There was attraction toward the use of polycaprolactone (PCL) due to its proven biocompatibility as its Food and Drug Administration approval in some human body applications [31]. Also, PCL with a molecular weight of 80,000 Mn has proven to elicit desirable results based on the studies outlined previously. The use of PCL was also attractive based on the price of the quantity required for multiple tests. Based on the properties of solvents, chloroform was selected for its high PCL solubility, while dimethylformamide (DMF) was selected due to its high dielectric constant and electrical conductivity. With focus on the use of PCL in combination with various concentrations of chloroform and DMF, this study will aim for the best results with these materials and within the electrospinning machine specifications.

2.8.4 Overview of Experimental Method

Given the concentration ranges of the polymers in Table 6, the PCL will be tested in concentrations of 10, 13, 15, 18 and 21% w/v. As the PCL tested has a relatively high molecular weight, it will be important to ensure the polymer is completely capable of dissolving in the solvents. There is more difficulty in dissolving PCL in DMF compared to chloroform, however DMF does prove to have benefits in fibre production, as seen in three of the four top experimental picks (Table 6). For this reason, it will be valuable to establish various solvent ratios to determine which solutions produce better performing fibres. For each concentration, the solvent ratios will be 100:0, 25:75 and 50:50 in favour of both DMF and chloroform, producing 5 solvent combinations for each polymer concentration.

Naturally, with variation in concentration and solvent ratios, the viscosity of the solutions will vary. This may impact the needle type that should be used and the flow rate of the solution coming through it. The range established from the studies is from 1 to 2.5 mL/h with 19G or 18G needles. Although a reliable guide, it will be important to experimentally establish what the ideal fibre

production case is. If the development of fibres is not consistent within these ranges, further testing will need to be done to do so.

The electric field can be adjusted by the voltage applied but is most likely limited by the distance between the electrodes. If the position of the rotating mandrel cannot be adjusted, the applied voltage will determine the strength of the electric field during testing. With the voltages ranging from 6 to 20 kV, the potential difference is expected to be in this range but will be more reflected on the amount which produces a consistent fibre stream. This will need to be experimentally tested as some applied voltages exhibit consistent fibre streams for a short period of time before the voltage dries the solution at the tip of the needle, inhibiting solution flow. To avoid this, it is important to determine a voltage which is capable of producing consistent results for a longer duration, allowing a large amount of fibre collection with each test.

The rotational speed of the mandrel in the studies vary from 1500 to 3000 rpm. It has been discovered that higher speeds produce smaller fibre diameters which may impact the elastic modulus of the overall sample, but the combination of the other parameters will also have an impact. There is benefit in varying the rotational speeds in attempt to create some crimping within the fibre bundles but the importance lies in having aligned fibres in the collection method.

The assessment of the electrospun ligaments will be determined by scanning electron microscope (SEM) imaging. These images will be vital in determining whether the fibres have been collected in an aligned manor and if the microarchitecture matches a native ligament. Image processing techniques will also be employed to calculate the average fibre diameter of the samples. Although not a key objective, there is value in determining how the parameter combinations affect the fibre diameters.

Tensile testing where force and displacement are measured is important to determine the stiffness of the samples and ensure it lies within the native ligament range established previously. This is another key aspect which will determine if the samples are sufficient for use as a synthetic knee ligament.

3. Methodology

The method established was done so for the consistency of ligament sample formation. Although sections of the procedure were subject to systematic error, the procedure was aimed to lie within the testing bounds. Experiments were conducted on the NEU-Pro Electrospinning Unit (Manufactured in China).

3.1 Solution Preparation

Chemical materials were purchased from Sigma-Aldrich, where the PCL had a molecular weight of 80,000 Mn. Solutions were made with various amounts of PCL and solvent combinations to uphold with the previously outlined concentrations and ratios. The concentrations were based on all samples being made up of 10mL of solvent, according to which ratio was being used (Table 7).

Table 7 - Solvent Ratios

Solvent ratio type	Chloroform (mL)	DMF (mL)
1	10	0
2	7.5	2.5
3	5	5
4	2.5	7.5
5	0	10

All solutions required a relatively long dissolving time so were placed on a magnetic mixer with a small magnet inside the solution. Chloroform-heavy solutions dissolved at a quicker rate than those with predominantly DMF as the solvent. Despite the solvent ratio, dissolving time was approximately 24 hours. Even after 48 hours and more, the PCL did not dissolve in the 100% or 75% DMF solutions, proving early on that this particular molecular weight PCL is too high for the DMF to dissolve and could not be tested.

Although the other three solvent combinations were completely dissolving the PCL, not all were worth testing. The 100% chloroform solution proved to be difficult to test in the electrospinning device, with inconsistent parameters and unpredictable fibre jet making it difficult to produce consistent results. Due to these complications, only type two and three solvent ratios were used in further testing.

3.2 Electrospinning Procedure

The solution was placed into the 10mL syringe which was connected to one end of the plastic tubing. On the other end of the tubing, the 18G flat tip needle was connected. The 18G needle was trimmed and filed down in order to have a flat tip. This was necessary in testing as charges would accumulate on the tip of the needle when it was subject to high voltage. This charge accumulation may affect the development of the Taylor cone when it comes to fibre production as well as the trajectory of the fibre jet. The needle distance from the collector was kept constant for all tests at 15cm.

Between each test, the tube was flushed with chloroform to prevent and contamination between the solutions. For the electrospinning testing, the needle was fed through the device and placed in the left needle holder, while the syringe on the other end was placed into the flow rate pump (Figure 8). Prior to setting the flow rate, the solution was purged in order to push the solution to the tip of the needle. Some cases required purging until the solution was consistent and free of air bubbles in the tubing. Once the solution was set up, it was placed in the syringe pump where the flow rate could be set.



Figure 8 - Syringe Pump and Flow Rate Control

The 8cm diameter rotating mandrel was covered in baking paper for ease of fibre removal postexperiment (Figure 9). The fibres did not have the tendency to stick to the paper so they could be removed without much compromise to their structure. Tape was used to join either end of the baking paper and provide tight coverage. Light wrapping of the mandrel could result in paper movement during rotation which is undesirable during testing.

Once the collector covered and ready for experimenting, all parameters were set except for the voltage. The flow rate was set between 1.5mL/h and 2mL/h. The rotation of the collector and the x axis needle speed were also set, however, both of these parameters were prone to independent alteration. The x axis needle speed was set at 2mm/h, yet was always increased by the end of the test. The rotational speed of the mandrel was also subject to increase over the experiment duration. While the electrospinning device included a tachometer, values could not be measured above 1000 rpm, hence why an external tachometer was required to measure the final rotational speed. Despite the slight increase over time for these parameters, the ranges for both were between 2 - 2.4 mm/s and 1000 – 1200 rpm for each test.

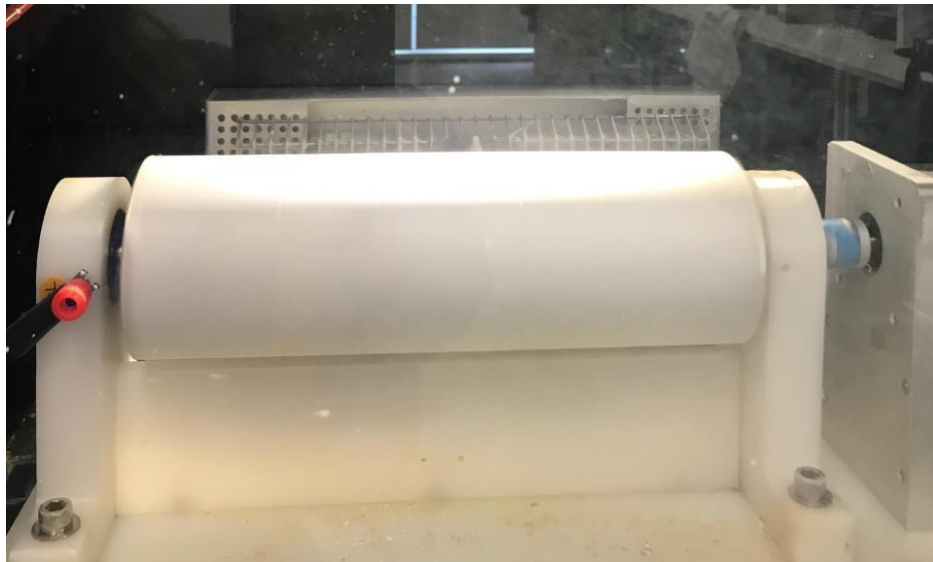


Figure 9 - Rotating Mandrel Collector Covered in Baking Paper



Figure 10 – NEU-Pro Electrospinning Unit

The flow rate parameter was turned on and once solution consistency through the tube was achieved, the voltage was increased until a continuous fibre jet was created. As fibre streams and jets were fine and difficult to see, caution was taken with parameter adjustments. Smaller concentration solutions would produce shorter streams and larger, more visible fibre jets (Figure 11), while solutions with larger concentrations generally produced longer streams but much finer and shorter fibre jets (Figure 12). The best fibre jet results were seen at approximately 20kV, however adjustment of voltage was made until a continuous fibre jet was formed. For instances where the fibre jet was inconsistent or splattering, for the purpose of consistency amongst other parameters, the voltage was the only parameter changed to produce a more desirable fibre jet. If splattering of the jet or solution dripping was occurring, to produce stability the voltage was increased. In cases where the fibre jet was becoming small or the Taylor cone was appearing to dry out, the applied voltage was decreased.

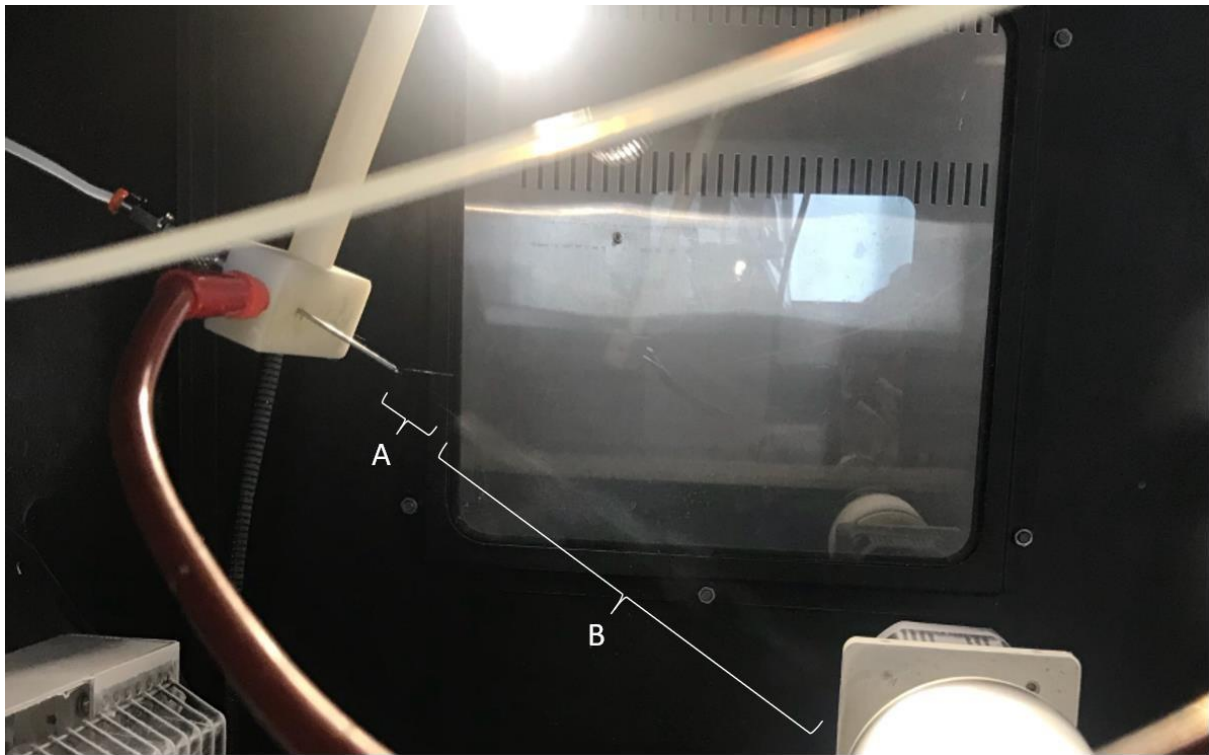


Figure 11 - A) Short Fibre Stream B) Long Fibre Jet

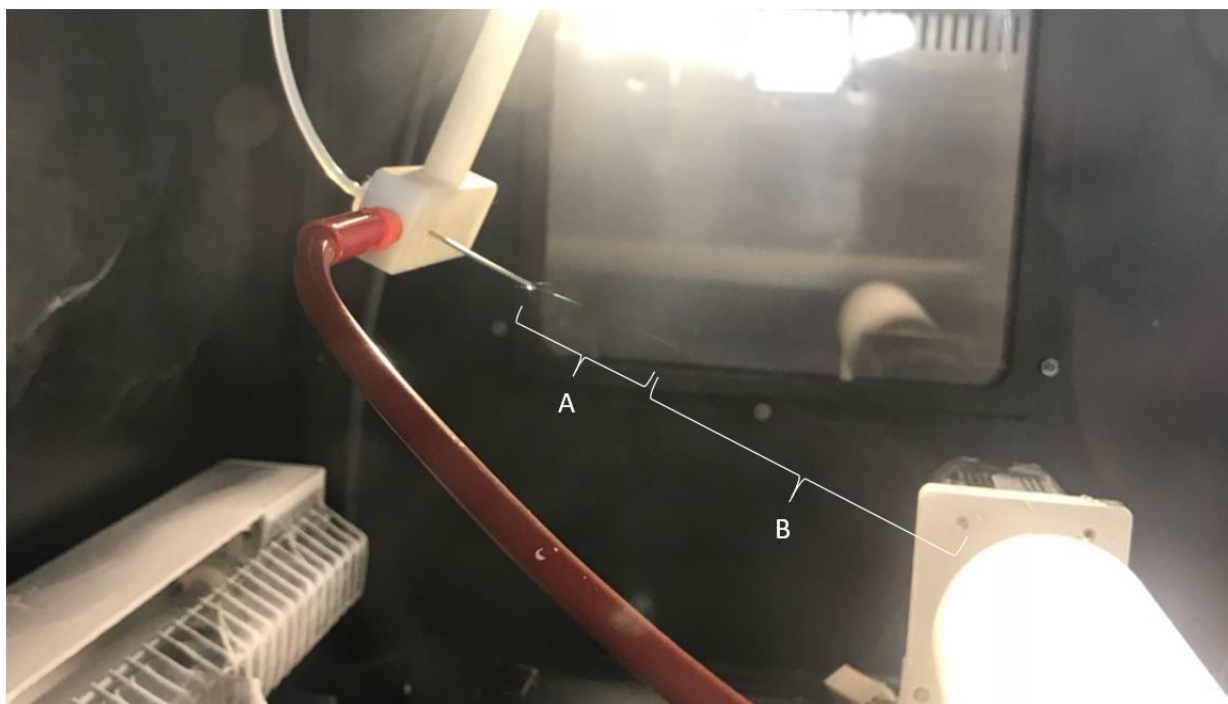


Figure 12 - A) Long Fibre Stream B) Shorter, Finer Fibre Jet

Each test was given a two-hour time period for fibre collection. Some test has a shorter duration of if the solution in the syringe ran out before the two-hour time had been reached. Upon completion, the parameters would all be safely stopped, with consideration towards not having remaining solution droplets onto the collected fibres. The fibre sheet was removed by horizontally slicing the baking paper with a scalpel while on the mandrel, allowing the sheet to be spread out flat (Figure 13). Once the baking paper was removed, the section of the sheet with tape was also sliced out. This section was saved in some samples for later SEM imaging. The remainder of the sheet was halved so that from one test, two ligament sample could be made.

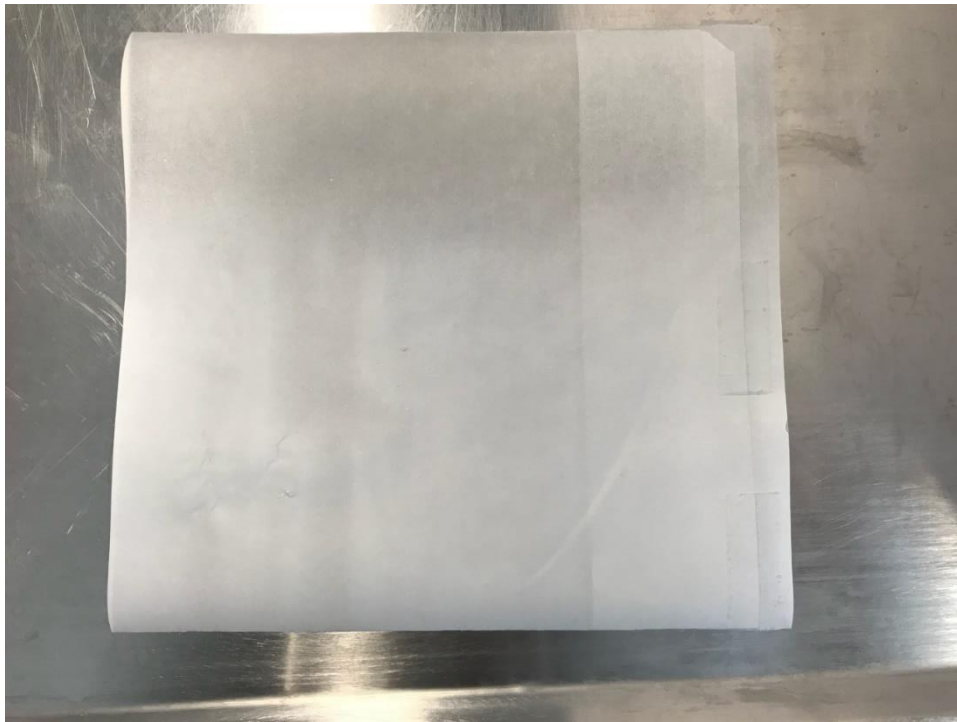


Figure 13 - Removed Baking Paper with Fibre Sheet

The ligament samples were created by rolling up the fibres in the same, longitudinal direction of collection. This was done by placing another sheet of baking paper on top on the edge of the sheet. Since fibre amounts are scarcer along the edges, to start the rolling up of the fibres they need to be handled delicately. Once the edge was lifted, the remainder of the fibre sheet could be consistently and carefully rolled up (Figure 14).



Figure 14 - Rolled-up Fibre Sheet into Ligament Sample

The weight and length of each sample was measured and recorded so that data normalisation could be done for the mechanical tests. The length was considered from each edge of the fibre sheet. If

the ends were thin due to uneven rolling, the length was considered from the visible edge of the fibre sheet on either end. Callipers were also used to carefully measure the diameter of the sample, taking care not to compress the fibres. This measurement was taken in a middle portion of the bundle, where the most consistent thickness was found to be. The diameter was halved, using the radius to find the cross-sectional area of the circular fibre bundle. There was some difficulty in taking this measurement as not all fibre bundles were tightly wrapped, introducing possible error in the diameter measurements. This however, would be accounted for in the data normalization.

The electrospinning tests were conducted in three different rounds. The first round covered a range of polymer concentrations in order to determine which solutions are most successful to electrospin with as well as to gain understanding of the material properties of each. Following the first round, the second and third lot of electrospinning tests were done with focus on the more successful solutions. The success of the solution is based on its cooperation in the electrospinning environment and the mechanical information it provides.

3.3 Mechanical Testing

Mechanical testing and data analysis was followed by each significant electrospinning round. Evaluation of the sample's material properties would be achieved through tensile testing, using the

Test Resources Machine with clamp attachments (Figure 15). Tests were conducted with a 5 kN load cell to conduct a position based tensile test at 30% strain rate for each sample. This was decided as 33% per second strain rate is approximately the strain experienced on the knee ligaments during walking [4]. Each end of the sample was clamped into the device from which the tests would begin from. The rate of strain was dependent on the starting distance between the clamps, which was slightly different with each run. Vertical alignment was maintained by clamp both ends with the guidance of a metal ruler.

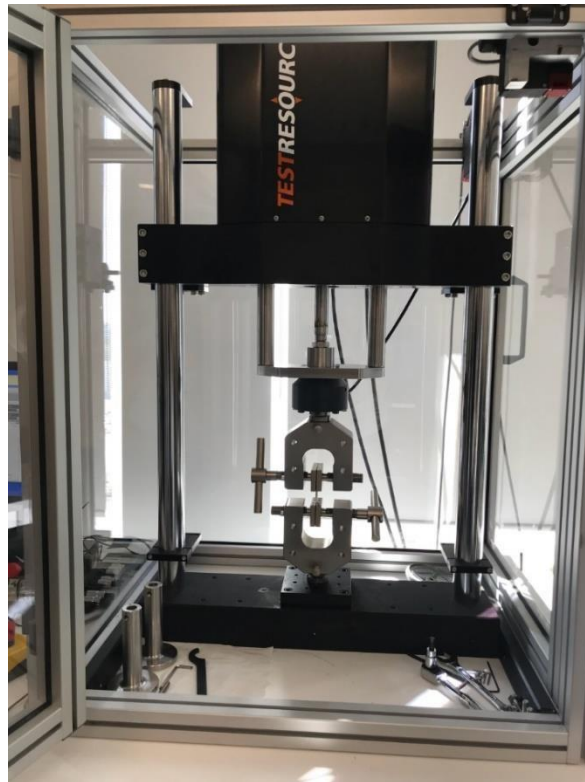


Figure 15 - Test Resources Device for Tensile Testing

Ideally the breaking of the ligament would occur in the middle of the testing region, however due to the stress concentration at the clamps, occasionally the ligament samples would break directly at the clamped location (Figure 16). The inside of the clamps were entirely made up of knurling grip, which with its sharp nature, the tight clamping had a tendency to potentially produce cuts in the samples. The data resulting from these types of test can still indicate the linear region of material but cannot account for the ultimate load the sample can withstand. This is particularly evident in cases where data appears to enter a second linear phase, suggesting some yielding has occurred sooner than anticipated.

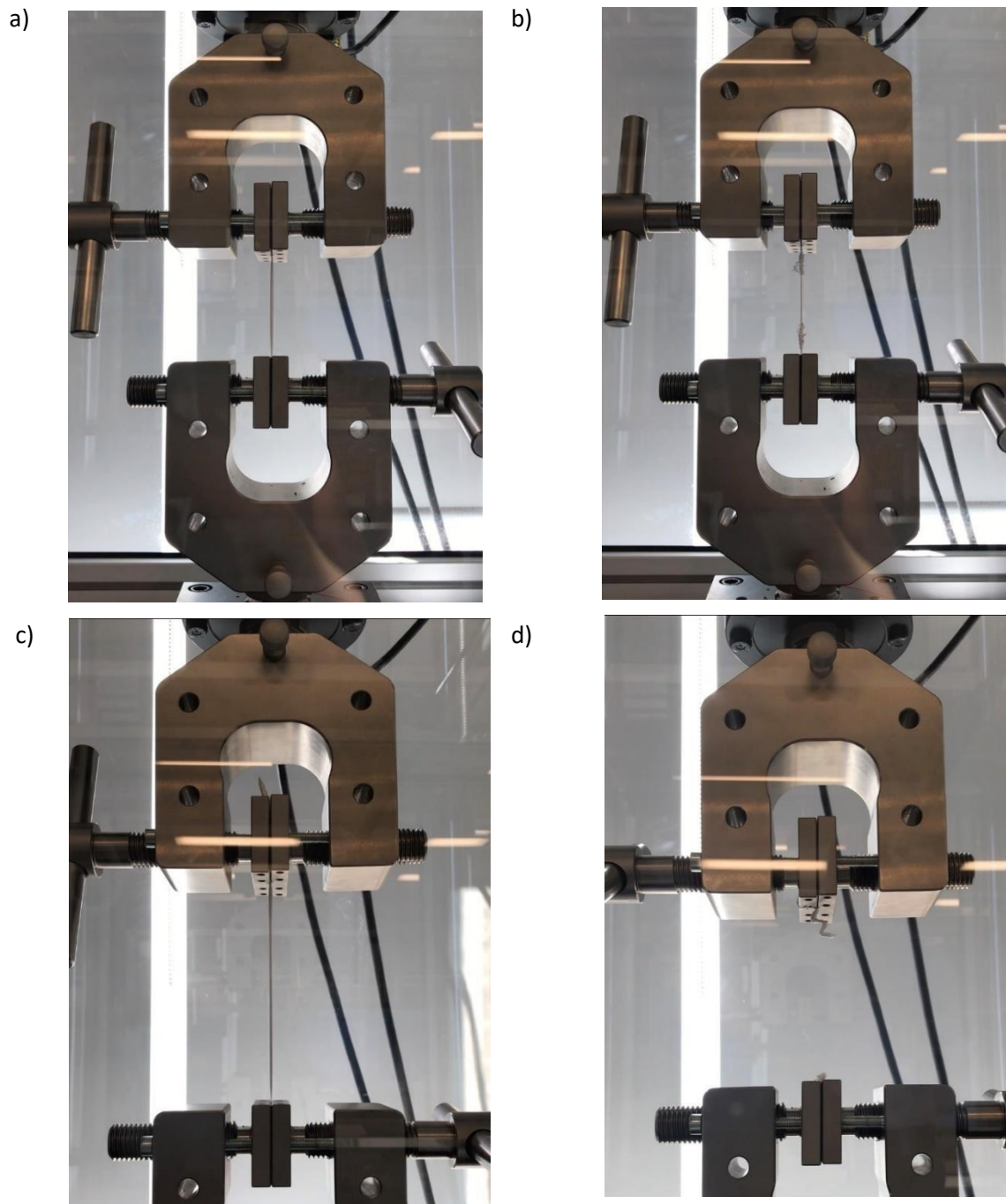


Figure 16 - a) Increased strain prior to b) Incremental breaking c) Increased strain prior to d) Clamp breaking

To avoid premature yielding or any other impacts from the knurling grip, an addition testing method was employed for later third round tests. The samples were folded over on either and looped once through metal rings fashioned out of thin wire. The ends were then secured with electrical tape and securely tightened with a clinch knot (Figure 17). The distance measured for each of the tests was done from knot to knot rather than from clamp edge to clamp edge while the remaining test methods were kept consistent. This information is vital for the determination of the strain rate the test would operate at and later required for the calculations for overall strain of the sample. The metal ring was then placed in the clamps, avoiding any force on the samples. The tensile test would then be conducted with data recorded for interpretation of the mechanical behaviour.

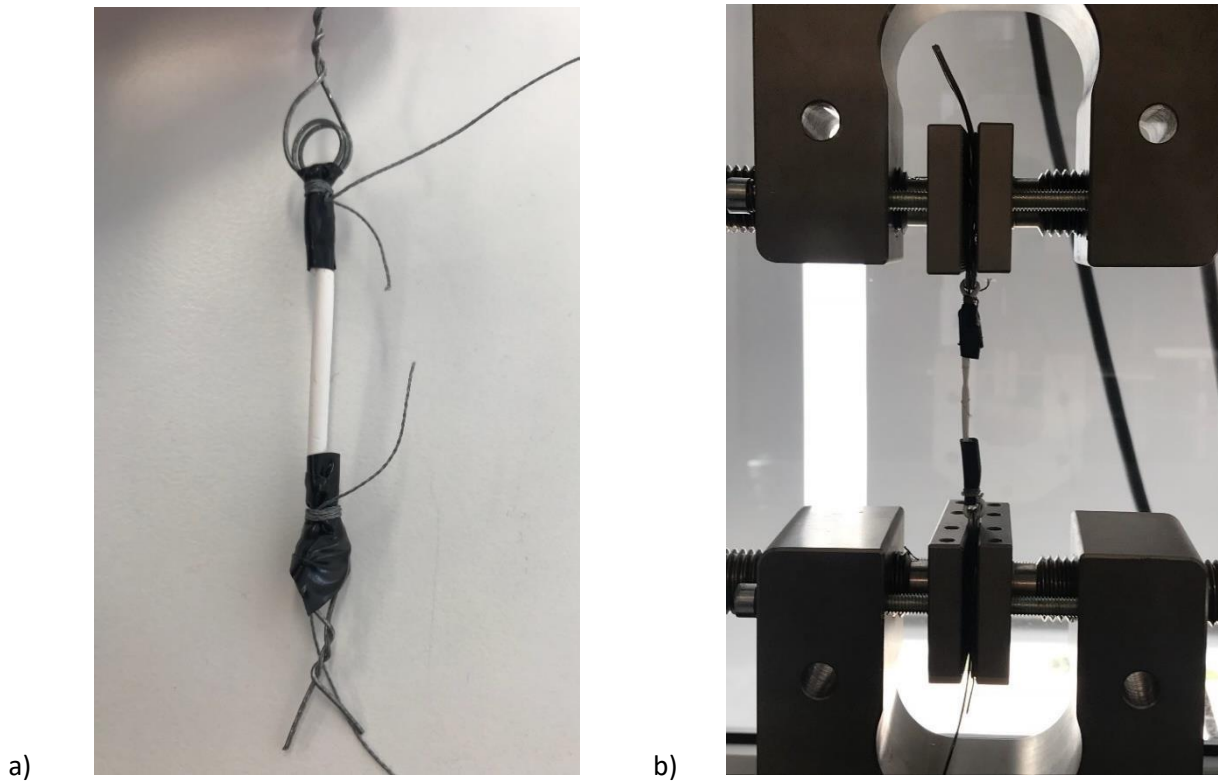


Figure 17 – a) Looped end sample prior to testing b) Looped end samples during testing

3.4 Normalising Data

As each sample had a different length, weight and cross-sectional area, it was important to use this information to normalize the mechanical testing data. Although the majority of tests were conducted with a 1.5mL/h flow rate and a two-hour duration, the fibre jets created for each run varied, meaning the types of fibres being formed were dependent on the other parameters. Due to these impacts, fibre sheet thickness varied for each run, which also made an impact on the type of rolling each test was capable of. Thin fibre sheets were more subject to scrunching or folding, making it difficult to tightly roll the sheet. In these instances, the cross-sectional area would appear slightly larger than it should be, impacting the comparison for stress calculations. The stress formula accounts for a solid object, which these samples are not. However, dividing apparent stress by the material volume fraction accounts for the lack of solid material in the samples (Equation 1).

$$\text{Material Volume Fraction } (v) = L \frac{w \text{ (kg)}}{(m) \times A(m^2) \times \rho(kgm^{-3})} \quad (1)$$

The data recorded from the Test Resources machine was the relative force and stroke, both which were used to calculate the respective stress and strain for each sample. The data was recorded just prior to testing and the force and stroke values were negative or close to zero during this time. The

data used in the plots would be from when the stroke value was greater than zero, indicating the test had begun. The corresponding force value in each case was always slightly above zero, due to the weight of the clamps. The force was not reduced to a starting point of zero since the values were so minute and there would be no impact to the slope of the linear region. The calculated crosssectional area and the initial distance between the clamps were used in the stress and strain equations (Equation 2, 3). The stress was normalized by dividing through by the material volume fraction. The stress-strain curves were graphed using MATLAB, where the strain was not graphed as a percentage in order to calculate the Young's modulus from the graph (Equation 4). Since each case was very specific in terms of breaking and data noise, the linear region's varied and needed to be judged accordingly. The noisy graphs were smoothed in MATLAB, clearing the visual aspect of the graph. The slope was found between two points which were evidently linear in the smooth graphs, which were proved with the R^2 , however noisier graphs required multiple measurements to find an appropriate average.

$$\text{Stress } (\sigma) = \frac{F \text{ (Newtons)}}{A \text{ (m}^2\text{)} v} \quad (2)$$

$$\text{Strain } (\varepsilon) = \frac{\Delta l}{l_0} \quad (3)$$

$$\text{'s Modulus } (E) = \sigma \text{ (Pascals)} \frac{\text{Young}}{\varepsilon \text{ (unitless)}} \quad (4)$$

3.5 SEM Imaging Method

A small section of the fibre sheet was saved from each test in order to analyse the fibres on a microscale with the FEI Inspect F50 model scanning electron microscope. Since the drum was covered in baking paper, the join of the paper was connected using tape. The fibres between the tape were left flat as they landed. Each sample was prepared on a small metal stage and pressed on a secured to double-sided tape.

The samples then underwent sputter coating which covered the surface of the fibres with a thin platinum film (

Figure 18). Since imaging takes place through the reflection of an electron beam the samples were layered with additional platinum coating to make the surface of the fibres more conductive. The fibres are conductive enough to be imaged without the coating, however, the additional layer makes the fibres less subject to movement due to the electron beam, since the fibres are not tightly secured. The samples were placed in the device mount and vacuumed sealed for five minutes. After the coating, the fibres appear to have a slightly grey tinge, none of which negatively impacts the imaging process.



Figure 18 - Samples post sputter coating

Upon sputter coating, the metal fibre holders were placed onto a dedicated imaging stage within the SEM vacuum (Figure 19). This section could be opened for samples to be placed, while the filament and anode which drive the electron beam remain in a sealed off vacuum which cannot be accessed. Once placed, this section was closed off and vented in order to match the vacuum of the beam section. The closed section can still be viewed via an internal camera and imaging software to the linked computer. This enables the controlled imaging of each sample while still being to identify each sample.

The saved images were imported into Fiji, where the scale was set according to the magnification of each image. The known distance in the images were used to find a ratio to the number of pixels in that given length. Setting the scale enabled for measuring of the fibre diameters seen on the surface. It was important not to consider the fibres which were placed under other fibres or in the distance of the image as there was no method to determine the depth at which they were.

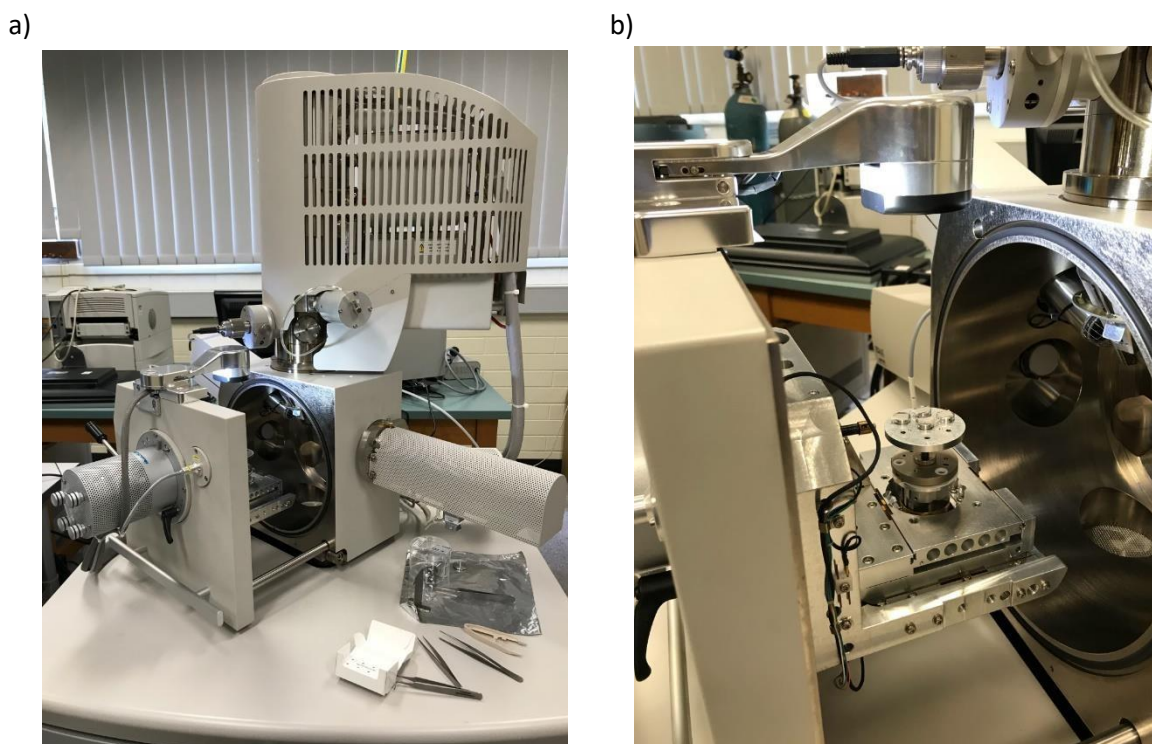


Figure 19 - a) SEM with open chamber b) Samples placed on chamber stage prior to imaging

4. Results

4.1 Electrospinning Outcomes

The parameters were aimed to be as consistent as possible, however, some variation was experienced with each test. Each electrospinning round divided and the parameters recorded so that variations or outliers could be easily identified (Table 8, Table 9, Table 10). The samples were paired off since each electrospinning run would produce a fibre sheet long enough for two samples, hence the sharing of parameters. Even with difficulty in controlling the rotational speed, the values were measured in order to correlate to fibre diameter upon imaging. The values for applied voltage had the greatest variation, however, adjustment was required to produce worthwhile fibres. The inconsistencies may be due to ambient conditions or other external factors.

Table 8 - Round One Electrospinning Test Parameters

Ligament sample no.	Conc. Of PCL (%)	Solvent ratio (DMF:CHCl ₃)	Flow rate (mL/h)	Voltage (kV)	Final Rpm	Run time
L1/L2	10	25:75	1.5	20-22	1000+	2h
L3/L4	10	50:50	1.5	20.04	1000+	2h
L5/L6	15	25:75	1.5	20.02	1000+	94 min
L7/L8	15	50: 50	1.5	25	1000+	2h
L9/L10	18	25:75	1.5	20.09	1098	2h
L11/L12	18	50:50	1.5	20.05-22	1108	2h
L13/L14	21	25:75	2	20.08	1538	<2h

L15/L16	21	50:50	1.5	20.07 – 22.05	950 -1257	2h
---------	----	-------	-----	---------------	-----------	----

Table 9 - Round Two Electrospinning Test Parameters

Ligament sample no.	Conc. Of PCL (%)	Solvent ratio (DMF:CHCl ₃)	X axis needle speed (mm/s)	Flow Rate (mL/h)	Voltage (kV)	Final Rpm	Run time
L17/L18	10	25:75	2.1-2.4	1.5	20.05	1233	2h
L19/L20	10	25:75	2.1-2.4	1.5	20.02	1080	2h
L21/L22	10	50:50	2-2.4	1.5	20.03	1080	2h
L23/L24	10	25:75	2.1-2.4	1.5	20.08-23.03	1032	2h
L25/L26	10	50:50	2-2.3	1.5	25.11-30.12	1088	2h
L27/28	10	50:50	2.2-2.3	1.5	25.49	1047	2h
L29/30	10	50:50	2.3-2.4	1.5	20.02	1050	2h

Table 10 - Round Three Electrospinning Test Parameters

Ligament sample no.	Conc. Of PCL (%)	Solvent ratio	X axis needle speed (mm/s)	Flow Rate (mL/h)	Voltage (kV)	Final Rpm	Run time
L31/L32	13	25:75	2-2.3	1.5	26.3-35.01	1102	2h
L33/L34	13	50:50	2-2.3	1.5	25.05	1102	2h
L35/L36	13	50:50	2.3-2.4	1.5	20.06	1105	2h
L37/L38	13	25:75	2.3-2.4	1.5	20.02-23.03	1107	2h

4.2 Material Properties of Ligament Samples

The stress-strain curves were used to determine the Elastic Modulus (Young's Modulus (E)) for each of the ligament samples. This value was determined by the slope in what appeared to be the linear region for each case. Some linear regions were prematurely shortened due to clamp stresses, however the slopes were determined across the entire span of each linear region. The strain was not represented in percentage in the graphs so that the values could be used in elastic modulus calculations. The type of break or whether the sample broke at all can be seen in the stress-strain graphs. The evidence in premature clamp breaking due to the knurling grip can be seen in cases such as sample L6 since the linear region is relatively short and a second linear region is experienced, possibly where the remainder of the fibres were elongated prior to the complete break load (Figure 20). Despite premature yielding in some cases, there were samples which still experienced incremental breaks, such as sample L12 (Figure 21). In the direct knurling clamp cases, no toe region

is seen, which suggests the fibres are already straightened, or a portion of them were damaged and cannot be incrementally recruited.

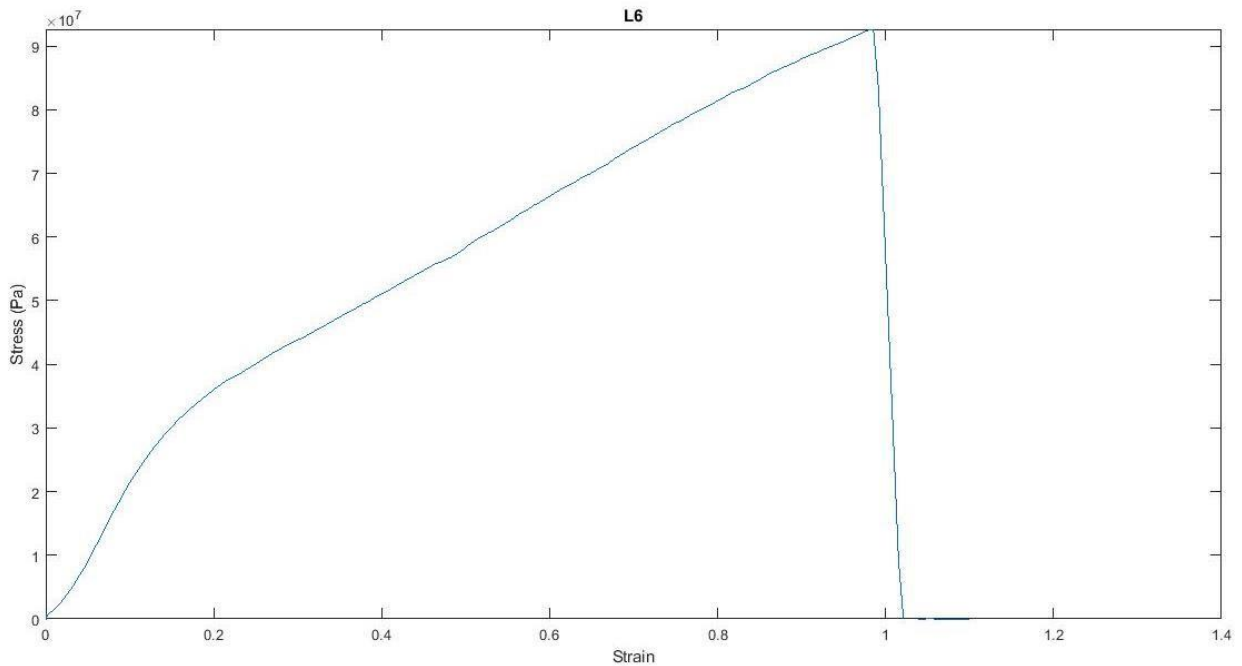


Figure 20 - Stress-strain graph of sample L6

There were also clamped method cases which did not break, this was a common occurrence for the ligament samples made with concentrations of 18 or 21% w/v. These samples also prove to have a very distinct elastic region and yielding point. An ultimate load cannot be determined since failure did not occur, as evident in sample L9 (Figure 22). For those ligaments that did not break, the real time data showed that at the constant strain the was held at the end of the test, the force experienced was slightly lowered overtime, also relates to the stress being reduced with time. This is an indication that the material exhibits stress relaxation when subject to a constant strain, proving its viscoelastic properties.

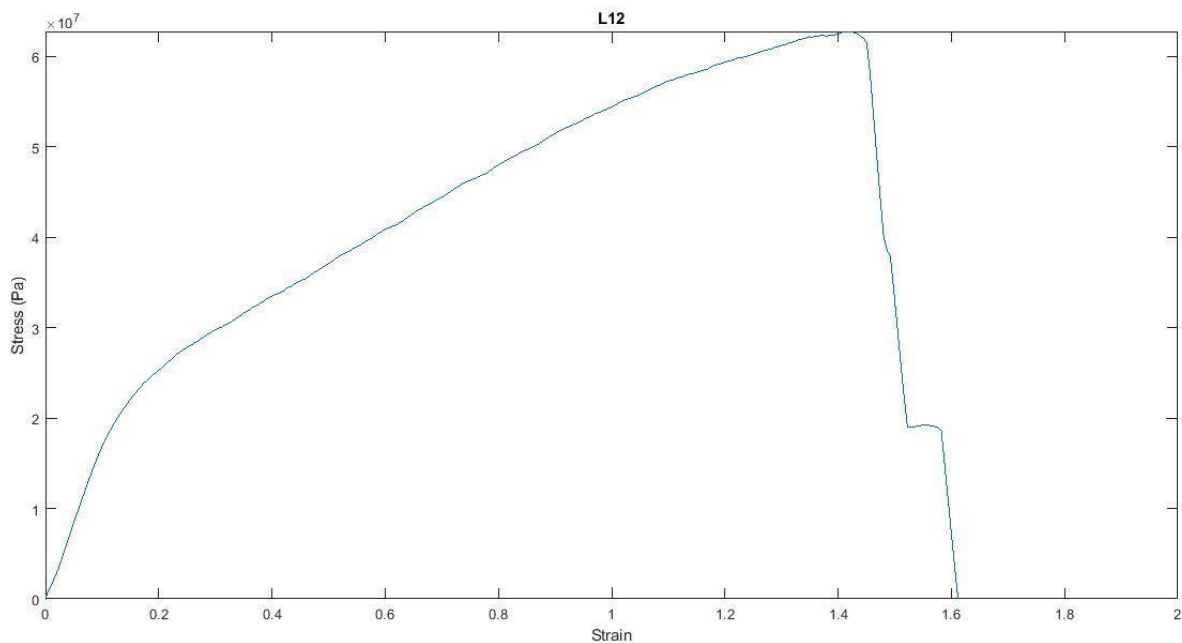


Figure 21 - Stress-strain curve for sample L12

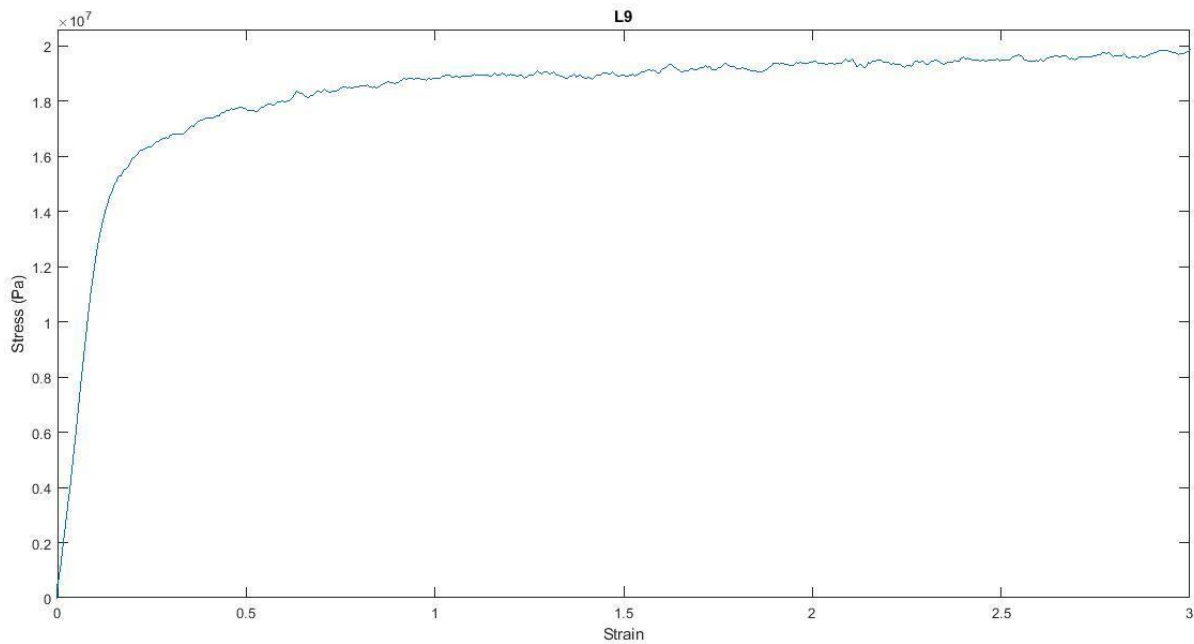
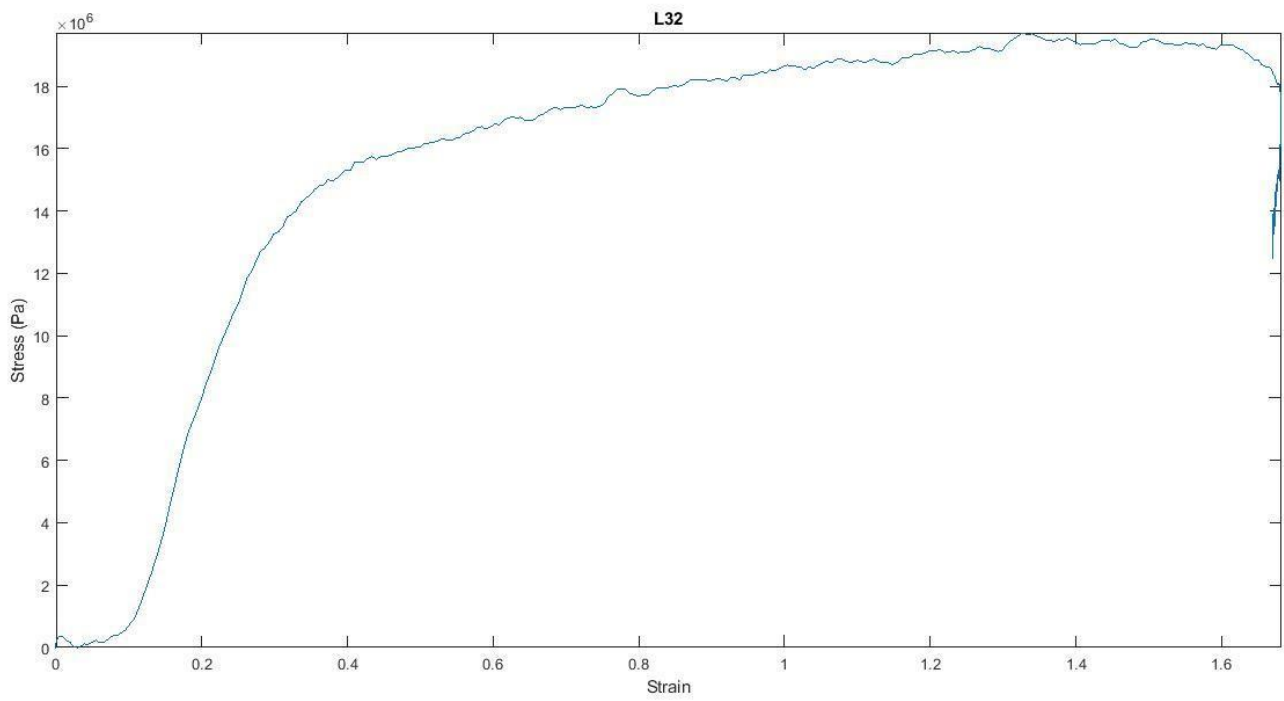


Figure 22 - Stress-strain curve for sample L9

An improvement was seen in the graphs when the looped end method was employed over the clamping test method. The fibres were less subject to early breakage at the clamps, which enabled a less interrupted linear region in most cases. While some ligament samples broke in the middle and not at the clamping site, others experienced abnormal breaks where the outer layer of fibres was pulled away from the middle layers. This is most likely due to too much tightening of the string at the sample's end, slicing through the outer layer of fibres. There was however, more opportunity for a toe region to be seen in this method. Despite not all tests being in tension prior to commencing, there is evidence of incremental fibre recruitment once forces are positive in the recorded data. This type of behaviour is shown in a cases such as L32 and L34, (Figure 23, Figure 24). It is difficult to declare whether this is due to some crimping experienced in the fibres or whether the multidirectional orientation and initial resistance to strain are causing the toe region reaction. There is some evidence in sample L34, that premature yielding is occurring, with uncertainty to if its dependent on the tightness of the string. However, the overall result of the graphs in the thirdround testing had a smaller occurrence of premature yielding.

Figure 23 - Stress-strain curve of sample L32



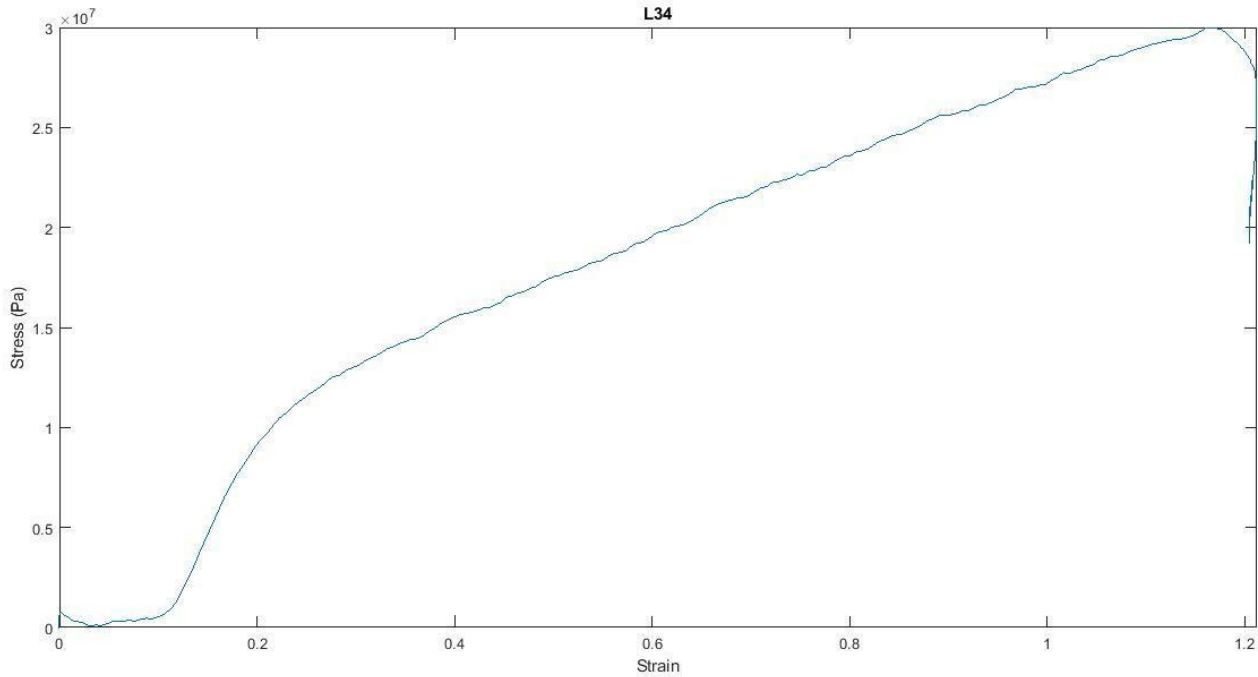


Figure 24 - Stress-strain curve of sample L34

The first round of electrospinning was done to compare the concentration of the PCL in the solution to Young's modulus. The most closely matched outcome to the native ligament elastic modulus range would later be reproduced in order to determine the repeatability of the sample development and testing. The measurements, volume fraction and elastic modulus is for each sample in the first round of testing is outline for comparison (Table 11).

It was expected that there would be a linear relationship between the polymer concentration and the elastic modulus, where the modulus would increase with an increase of PCL in the solution. However, for these testing conditions it is seen that there is the greatest variation across the elastic moduli experienced for 15% w/v solutions (Figure 25). The large range seen for the 15% solutions suggests a potential source of error. For samples L5 and L6, test time was slightly below two hours due to solution limitations. The fibre sheets are likely thinner than in other tests, explaining the difficulty in rolling them smoothly. Difficulty in rolling may translate into inaccurate cross-sectional area measurements, which as a result impacts the stress calculations. Although a potential source of error, there is still an inconsistency in trends for higher concentrations. The lack of trend is indicative of other electrospinning parameters possibly interfering with fibre production and as a result, the samples material properties.

Although the 10% concentration samples were slightly below the native ligament range, their least drastic and fairly consistent modulus range made them attractive for secondary testing. Other concentrations proved to have moduli within the range of native ligaments, but were too inconsistent to determine which would be best for secondary testing.

Table 11 - Round One Ligament Sample Measurements and Properties

Ligament Sample No.	Conc. of PCL (%)	Weight (mg)	Length (mm)	Diameter (mm)	Crosssectional Area (mm ²)	Material Volume Fraction	Elastic Modulus (MPa)
L1	10	141.2	105	2.64	5.47	0.215	45.35
L2	10	146.8	104	2.32	4.23	0.292	40.36
L3	10	144	97	2.71	5.77	0.225	31.72
L4	10	146.1	96	2.35	4.34	0.307	40.36
L5	15	166.5	107	3.41	9.13	0.149	207.27
L6	15	162.8	100	2.81	6.20	0.229	243.07
L8	15	217.3	105	3.25	8.29	0.218	115.18
L9	18	262.8	110	4.04	12.82	0.163	123.26
L10	18	234.6	115	3.73	10.93	0.179	129.77
L11	18	256.7	105	3.34	8.76	0.244	179.62
L12	18	241.8	104	3.63	10.35	0.196	179.59
L13	21	406.3	106	6.11	29.321	0.114	157.86
L14	21	320.9	107	4.75	17.7205	0.148	148.99
L16	21	210.9	101	3.29	8.5012	0.215	114.12

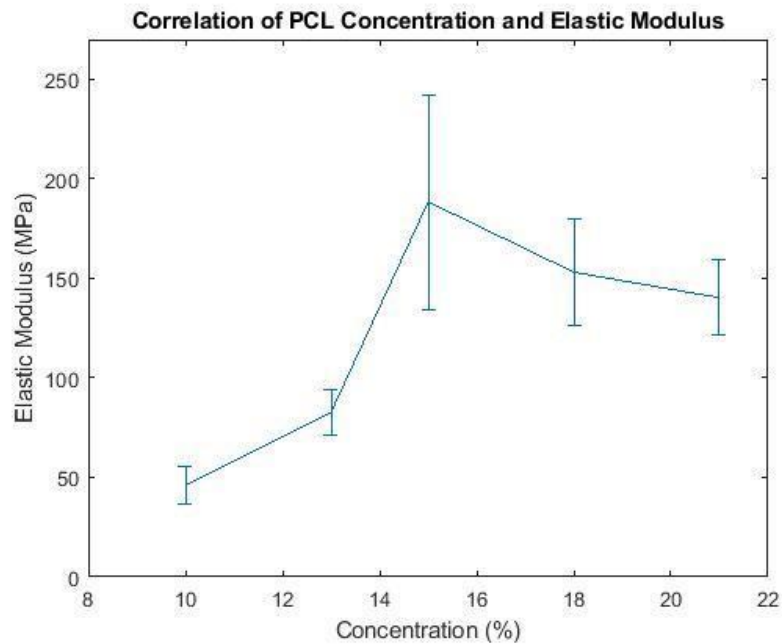


Figure 25 - Relationship between PCL concentration in solutions and elastic modulus

The formation of a second round of electrospinning tests was conducted to produce a larger sample size of the 10% polymer ligaments. The same Young's calculation method was employed as previously, using sample measurements, and volume fraction to determine the elastic modulus (Table 12). The initial clamping test method was kept consistent for all tensile tests, except sample L26. This sample was tested with the looped end method to inspect the differences in testing method. It experienced a break at the clinch knot, however the stress strain curve proved otherwise, with a longer linear region and a toe region (Figure 26).

The elastic modulus range was kept fairly consistent, with some values exceeding the previously found range (31 – 45 MPa). Even with increase in the modulus in some samples, the overall material property of the 10% solutions was not meeting that of a real ACL. Since only the lower range of the native ACL was being met in these samples, and the 15% solutions exceeded the desirable elastic modulus, it was decided third round testing would take place on 13% w/v PCL solutions.

Table 12 - Round Two Ligament Sample Measurements and Properties

Ligament Sample No. (10% PCL)	Weight (mg)	Length (mm)	Diameter (mm)	Cross-Sectional Area (mm ²)	Volume Fraction	Elastic Modulus (MPa)
L17	156.5	108	2.68	5.641	0.224	51.94
L18	156.4	104	2.43	4.6377	0.283	44.53
L19	161.1	104	2.51	4.9481	0.274	63.55
L20	155.5	100	2.44	4.6759	0.290	58.08
L21	151.8	105	2.37	4.4115	0.286	35.15
L22	146.6	100	2.23	3.9057	0.328	45.80
L23	155.9	105	2.41	4.5617	0.284	54.50
L24	162.7	104	2.54	5.0671	0.269	56.59
L25	140.8	104	2.3	4.1548	0.285	31.57
L26	134.9	96	2.1	3.4636	0.354	54.64
L27	144.3	102	2.32	4.2273	0.292	33.74
L28	141.9	99	2.41	4.5617	0.274	38.88
L29	139.6	101	2.4	4.5239	0.267	53.65
L30	141.4	96	2.28	4.0828	0.315	48.78

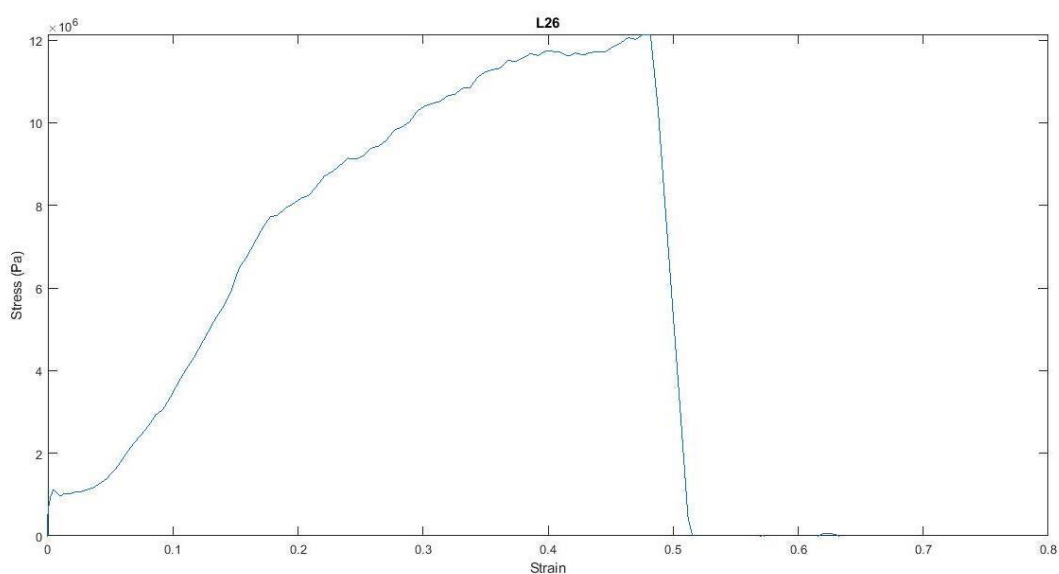


Figure 26 - Stress-strain curve for sample L26

The third round of electrospinning was conducted with all 13% PCL solutions in the same solvent ratios used for previous tests. Measurements of samples was consistent to previous methods, summarising the values Table 13). The mechanical testing method was changed from the clamping set up to the looped ligament end method for all round three samples. This method avoided premature breaks in most cases and allowed for the incremental recruitment of fibres, showing a toe region in 50% of the stress-strain graphs. The complete graph summary for round one, two and three of testing can be seen respectively in Appendix A, B and C.

Table 13 - Round Three Ligament Samples Measurements and Properties

Ligament Sample No. (13% PCL)	Weight (mg)	Length (mm)	Diameter (mm)	Cross-Sectional Area (mm ²)	Volume Fraction	Elastic Modulus (MPa)
L31	176.4	102	3.15	7.79	0.194	92.16
L32	180.9	106	2.98	6.97	0.214	72.49
L33	186.4	104	2.62	5.39	0.290	86.68
L34	199.8	108	2.86	6.42	0.252	106.26
L35	178.5	106	2.61	5.35	0.275	73.73
L36	174.0	106	2.51	4.95	0.289	78.99
L37	191.0	107	3.03	7.21	0.216	69.58
L38	178.9	104	2.80	6.16	0.244	81.86

Based on the summary tables for each electrospinning round, the elastic modulus results most consistent with native ACL is exhibited by the 13% PCL solutions (Table 13). Despite the variation across the samples, the values are all within the desired range (65 – 128 MPa) and prove to have a similar elasticity of real human knee ligaments.

As not all samples broke within the middle segment of the sample, and some samples did not break within the testing limits, the ultimate load was difficult to obtain. The ligament samples also have a significantly smaller cross-sectional area than native ligaments, so a direct comparison of ultimate load cannot be made. The cross-sectional area of the ligaments can be scaled against a native ligament measurement, determining the factor by which force would be increased. An average measurement of the ACL cross-sectional area (46.9 mm²) was used to scale against the sample cross-sectional area [42]. Sample L33 was selected due to the nature of its incremental break, where it experiences a peak load of 41.67 N (Figure 27).

The ACL cross-sectional area was found to be larger than sample L33 by a factor of 8.7. The Young's modulus calculation can be rearranged to find an approximation of the force L33 would experience if it had the cross-sectional area of a native ACL [43]. Due to the nature of the synthetic ligament, the volume fraction was also included in this calculation, where it is assumed the native ACL has a volume fraction of one.

$$\begin{aligned}
 & \frac{8.7AE\Delta l}{vl_0} \\
 \frac{F'}{F} &= \frac{vl_0}{\frac{AE\Delta l}{vl_0}} \quad (5) \\
 & \frac{8.7AE\Delta l}{0.29l_0} \\
 \frac{F'}{F} &= \frac{AE\Delta l}{vl_0} \\
 & \frac{F'}{F} = 30
 \end{aligned}$$

The ultimate load experienced by L33 would be increased by a factor of 30 in the case it was the size of a native ACL, which equates to an ultimate force of 1250 N. Despite not matching the failure load of a native ACL, which is approximately 2160 N [39], in the case it was developed in to a larger scale, the synthetic ligament would experience a much larger failure force than what is being experienced currently. This scaled value is an approximation for one of the samples which experienced an ideal break, suggesting other samples may have been able to withstand an even larger load. Exact conclusions cannot be made from this calculation; however, the approximate load value provides an outline of what would be expected of a synthetic sample had it been manufactured to the size of a real ACL.

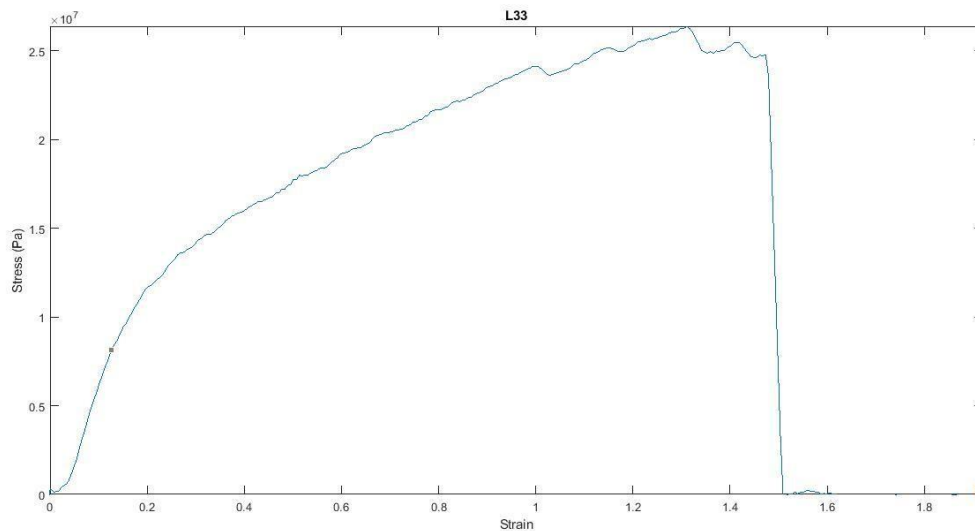


Figure 27 - Stress-strain curve for sample L33

4.3 Fibre Morphology

SEM imaging was taken with various magnifications, with adjustments made to produce the best possible focus in the image. Zoomed out images were taken to get an overall view of the fibre sheet (Figure 28). Small scale droplets were seen on all imaged samples. Although undesirable, the overall structure is fibre dependent so it is unlikely that the droplets can make a detrimental impact. A closer magnification image was taken of each sample in order to assess the fibres and make diameter

measurements free of droplets (Figure 29). Suitable images were used in the image processing program, Fiji, which used the microscope scale and program plugins to find fibre diameters and pore size.

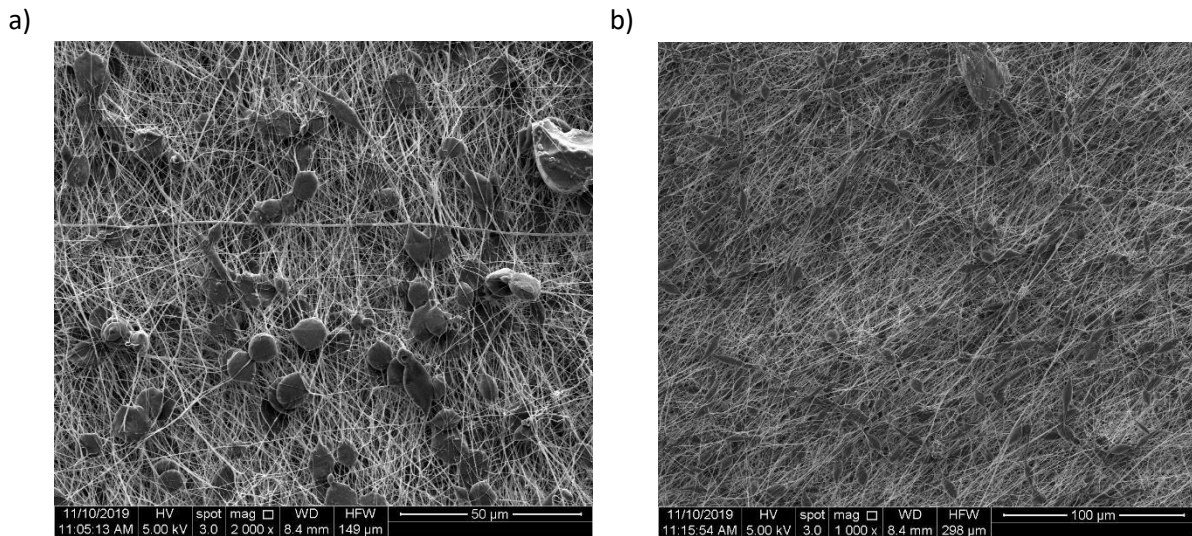


Figure 28 - **a)** Sample L19/L20 at 2000x magnification **b)** Sample L29/30 at 1000x magnification

The images are very small portions of the entire fibre sheet, but there appears to be some type of crosslinking and intertwining of fibres. It is difficult to determine whether this is due to high speed fibre whipping in the jet or if tis from the nature of PCL as a polymer. Despite the cause, it is preferred that there is small amounts of this occurring. In the case that there was a great deal of crosslinking, the overall structure of the fibres would become more rigid, potentially moving away from the elastic modulus value.

The greatest variability across the electrospinning parameters are seen in the voltage and the final rotational speed of the collector drum. Theoretically, the increase in both parameters results in smaller fibre diameters, however the inconsistency in both variables across the tests makes it difficult to establish a distinct relationship (Table 14).

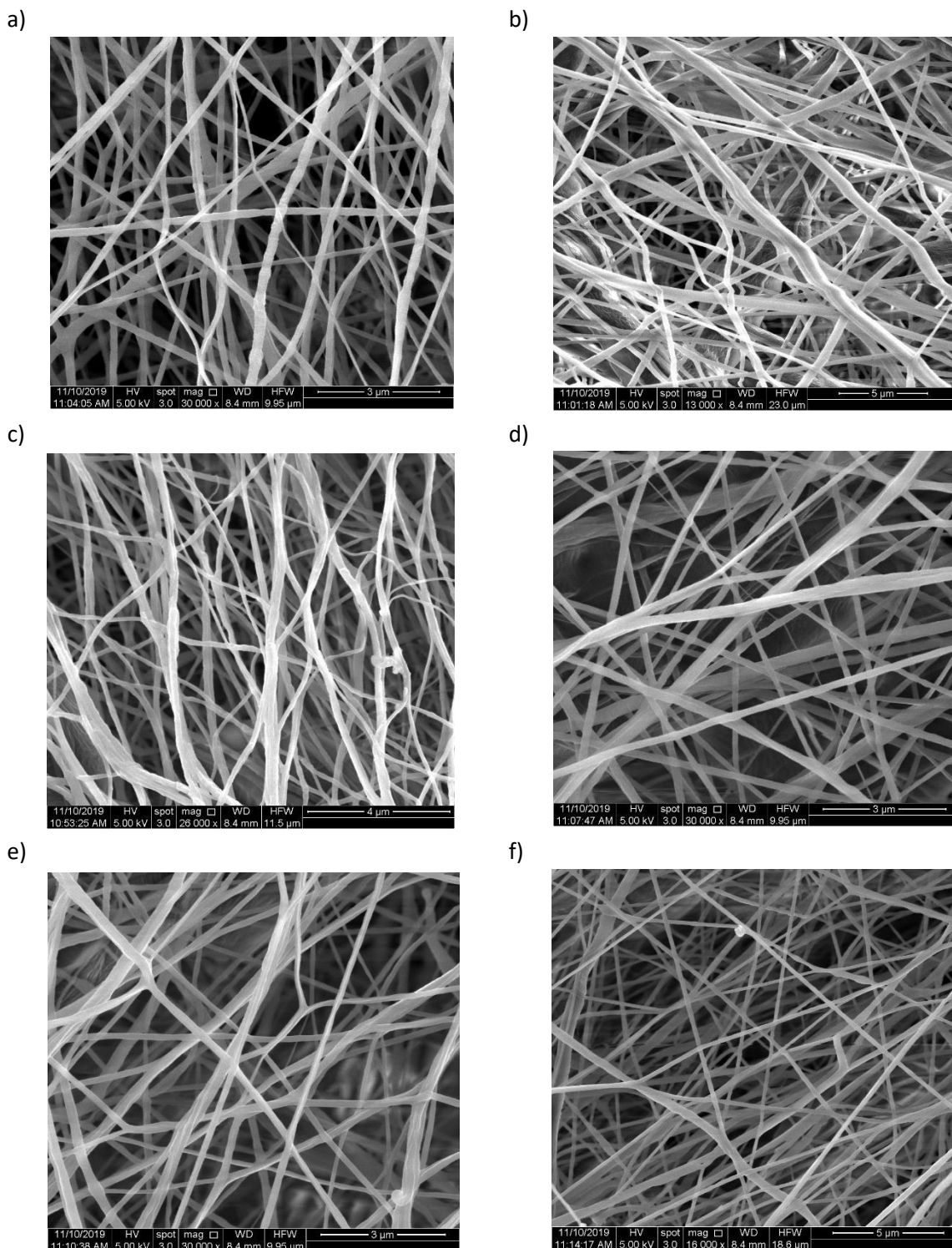


Figure 29 - a) Sample L19/20 b) Sample L21/22 c) Sample L23/24 d) Sample L25/26 e) Sample L27/28 f) Sample L29/30 Table 14 - Summary of Voltage and Collector RPM in comparison to Average Fibre Diameter and Pore Size for 10% solutions

Ligament Sample no.	Solvent Ratio (DMF:CHCl ₃)	Voltage (kV)	Final Rpm	Average Diameter (nm)	Average Pore Size (μm ²)
L19/20	25:75	20.02	1080	198 ± 47	9 ± 1.3
L21/22	50:50	20.03	1080	366 ± 131	19 ± 4.9
L23/24	25:75	20.08-23.03	1032	221 ± 63	9 ± 0.9
L25/26	50:50	30.12-25.11	1088	195 ± 28	4 ± 0.5

L27/28	50:50	25.49	1047	169 ± 19	7 ± 1.7
L29/30	50:50	20.02	1050	277 ± 81	21 ± 8.6

It is apparent that the fibre diameters cannot be concluded from the impact of either the voltage or final rpm, but rather need to be considered jointly. This is difficult to determine since it is not known to which extent each parameter affects the diameter. The solvent ratio may need to be considered as this impacts the overall conductivity of the solution, particularly as DMF has a significantly higher dipole moment which may impact the voltage required to elicit a successful fibre jet response. The ambient conditions may also contribute to this result, since humidity contributes to how the solvents evaporate during fibre production. In cases where evaporation is rapid, elongation of fibres prior to jet formation may also be altered, contributing to the fibre diameters. Elongation to fibre formation is difficult to view and quantify so there is much uncertainty in determining the extent of impact to the final results.

Correlation graphs between the fibre diameter and the voltage and rpm were constructed to visualise the relationship between the parameters and the diameter results (Figure 30). From the correlation graphs it can be seen that there is not a direct relationship since both parameters are impacting the fibre diameters. There is some evidence that the smallest fibres come from the largest voltages tested, while rpm alone is difficult to account for. There are also limitations in constructing a relationship to the parameters since such small sample sizes were used. The 10% solution with the 50:50 solvent ratio has four points, so multilinear regression was investigated using MATLAB. From this function it was found to have an R-squared value of 0.9 and a p-value of 0.05, proving there is significance to the two sets of results.

The pore size was also investigated for each of the samples. This can give an indication on how dense the fibre jet is during electrospinning. There is difficulty in measuring such values since the pores are based on the first layer of fibres rather than the fibres in the depths of the image. Fibres in the background are further and may not correspond to the image's scale. There are challenged to using only the first layer of fibres since there are limited complete pores on such a magnified image. Based on this limitation, the measurement sample sizes are approximately n=5 for each image.

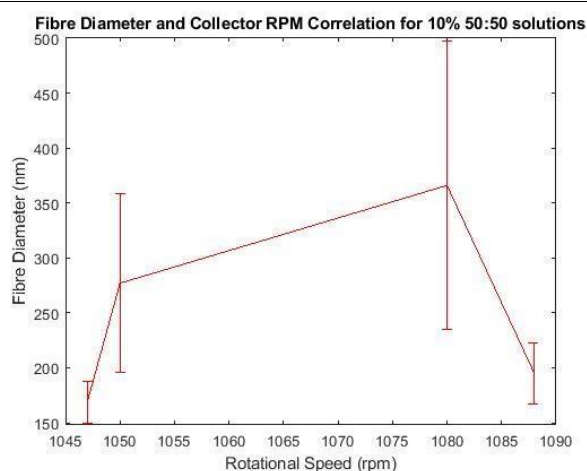
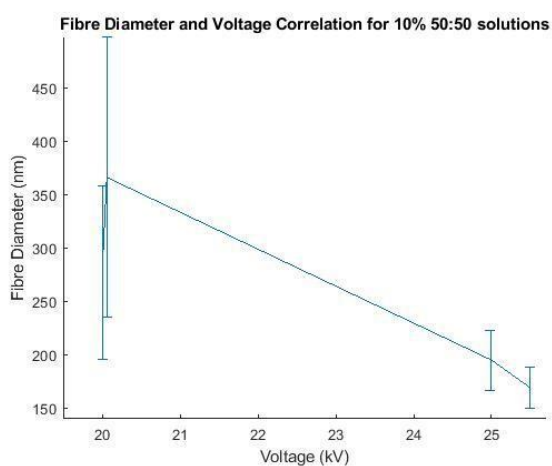
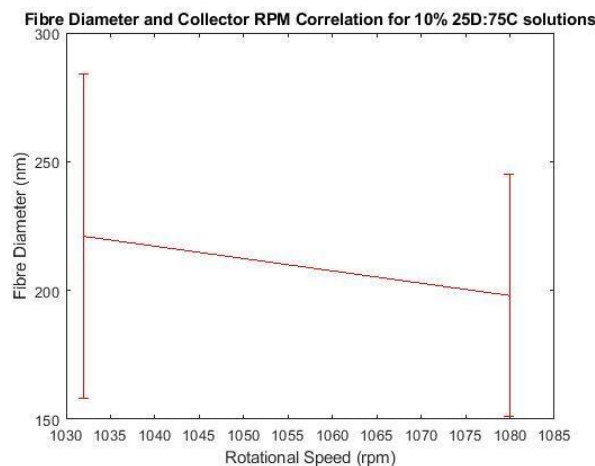
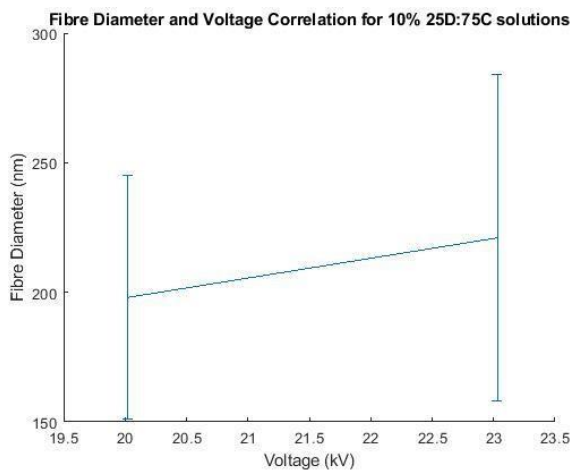


Figure 30 - Correlation graphs for 10% solution fibre diameters against voltage and final rpm

The round three 13% solutions were also imaged to determine the nature of the fibres. There was less evidence of droplets seen on the fibre sheets, with both instances of the 27D:75C solvent solutions being completely free of droplets (Figure 31, Figure 32, Figure 33, Figure 34). The 50:50 solvent solutions however, proved to have many more droplets than anticipated, showing many large formations riddled between the fibre layers. Some diameters appear very thick and directed out of a droplet. This suggests that there was not sufficient opportunity for fibres to form out of the solution. Jet formation during electrospinning is adjustable to an extent through voltage manipulation, however it is impossible to see if nanoscale droplets are impeding the stream. It is difficult to have certainty to whether this issue could have been avoided during testing or if it is a consequence of this particular solution combination.

The closest possible focus images were taken in order to get assess fibre diameters and pore sizes (Figure 35). The fibre diameters were compared to the voltage and rpm during experiments (Table 15). Sample L37/38 was subject to some damage by the electron beam, hence the dark fibres in the images. The closest structures should reflect the beam to the greatest extent, appearing brighter on the images. In this case fibres are lacking reflective ability so some sample damage has occurred through imaging and not due to conditions during electrospinning.

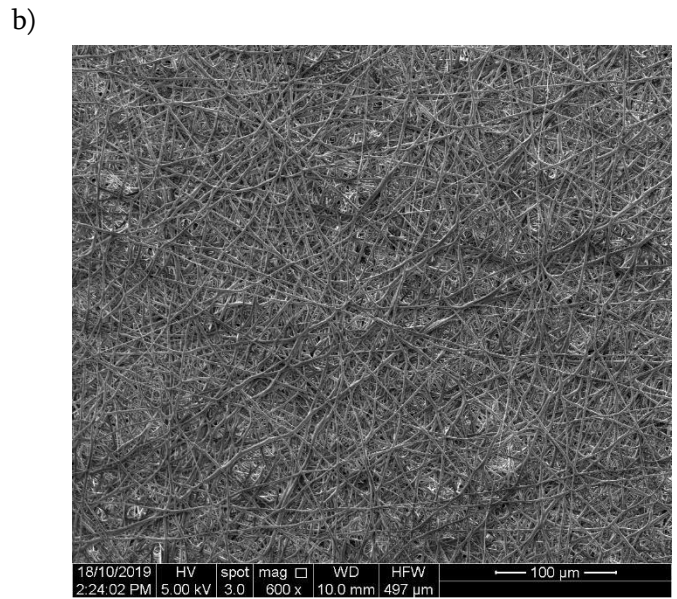
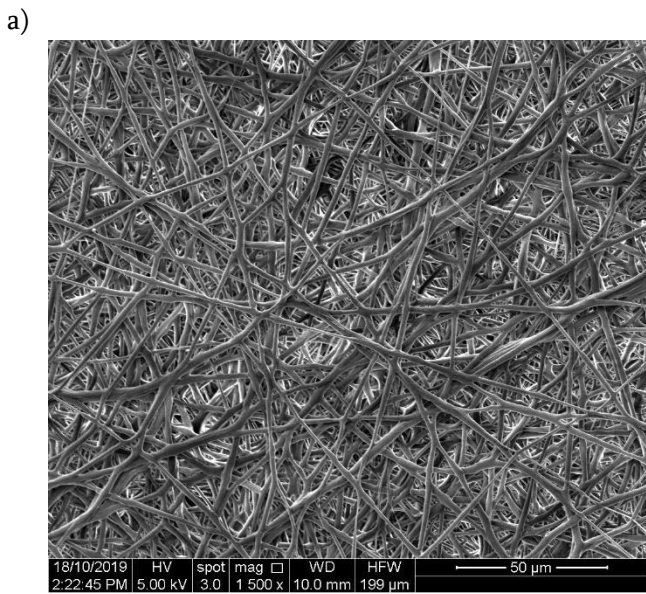


Figure 31 - Sample L31/32 at **a)** 1500 magnification and **b)** 600x magnification

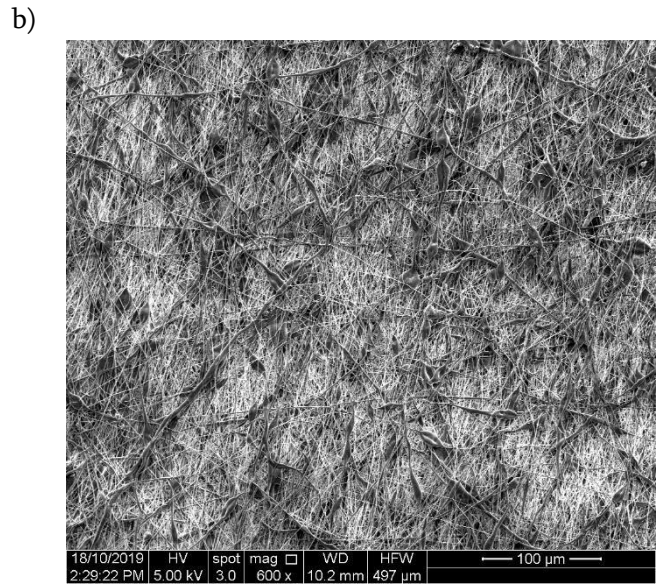
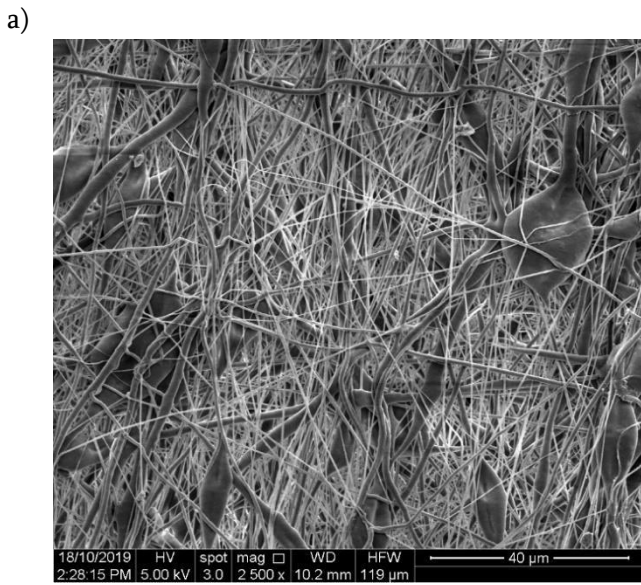


Figure 32 - Sample L33/34 at **a)** 2500x magnification and **b)** 600x magnification

a)

b)

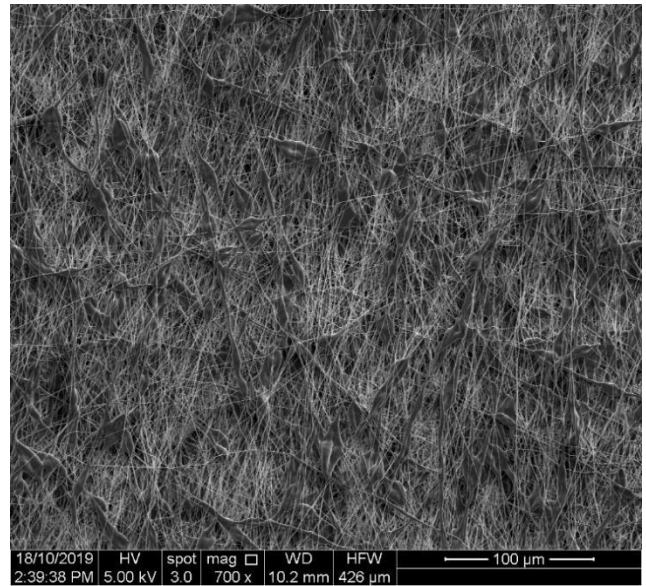
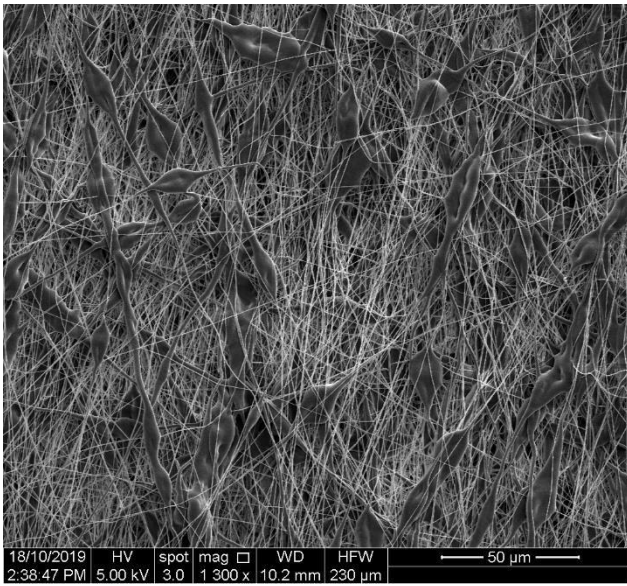


Figure 33 - Sample L35/36 at **a)** 1300x magnification and **b)** 700x magnification

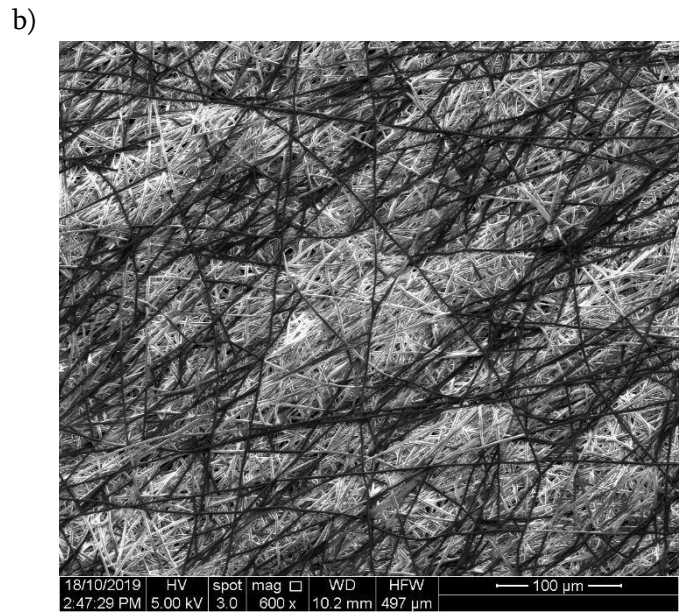
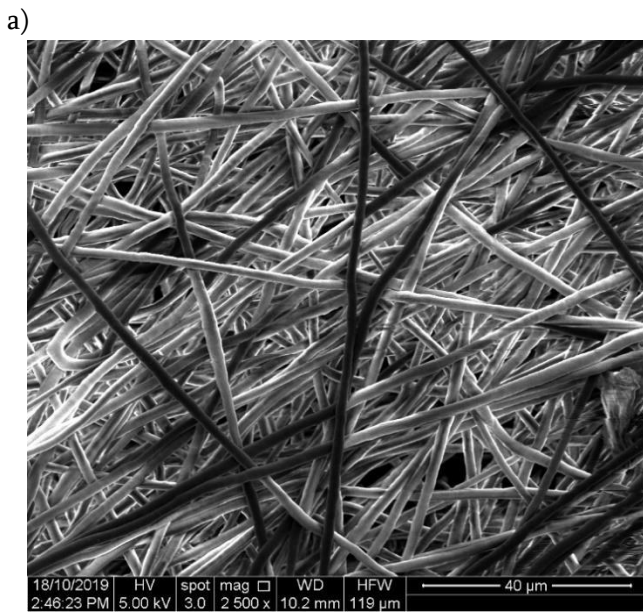


Figure 34 - Sample L37/38 at **a)** 2500x magnification and **b)** 600x magnification

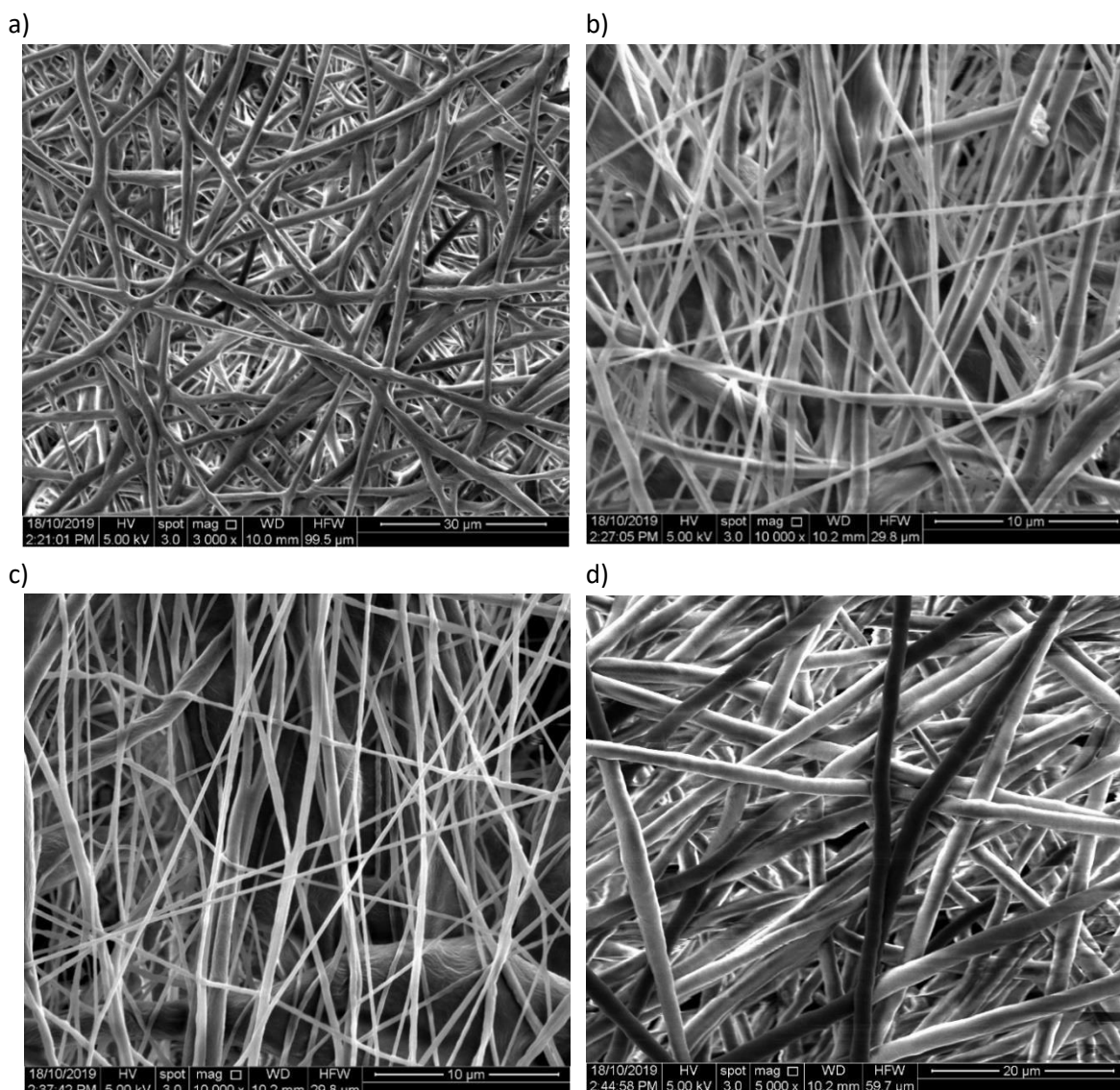


Figure 35 - a) L31/32 b) L33/34 c) L35/36 d) L37/38

Table 15 - Summary of Voltage and Collector RPM in comparison to Average Fibre Diameter and Pore Size for 13% solutions

Ligament Sample no.	Solvent Ratio (DMF:CHCl ₃)	Voltage (kV)	Final Rpm	Average Diameter (μm)	Average Pore Size (μm ²)
L31/L32	25:75	35.01-26.3	1102	1.9 ± 0.55	211 ± 74
L33/L34	50:50	25.05	1102	0.5 ± 0.23	61 ± 25
L35/L36	50:50	20.06	1105	0.39 ± 0.22	29 ± 8
L37/L38	25:75	20.02-23.03	1107	2.1 ± 0.13	366 ± 148

The fibres for the 13% solutions are much thicker than the 10% solution fibre diameters. It is expected the higher polymer solutions will produce fibres with larger diameters due to the

remainder of polymer once the solvents dissolve and dry in the process. The pore sized are also much larger than seen in the 10% solutions. There appears to be a great deal of variation within the samples also. The 50:50 solvent solutions prove to be much smaller than the 25:75 solvent solutions, yet the 25:75 solvent fibres are more homogenous in nature. With little variation between the voltage and rpm parameters, it is likely the solvent combinations had the greatest impact for this polymer concentration.

Correlation graphs were once again constructed to establish a relation for voltage and rpm against the fibre diameter (Figure 36). The parameters appear to work inversely between each other and amongst the different solvent solutions. The lack of distinct parameter relationship again indicates that other contributing factors, such as ambient conditions of testing contribute to the fibre diameter.

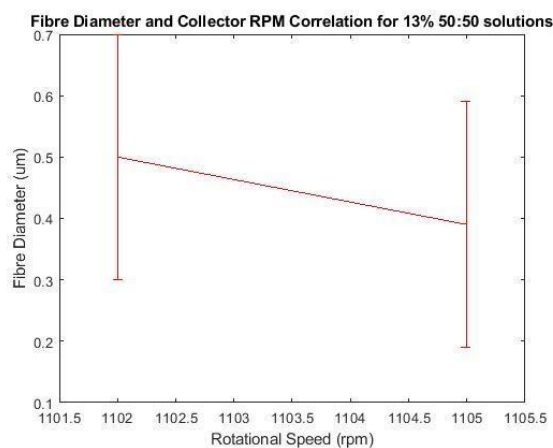
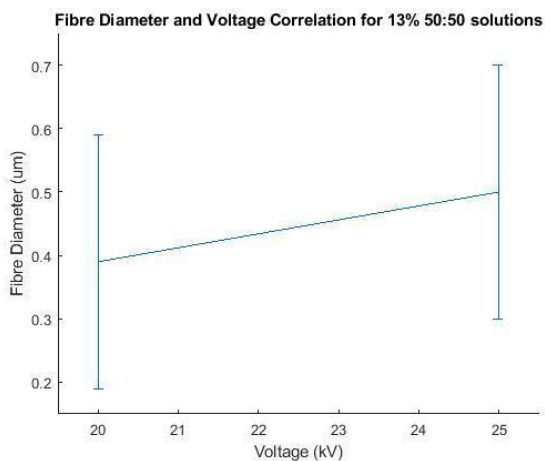
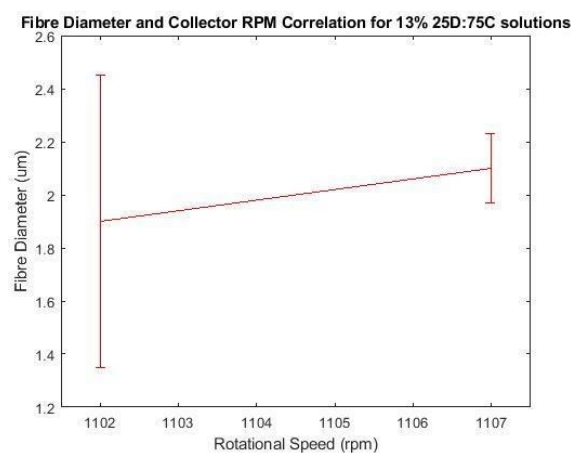
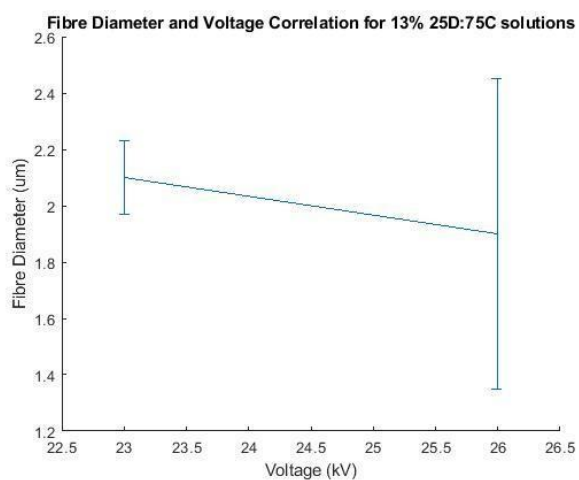


Figure 36 - Correlation graphs for 13% solution fibre diameters against voltage and final rpm

5. Discussion

5.1 Key Findings

The results support the value in developing synthetic knee ligaments through electrospinning methods to closely replicate the elastic modulus of the original ligament. The modulus values obtained in the 13% PCL solutions prove that this aspect of native ligaments can be replicated in synthetic samples. The calculations used to determine a scaled failure load provide insight to the expected forces experience had the sample been produced to a larger size. Although not ideal, the calculated force suggests that the overall mechanical properties are not far from native ligaments. The fibre diameters produced across all samples lie within the collagen fibril and fibre range, proving there is a less structured yet hierarchical nature to the synthetic samples. Even with lack of obvious crimping in the fibres, the synthetic ligaments experienced an eventual recruitment of fibres with increased tension, producing a toe region, much like what is experienced in native ligaments. Findings suggest that important aspects of real ligaments can be replicated in synthetic electrospun samples.

5.1 Polymer Concentrations and Solution Preparation

Initially, it was predicted that a higher concentration would provide better outcomes in terms of elastic modulus and hence why such a high focus was placed on the higher concentrations. The PCL used, although a high molecular weight in comparison to other polymers, it was expected that a high concentration would be needed to compensate for the polymer used. However, it was found that in the initial tests the 10% solution had the most consistent performance in terms of electrospinning testing and material properties of the ligament samples. The size of the fibre jet also appeared to be much larger in the 10% solutions when compared to the larger concentrations tested. The 10% solutions produced a short stream between the Taylor cone and the large fibre jet. The higher the concentration of the polymer, the longer the solution stream was, eventuating to a thinner and finer fibre jet. There are limitations with measuring this phenomenon, so this trend was discovered through observations during electrospinning tests. There is difficulty in determining whether this impacted the amount of fibres produced, or if higher concentrations produced thicker fibres and therefore less in the jets.

Despite large and visible fibre jet production, the 10% solutions did not however, meet requirements for the native ligament modulus ranges in both the first and second round of testing. Rather than retest with the established concentrations, it was decided to explore the nature of the 13% concentration solution. The inconsistency and potential error in the 15% solutions created uncertainty on whether there was enough reliability in testing method and results to conduct secondary tests. Even with some variation in the critical voltage for the 13% solutions, the samples did produce desirable mechanical responses, proving their worth for this application.

There would have been benefit had the initial concentrations outline been more consistent between the values. It was predicted that the higher concentrations would produce better results in terms of elasticity, however the smaller scale concentrations are better suited for knee ligament applications. It would have also been interesting to evaluate 1% w/v increments between the concentrations, covering a wider range of solutions. This method is unfortunately limited by the timeframe of the project.

5.2 Electrospinning Procedure and Outcome

The outcome of electrospinning is directly linked to the combination of parameters used in testing. The alteration of just one parameter has the ability to impact the way in which the fibres form or whether they are created at all. Even with the outlined range being followed for each parameter, the testing was occasionally subject to systematic or procedural error.

The collection drum and the distance between it and the needle electrode were kept constant for all tests. The other parameters however, could have been subject to slight variation which may as a result, impact the type of jet and fibres being produced. Even with efforts to maintain consistency between tests, small impacts the fibre development can result in larger impacts for the entire ligament sample. Prior to setting all parameters, the solution was purged through the tubing to ensure it had travelled consistently through the tube to the needle. As the flow rate was set, the voltage was increased to find the critical point at which a consistent jet was formed. The purging of the solution prior to voltage adjustment would occasionally mean there was an excessive build of solution at the tip of the needle. Occasionally this meant a higher voltage was required to form the fibres and prevent wet solution droplets on the collector. A few minutes was allocated to determine whether the applied voltage could consistently produce fibres overtime, or if it required reduction to match the demand of the flow rate. The flow rate also required some settling time since the needle was slightly tilted downwards, so solutions were subject to additional gravitational influence. While only slight influences of testing, these factors needed to be considered when establishing each electrospinning test.

5.3 Potential Sources of Error

The syringe containing the solution and the needle electrode were connected via plastic tubing. Due to equipment availability two different types of tubes were used throughout the testing. The initial tube used was connected to metal attachments on either end while the other had plastic connectors. While this seems minute, there is a likely hood that the metal connector attached to the needle was subject to the high voltages in the device, possibly contributing to fibre production.

Between the testing, the tubing was flushed with chloroform to eliminate contamination between the solutions tested. Following, an air-filled syringe was used to rapidly pump out the excess droplets. Occasionally, there would be droplets left in the tubing, in which case the new solution would be purged through until the tube was consistently full with the new solution only. Despite doing this, if the newly filled syringe has any air bubbles, there would cause interference in testing if they passed through the tube while in the device. This meant that when the air bubble reached the tip of the needle, the fibre jet would experience a bursting type effect before the solution would consistently continue to flow. When this situation occurred the fibre flow would be impeded but only momentarily, meaning its greatest impact on the fibre collection would be if the solution splattered on the collecting drum.

The needle was trimmed from its manufactured sharp tip to a flat tip. The end was manually filed and reopened to achieve an even, circular and flat tip. As there is some resistance in reshaping the metal needle, in the case that the trimming dented the end or the reopening was not made perfectly circular, fibre jet formation may be impacted. In high voltages, charges accumulate on sharp or non-uniform edges, which in turn would cause the fibre jet to be formed at this location rather than at the tip of the needle. Some tests did produce fibre jets that did not directly aim at the drum like intended, and possible non-uniformity in the needle may have been the cause of that. This however,

did not occur often and if it did, there fibres were still landing successfully on the collector. The trajectory of the jet may just have concentrated the fibre landing toward one side of the drum rather than across the entire length of the collector.

Two systematic errors which were caused by device limitation were the inconsistency in the collector rotational speed and the x axis needle speed. Both parameters proved to increase over time despite the initial set values. The two-hour test duration meant that, particularly the rotational speed was subject to significant increase. The issue linked to this was also that the device tachometer display was limited to 999 rpm. For values above 1000 rpm, the value could not be seen, inhibiting the real-time adjustment of high rotational speeds. In order to record the measurement of the final drum rpm, an external tachometer was used once the test has ceased. This was done as the reflective tape on the edge of the drum could not be seen through the window display of the electrospinning machine. Since the door of the electrospinning device could not be opened while the voltage was turned on, rpm measurements could not be taken during tests, hence the final value obtained with each run. This limitation impacted the initial experimental plan to vary the rpm of the drum from high and significantly higher speeds. At higher rotational speeds it is expected the fibres land with some stretch, elongating and thinning their diameters. The increased a decrease would theoretically create variation in the fibres collected, meaning they would be recruited differently in tensile testing. This variation in recruitment would ideally create a toe region in the graphs, resembling native ligament behaviour. Unfortunately, limitations in the device meant that there would be difficulty in creating intentional fibre crimping, hence why this aspect of testing was annulled.

The x axis needle speed was not as drastic in increase, where the initial 2mm/s speed would increase to nothing greater than 2.4mm/s. Although the slight increase did occur, it is unlikely that the fibre landing was impacted a great deal, rather just an inconsistency across the testing.

It was intended that each electrospinning test was conducted with parameters from the previously outlined range. In practice however, there are additional factors which impact the way in which the fibres are produced and naturally the overall outcome. The flow rate was set for 1.5mL/h for each test and it was planned to remain constant throughout all the testing. The higher concentration solutions did prove to be more viscous than the smaller concentrations, which resulted in the solution drying at the tip of the needle, inhibiting fibre production. In these cases, flow rate was increased to 2mL/h to prevent any drying. Although the set parameter was exceeded, there was more value in producing successful fibres than maintaining an identical flow rate for each run. This alteration to testing was also an indication that there is more difficulty in producing a consistent fibre stream with high viscosity solutions under the set test parameters.

The applied voltage was also another parameter which exceeded the intended testing value. Initially it was aimed to have a potential difference of no greater than 20kV. However, there were some cases where the voltage needed to be increased in order to produce a consistent fibre stream and to keep the other parameters consistent. There were cases where the same type of solution, with consistency in other parameters, required variation in applied voltage to produce a successful fibre stream. This was seen in the 13% solution both with 50:50 solvent ratio, where the first trial produced a consistent jet at 25kV and the second at 20kV. It is likely that this variation is based on ambient conditions such as room temperature and humidity. The way in which the solution will react in a high electric field is highly dependent on the dielectric constant of the solutions used. The known dielectric constant at 20 °C for chloroform and DMF are 4.81 and 36.7 respectively [28]. This value is an indication of the solvent's polarity and electric potential energy, where the higher

the value, the higher the dipole moment of the solution. This interaction on a molecular level impacts the way in which the overall solution will act in high electric fields. In cases where temperature is greater than 20 °C, the intramolecular forces between the polymer and solvents are weakened, potentially altering the overall polarity of the solution. It is difficult to draw meaningful conclusions regarding temperature on the high voltage tests as it was not recorded for each trial.

In cases where the temperature may have been higher, the solution, even at 20kV, was dripping and not forming a fibre jet. In these instances, rather than altering other parameters to reduce this issue, such as flow rate, the voltage was increased until a consistent jet was formed.

The solvents also undergo rapid evaporation in the high electric field when fibre jet whipping is achieved and fibres are formed. As humidity was also not controlled, it is probable that the varying conditions during testing impacted on the overall results of the fibres.

5.4 Mechanical Testing

The conducting of the tensile tests to obtain Young's modulus was most valuable in understanding the material properties of the synthetic ligament samples. There were however, aspects which added complication to the testing process and the data analysis. The samples were positioned vertically with clamps that had a rough knurling grip. Although necessary to have the samples in place, the tight nature of the clamps caused a stress concentration at the clamped location. Occasionally, during tensile testing, the breaking point would occur somewhere in the middle of the ligament sample. In most cases however, if a break did occur, it would happen exactly at the clamp. This is indicative that the sample was not at its limit but rather the stress concentration caused premature breaking. This was also evident in the stress-strain graphs as some linear regions were short and experiences some yielding before entering was appeared to be a secondary linear region. Ideally this type of behaviour should not be seen in data analysis, however this reflects the complications in testing rather than the material strength of the synthetic ligaments.

In attempt to remove this issue, rather than clamping, the test was set up by clamping metal loops in which the sample would be folded around. The folded over section was then secured with tape and string as a way to reduce the early breaking seen in the clamping method. This method was limited by the length of the sample since the testing area would be lost the more the ligament sample was folded. Initially, when this was first tested with one sample in the round two of testing, the break appeared to be the same, however, it was seen that a longer linear region was seen and a slight toe region. For this reason, all round three tensile tests were conducted with this method. The success rate was not 100%, yet an improvement was seen as clamp breaks were eliminated and an increase in toe region curves were seen. Had the benefits of this method been discovered earlier, it would have been worthwhile to test a wider range of samples with this method, rather than limiting most with a reduced linear region.

The mechanical tests could have also been conducted differently to assess the ligament samples in different biological conditions. The testing method was closely related to the strain rates experienced during walking. In the case of a greater sample size, there would be worth in testing a faster strain rate to replicate running and then, testing in the case of a rupture at 100% strain rate. Due to limitations in clamping it was also difficult to determine the ultimate strength of the samples. As many did not rupture, again in the case of a larger sample size of ligaments., there would be value in doing a load based tensile test, to determine values at which the ligaments rupture.

5.5 SEM Imaging

The SEM imaging proved to be extremely valuable in measuring fibre diameters and pore sizes. There would have been worth in taking several SEM images in different locations for each sample, so that a larger sample size for the each of the measurements could be taken. This would be particularly valuable for pore sizes since some first fibre layer pores are cut off within the image, excluding the opportunity for measurement. A similar limitation is seen in the fibre diameter measurements, where only the first layer of fibres can be considered. Fibres below the surface cannot be considered in measurements due to the unknown depth of the image.

5.6 Future Studies

There is much depth and room for further studies in the field of synthetic ligament development. Specifically, electrospinning has many routes which can be further explored in order to produce a better matched outcome to native ligaments.

5.6.1 Project Continuation

In order to achieve more control in the fibre outcomes, it would be worth managing ambient conditions to prevent any variations in results due to external factors. Applying a specific temperature may also contribute to the crimping of fibres. This would be highly regarded in an artificial ligament as it would more closely match the fibre structure seen in a native ligament.

Attempt in achieving thinner fibres to replicate the smaller sub-structures in native ligaments could be done through thinner needle testing. The production of thinner needles could compromise the mechanical properties established in successful tests, however multiple needle testing may be worthwhile. Using various needle sizes in one fibre sheet collection may also promote the desired fibre straightening in increased tension.

The material properties could be better understood and related to real ligament function if the tensile tests were conducted at the same angles experienced in the knee. This would be beneficial to determine the nature of the sample in different positions, much like what is experienced by the knee ligaments during movement. An angled testing method would also indicate the behaviour of the fibres and whether their elasticity and strength is seen in all directions. There would also be significance in testing the ligaments after soaking in a saline bath. They may behave differently when hydrated and close to in vivo conditions.

The mechanical testing could also take a further approach, where cyclic tensile testing could be conducted, producing load-elongation graphs. As a result, the test data would provide hysteresis curves which would give an indication of the energy losses in the samples. Tests could be repeated with increase in loads which would give an indication of the conditions which produce permanent deformation in the samples, when elongation does not return to the original point after unloading.

5.6.2 Further Research

Valuable future studies would also involve the assessment of the biocompatibility of the samples. Although PCL is a biocompatible polymer, acceptance of such a sample in the body is also dependent on whether or not it is a structure that supports cell in growth. A method which could be employed is cell seeding with focus on whether cells are capable of attachment. This is highly dependent on the pore size between the fibre layer which reflects if cells can interact and grow across the entire sample. Biocompatibility analysis could be also achieved with in vivo animal

testing to determine the nature of ligaments when implanted. Monitoring the models overtime would help determine the acceptance into the body and the type of rehabilitation time required.

In a study without budget limitations, there would be much value in testing a solution which contains collagen. Since it is found naturally in ligaments, it would be interesting to see how it contributes to the electrospinning process and the mechanical properties of the synthetic ligaments.

6. Conclusion

The high occurrence of knee ligament injuries in combination with a large number of unsatisfactory long-term results, indicates that an improvement in the replacement graft and its mechanical properties is necessary. The mechanical properties of the replacement play a vital role in whether or not original knee kinematics can be preserved after reconstructive surgery. For replacement grafts that lack the desired elastic modulus, the overall mechanics of the knee are compromised, highlighting the importance better suited ligament replication.

The use of electrospinning to achieve closely matched synthetic ligaments, proved to be successful with elastic modulus results within native ligament range. The properties and results of the ligament samples directly related to the combination of materials and electrospinning parameters. Familiarisation of the testing conditions progressed throughout the study duration, eventuating to the understanding of successful sample production. Despite not replicating aligned fibre orientation and crimping, the samples exhibited desirable responses under increased tensile load conditions. Investigating beneath the visible, the fibre diameters and make-up of the samples also prove that homogenous fibre production is achievable.

Overall, the results of the study prove to be worthwhile, with evidence of native ligament qualities replicated in the synthetic electrospun samples. The explorative nature of the study meant that avenues of testing could have been vast, yet the findings establish sound beginnings to the resolution of this problem and provides opportunity for further research.

7. References

- [1] Lee CH, Shin HJ, Cho IH, Kang YM, Kim IA, Park KD, Shin JW. Nanofiber alignment and direction of mechanical strain affect the ECM production of human ACL fibroblast. *Biomaterials*. 2005 Apr 1;26(11):1261-70.
- [2] Pauly HM, Kelly DJ, Popat KC, Trujillo NA, Dunne NJ, McCarthy HO, Donahue TL. Mechanical properties and cellular response of novel electrospun nanofibers for ligament tissue engineering: Effects of orientation and geometry. *Journal of the mechanical behavior of biomedical materials*. 2016 Aug 1;61:258-70.
- [3] Surrao DC, Hayami JW, Waldman SD, Amsden BG. Self-crimping, biodegradable, electrospun polymer microfibers. *Biomacromolecules*. 2010 Nov 3;11(12):3624-9.

- [4] Sensini A, Gualandi C, Focarete ML, Belcari J, Zucchelli A, Boyle L, Reilly GC, Kao AP, Tozzi G, Cristofolini L. Multiscale hierarchical bioresorbable scaffolds for the regeneration of tendons and ligaments. *Biofabrication*. 2019 Jun 12;11(3):035026.
- [5] Petrigliano FA, Arom GA, Nazemi AN, Yeraniosian MG, Wu BM, McAllister DR. In vivo evaluation of electrospun polycaprolactone graft for anterior cruciate ligament engineering. *Tissue Engineering Part A*. 2015 Jan 6;21(7-8):1228-36.
- [6] Shang S, Yang F, Cheng X, Walboomers XF, Jansen JA. The effect of electrospun fibre alignment on the behaviour of rat periodontal ligament cells.
- [7] Cardwell RD, Dahlgren LA, Goldstein AS. Electrospun fibre diameter, not alignment, affects mesenchymal stem cell differentiation into the tendon/ligament lineage. *Journal of tissue engineering and regenerative medicine*. 2014 Dec;8(12):937-45.
- [8] Vaquette C, Kahn C, Frochot C, Nouvel C, Six JL, De Isla N, Luo LH, Cooper-White J, Rahouadj R, Wang X. Aligned poly (l-lactic-co-ε-caprolactone) electrospun microfibers and knitted structure: A novel composite scaffold for ligament tissue engineering. *Journal of Biomedical Materials Research Part A*. 2010 Sep 15;94(4):1270-82.
- [9] Chen F, Hayami JW, Amsden BG. Electrospun poly (l-lactide-co-acryloyl carbonate) fiber scaffolds with a mechanically stable crimp structure for ligament tissue engineering. *Biomacromolecules*. 2014 Apr 11;15(5):1593-601.
- [10] Leong NL, Kabir N, Arshi A, Nazemi A, Jiang J, Wu BM, Petrigliano FA, McAllister DR. Use of ultra-high molecular weight polycaprolactone scaffolds for ACL reconstruction. *Journal of Orthopaedic Research*. 2016 May;34(5):828-35.
- [11] Leong NL, Kabir N, Arshi A, Nazemi A, Wu B, Petrigliano FA, McAllister DR. Evaluation of polycaprolactone scaffold with basic fibroblast growth factor and fibroblasts in an athymic rat model for anterior cruciate ligament reconstruction. *Tissue Engineering Part A*. 2015 Apr 7;21(11-12):1859-68.
- [12] Bashur CA, Dahlgren LA, Goldstein AS. Effect of fiber diameter and orientation on fibroblast morphology and proliferation on electrospun poly (D, L-lactic-co-glycolic acid) meshes. *Biomaterials*. 2006 Nov 1;27(33):5681-8.
- [13] Noyes FR, Grood ES. The strength of the anterior cruciate ligament in humans and Rhesus. *J Bone Joint Surg Am*. 1976;58:1074-82.
- [14] Chandrashekar N, Mansouri H, Slauterbeck J, Hashemi J. Sex-based differences in the tensile properties of the human anterior cruciate ligament. *Journal of biomechanics*. 2006 Jan 1;39(16):2943-50.
- [15] Sperling LE, Reis KP, Pozzobon LG, Girardi CS, Pranke P. Influence of random and oriented electrospun fibrous poly (lactic-co-glycolic acid) scaffolds on neural differentiation of mouse embryonic stem cells. *Journal of Biomedical Materials Research Part A*. 2017 May;105(5):1333-45.
- [16] Nau T, Teuschl A. Regeneration of the anterior cruciate ligament: current strategies in tissue engineering. *World journal of orthopedics*. 2015 Jan 18;6(1):127.
- [17] Machotka Z, Scarborough I, Duncan W, Kumar S, Perraton L. Anterior cruciate ligament repair with LARS (ligament advanced reinforcement system): a systematic review. *BMC Sports Science, Medicine and Rehabilitation*. 2010 Dec 1;2(1):29.
- [18] Corin, 2019. LARS ACL. ACL Augmentation and Reinforcement – Surgical Technique.[Internet] Accessed October 2019. Available from: <https://www.coringroup.com/assets/productresources/LARS/Resources-Product-Literature-LARS-ACL-Surgical-Technique.pdf>
- [19] Physiopedia, 2019. Anterior Cruciate Ligament (ACL) – Structure and Biomechanical Properties. [Internet] Accessed October 2019. Available from:

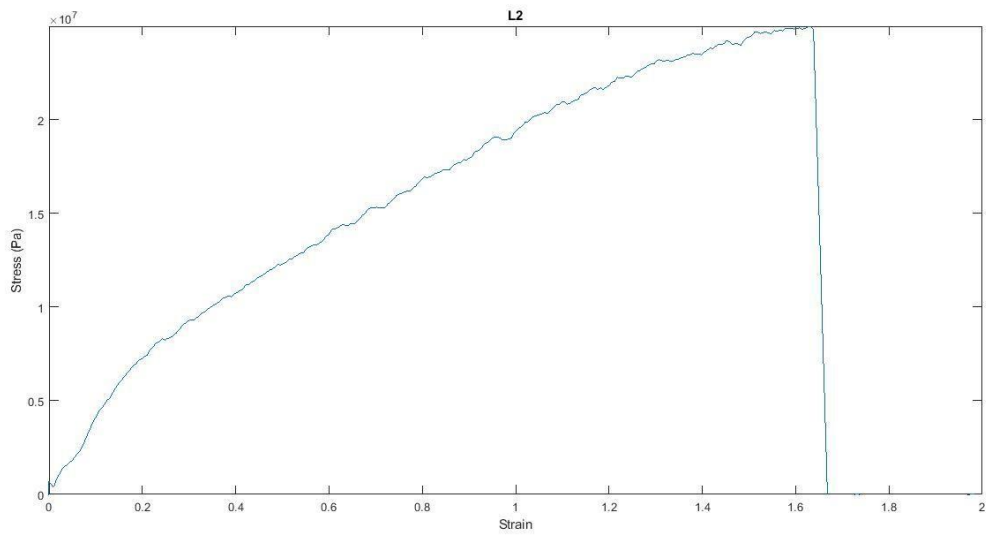
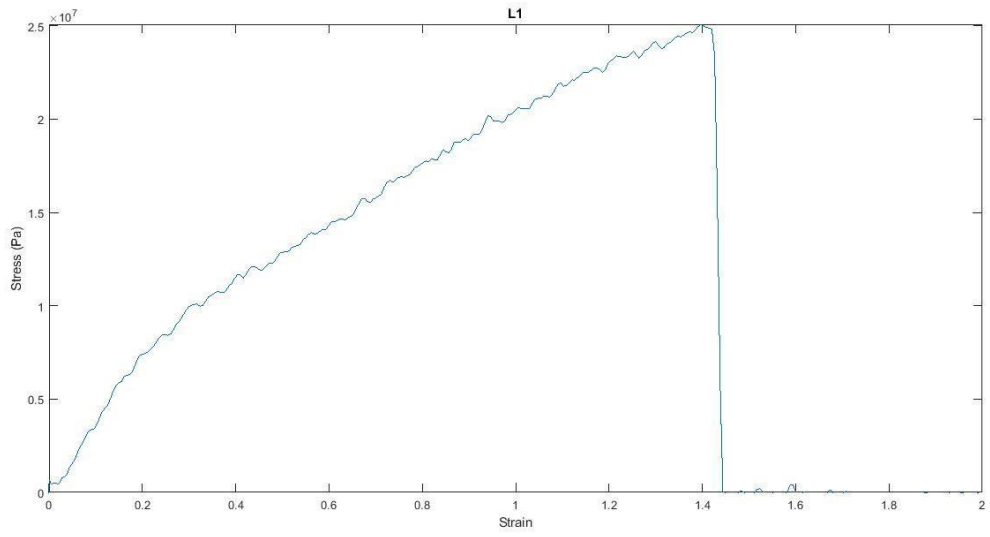
[https://www.physiopeedia.com/Anterior_Cruciate_Ligament_\(ACL\)_-Structure_and_Biomechanical_Properties](https://www.physiopeedia.com/Anterior_Cruciate_Ligament_(ACL)_-Structure_and_Biomechanical_Properties)

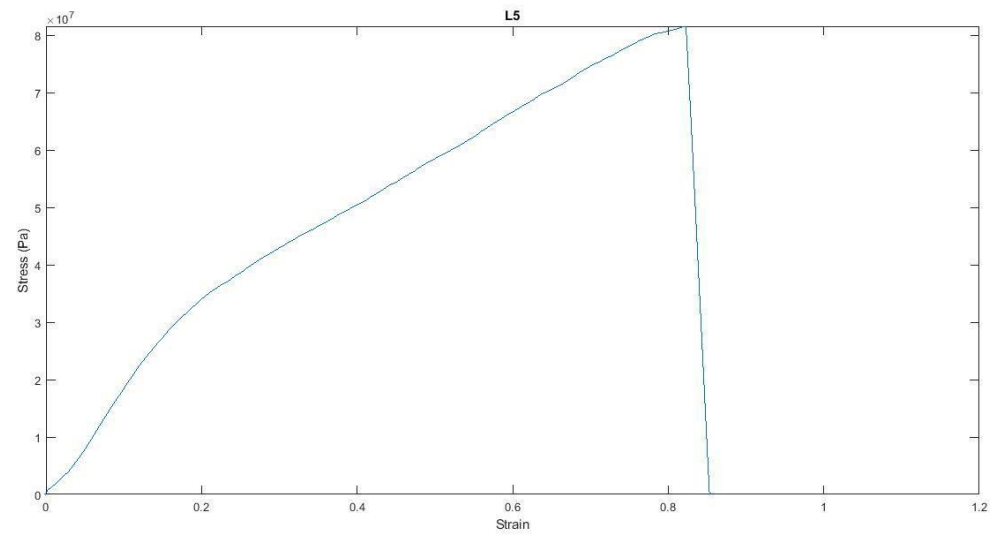
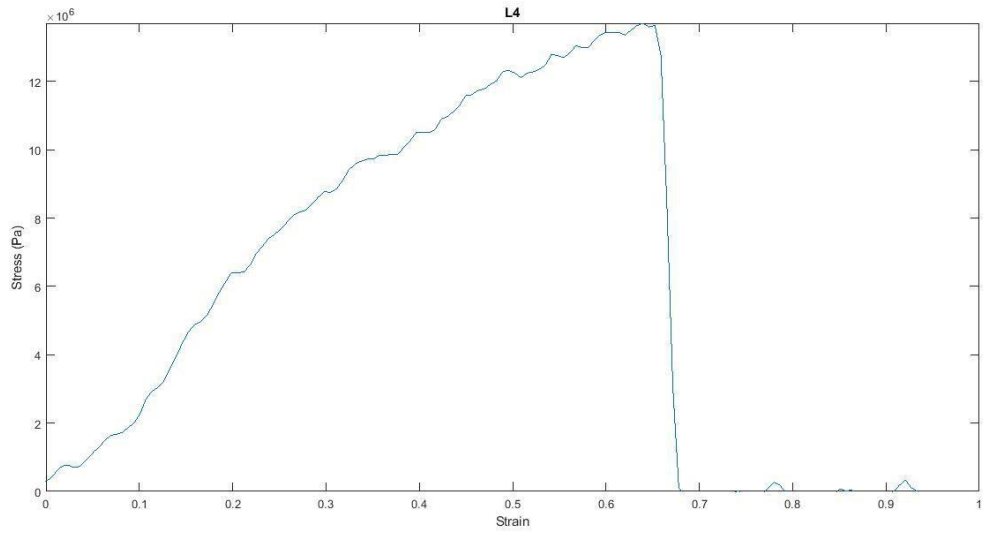
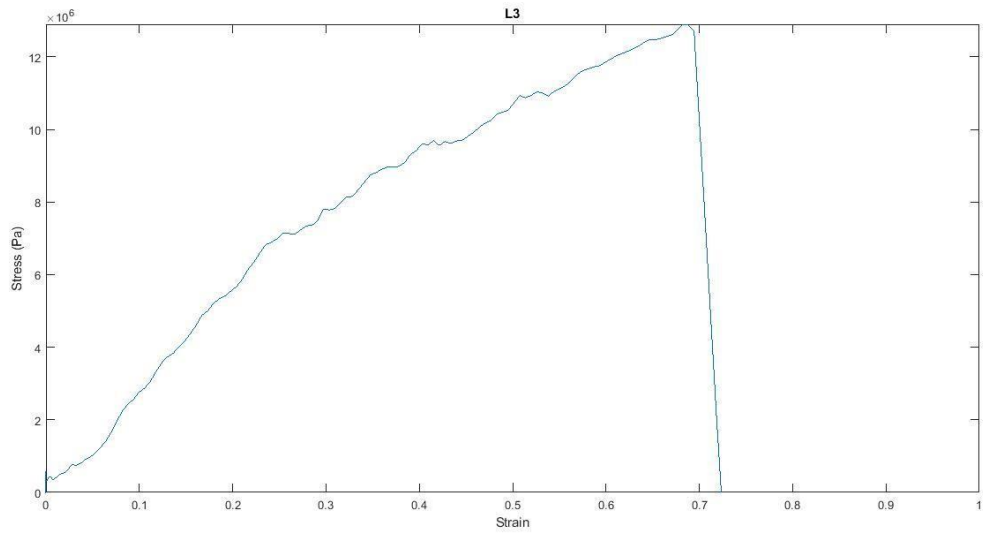
- [20] Sensini A, Cristofolini L. Biofabrication of electrospun scaffolds for the regeneration of tendons and ligaments. *Materials*. 2018 Oct;11(10):1963.
- [21] Wendorff JH, Agarwal S, Greiner A. *Electrospinning: materials, processing, and applications*. John Wiley & Sons; 2012 Feb 8.
- [22] Pinloche, JB., 2015. *Experimental Testing on Human Ligaments*. Flinders University
- [23] Black J, Hastings G, editors. *Handbook of biomaterial properties*. Springer Science & Business Media; 2013 Nov 27.
- [24] Elahi MF, Lu W, Guoping G, Khan F. Core-shell fibers for biomedical applications—A review. *J. Bioeng. Biomed. Sci.* 2013;3(1):1-4.
- [25] Shin SH, Purevdorj O, Castano O, Planell JA, Kim HW. A short review: recent advances in electrospinning for bone tissue regeneration. *Journal of tissue engineering*. 2012 Dec;3(1):2041731412443530.
- [26] Physiopedia, 2019. Knee. [Internet] Accessed August 2019. Available from: <https://www.physiopeedia.com/Knee>
- [27] Sensini A, Gualandi C, Zucchelli A, Boyle LA, Kao AP, Reilly GC, Tozzi G, Cristofolini L, Focarete ML. Tendon fascicle-inspired nanofibrous scaffold of polylactic acid/collagen with enhanced 3D-structure and biomechanical properties. *Scientific reports*. 2018 Nov 21;8(1):17167.
- [28] Moldoveanu SC, David V. *Essentials in modern HPLC separations*. Newnes; 2012 Nov 8.
- [29] Subbiah T, Bhat GS, Tock RW, Parameswaran S, Ramkumar SS. Electrospinning of nanofibers. *Journal of applied polymer science*. 2005 Apr 15;96(2):557-69.
- [30] Butler DL, Kay MD, Stouffer DC. Comparison of material properties in fascicle-bone units from human patellar tendon and knee ligaments. *Journal of biomechanics*. 1986 Jan 1;19(6):425-32.
- [31] US Food & Drug Administration, 2019. Environmental Assessment for Food Contact Notification No. 1761. [Internet]. Accessed October 2019. Available from: <https://search.usa.gov/search?query=polycaprolactone&affiliate=fda1>
- [32] Seon JK, Song EK, Park SJ. Osteoarthritis after anterior cruciate ligament reconstruction using a patellar tendon autograft. *International orthopaedics*. 2006 Apr 1;30(2):94.
- [33] Mow VC, Huiskes R, editors. *Basic orthopaedic biomechanics & mechano-biology*. Lippincott Williams & Wilkins; 2005. p. [184]
- [34] Dennis DA, Komistek RD, Mahfouz MR, Haas BD, Stiehl JB. Coventry Award Paper: Multicenter Determination of In Vivo Kinematics After Total Knee Arthroplasty. *Clinical Orthopaedics and Related Research (1976-2007)*. 2003 Nov 1;416:37-57.
- [35] Mow VC, Huiskes R, editors. *Basic orthopaedic biomechanics & mechano-biology*. Lippincott Williams & Wilkins; 2005. p. [302]
- [36] Tiefenboeck TM, Thurmaier E, Tiefenboeck MM, Ostermann RC, Joestl J, Winnisch M, Schurz M, Hajdu S, Hofbauer M. Clinical and functional outcome after anterior cruciate ligament reconstruction using the LARS™ system at a minimum follow-up of 10 years. *The Knee*. 2015 Dec 1;22(6):565-8.
- [37] Tzurbakis M, Diamantopoulos A, Xenakis T, Georgoulis A. Surgical treatment of multiple knee ligament injuries in 44 patients: 2–8 years follow-up results. *Knee Surgery, Sports Traumatology, Arthroscopy*. 2006 Aug 1;14(8):739-49.
- [38] Orthopedic Center of Illinois, 2019. Spotlight: ACL Reconstruction. [Internet]. Accessed October 2019. Available from: <https://orthocenterillinois.com>

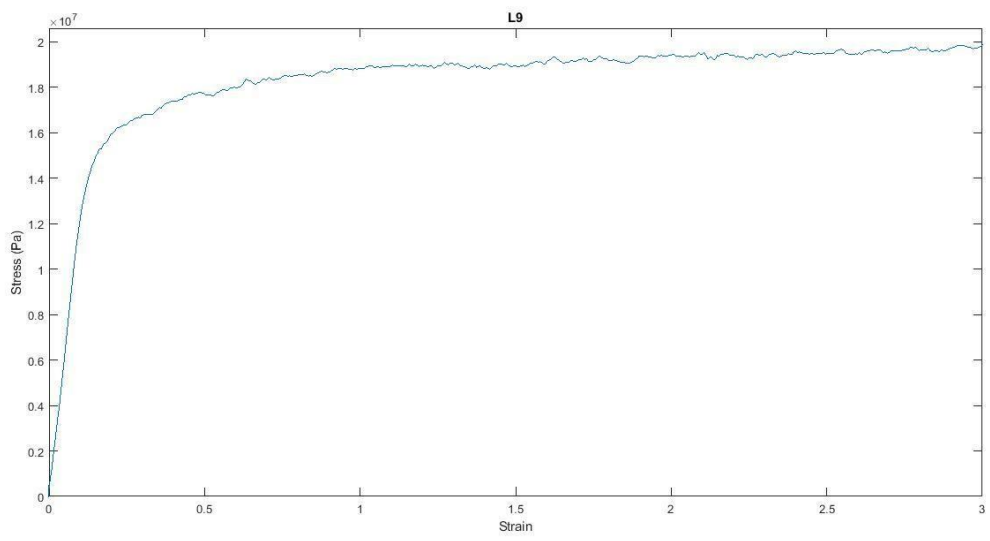
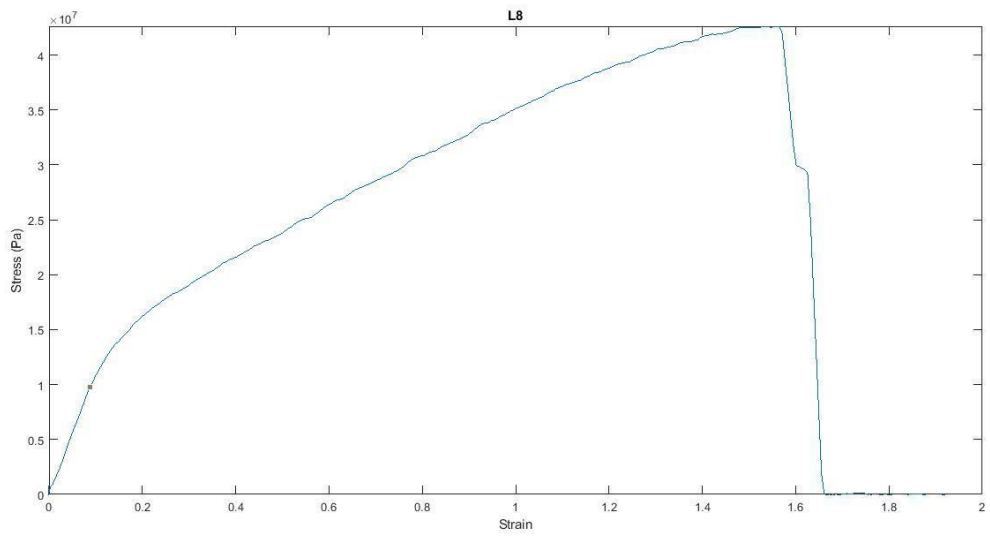
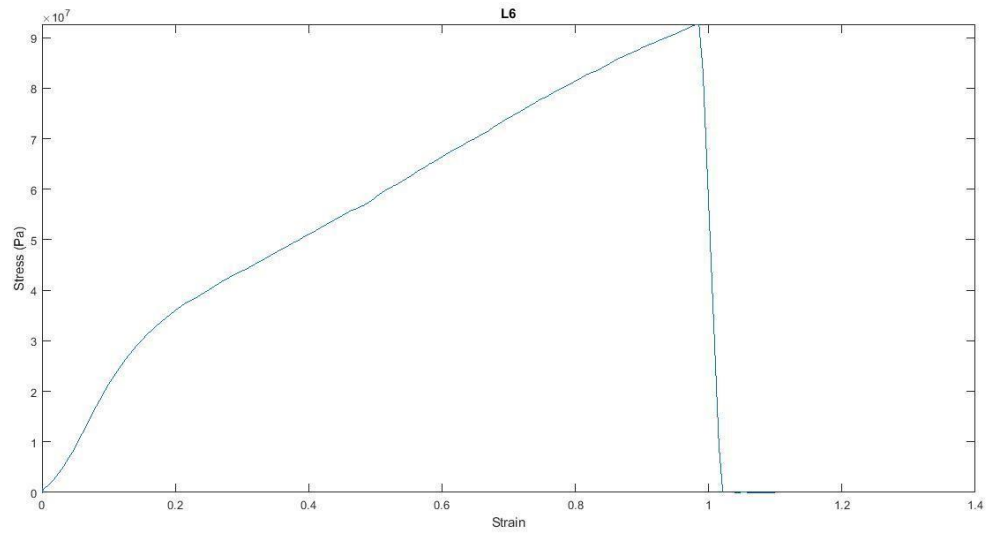
- [39] Dargel J, Gotter M, Mader K, Pennig D, Koebke J, Schmidt-Wiethoff R. Biomechanics of the anterior cruciate ligament and implications for surgical reconstruction. *Strategies in Trauma and Limb Reconstruction*. 2007 Apr 1;2(1):1-2.
- [40] Neoligaments, 2019. JewelACL. [Internet] Accessed October 2019. Available from: <https://www.neoligaments.com/product/jewel-acl/>
- [41] Rong GW, Wang YC. The role of cruciate ligaments in maintaining knee joint stability. *Clinical orthopaedics and related research*. 1987 Feb(215):65-71.
- [42] Iriuchishima T, Yorifuji H, Aizawa S, Tajika Y, Murakami T, Fu FH. Evaluation of ACL mid-substance cross-sectional area for reconstructed autograft selection. *Knee surgery, sports traumatology, arthroscopy*. 2014 Jan 1;22(1):207-13.
- [43] Mow VC, Huiskes R, editors. *Basic orthopaedic biomechanics & mechano-biology*. Lippincott Williams & Wilkins; 2005. p. [130]
- [44] Luo CJ, Stride E, Edirisinghe M. Mapping the influence of solubility and dielectric constant on electrospinning polycaprolactone solutions. *Macromolecules*. 2012 May 18;45(11):4669-80.
- [45] Kartus J, Movin T, Karlsson J. Donor-site morbidity and anterior knee problems after anterior cruciate ligament reconstruction using autografts. *Arthroscopy: The Journal of Arthroscopic & Related Surgery*. 2001 Nov 1;17(9):971-80.
- [46] Tiefenboeck, T.M., Thurmaier, E., Tiefenboeck, M.M., Ostermann, R.C., Joestl, J., Winnisch, M., Schurz, M., Hajdu, S. and Hofbauer, M., 2015. Clinical and functional outcome after anterior cruciate ligament reconstruction using the LARS™ system at a minimum follow-up of 10 years. *The Knee*, 22(6), pp.565-568.

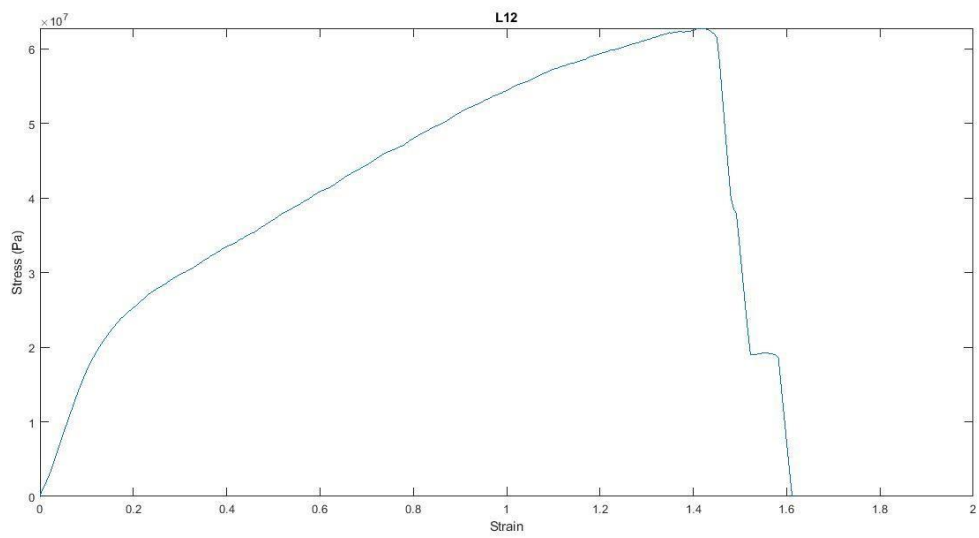
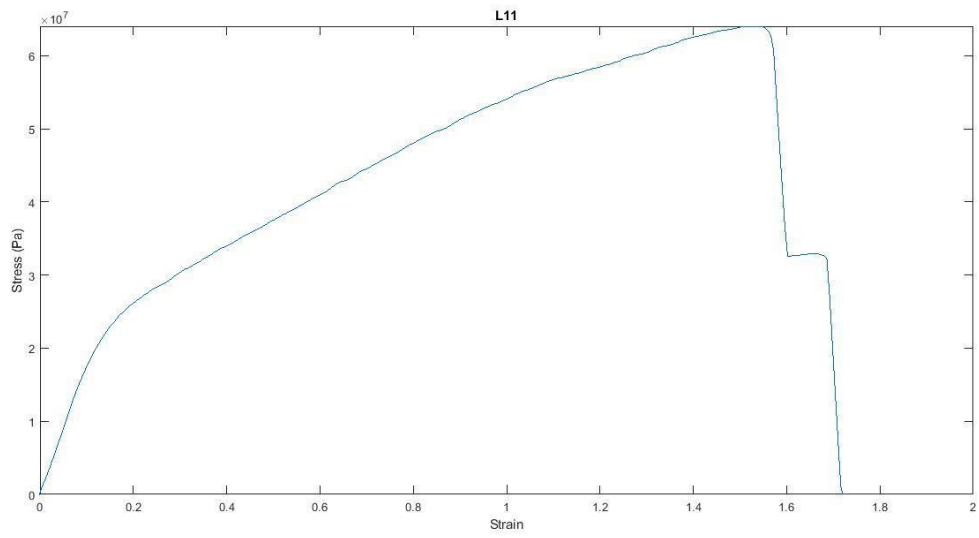
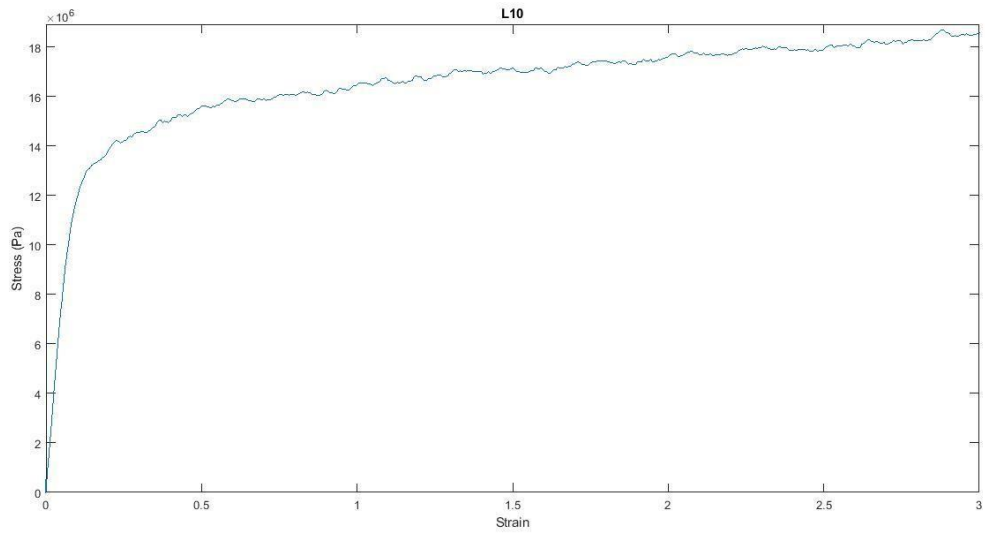
8. Appendices

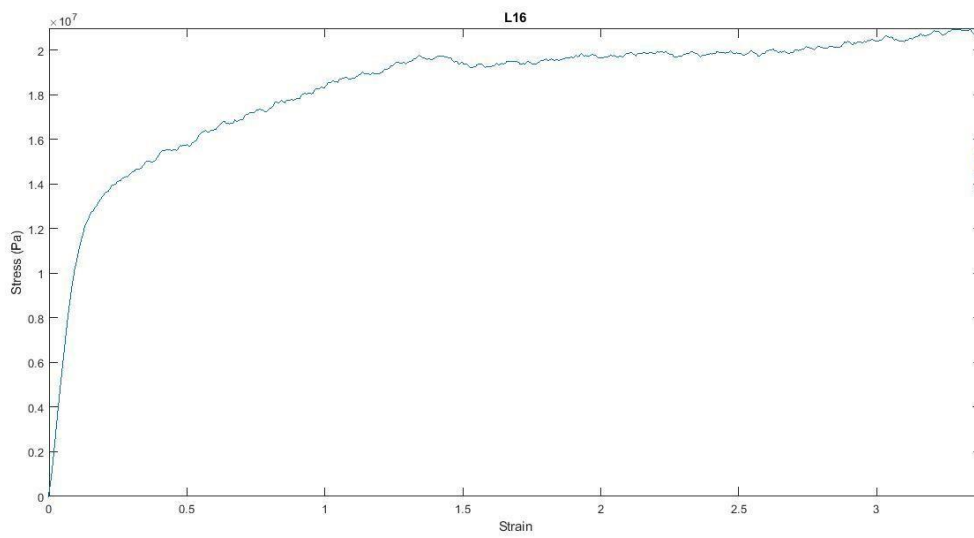
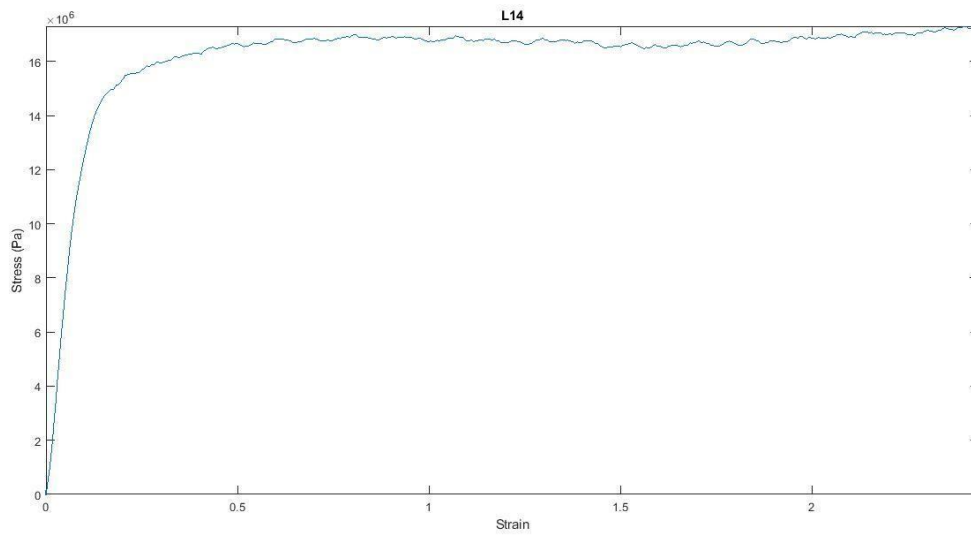
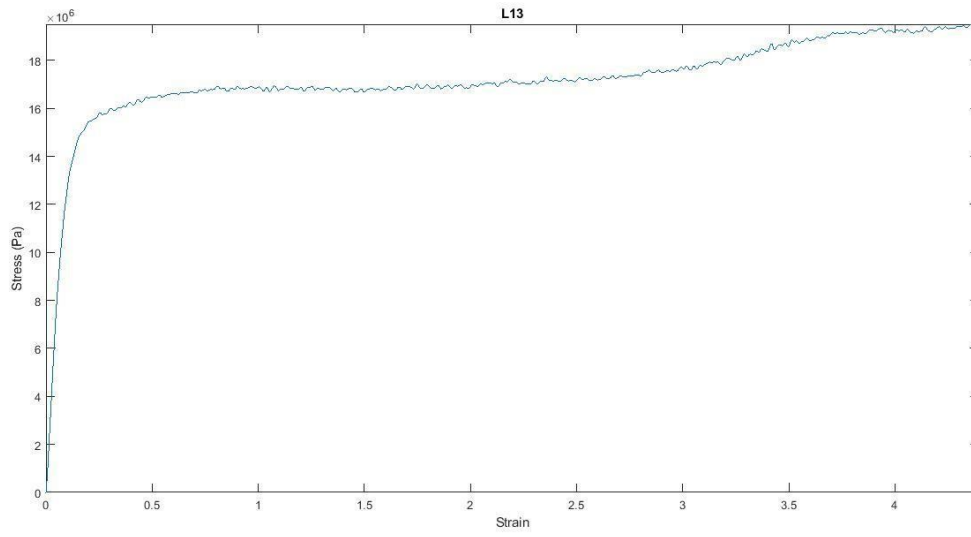
Appendix A – Round One Stress-Strain Graphs



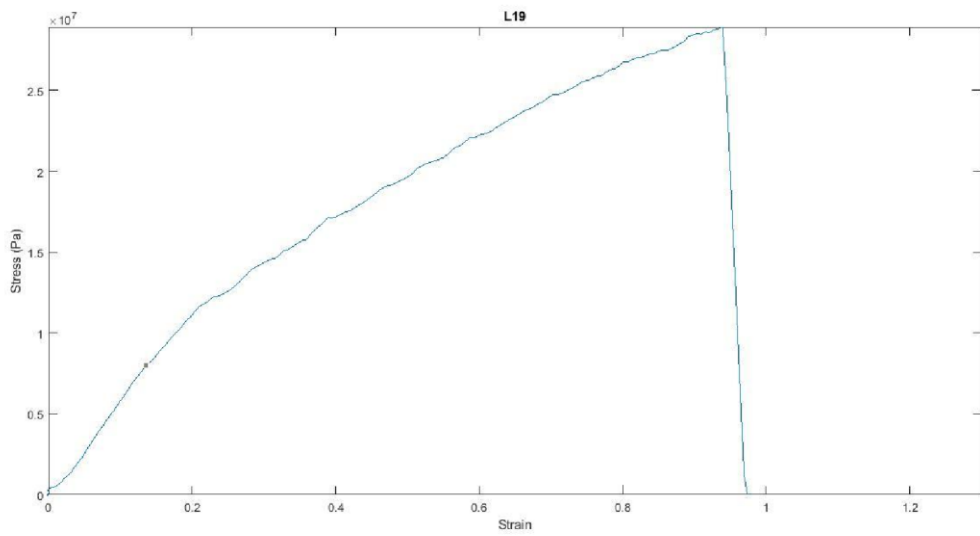
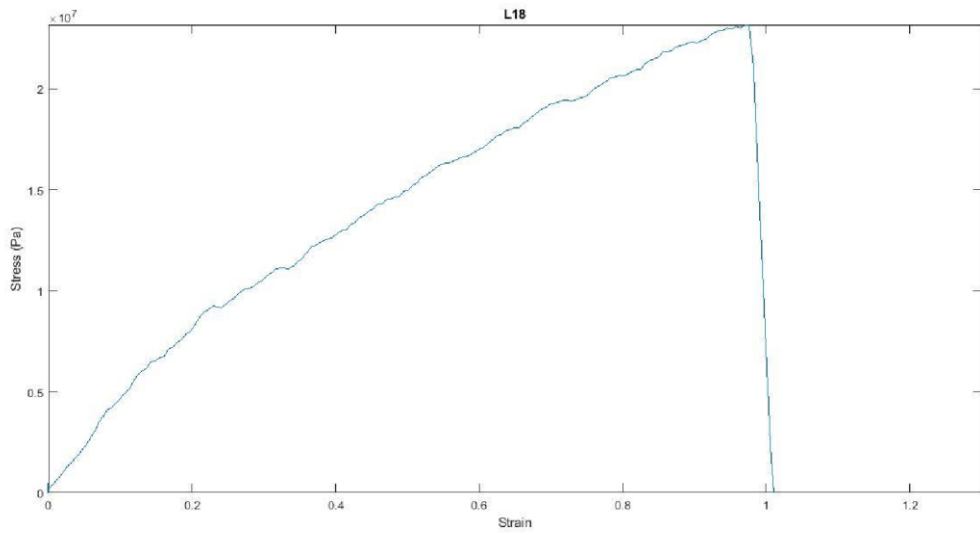
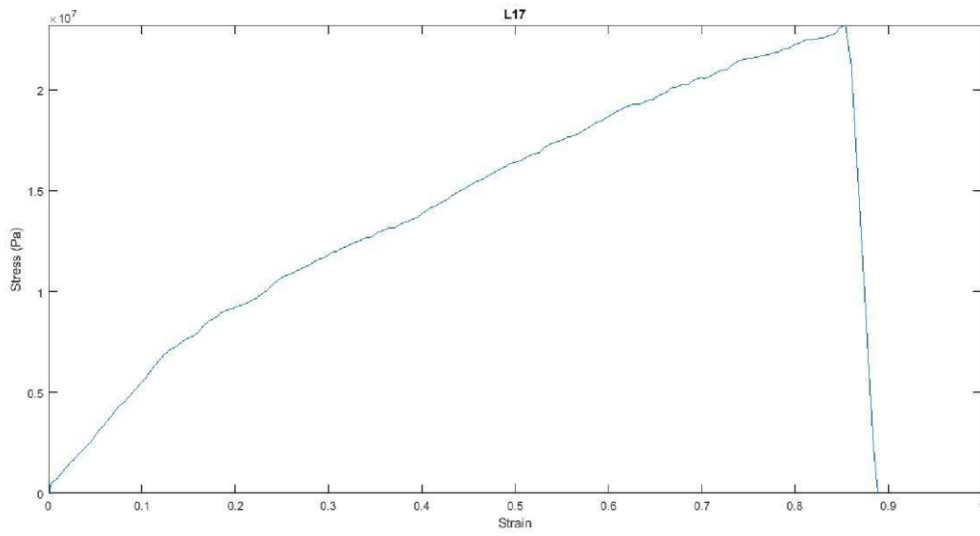


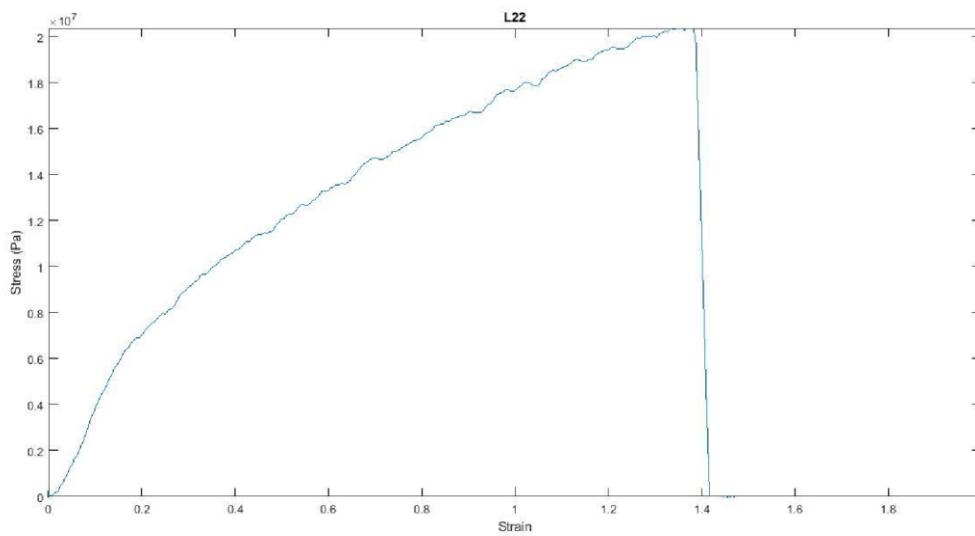
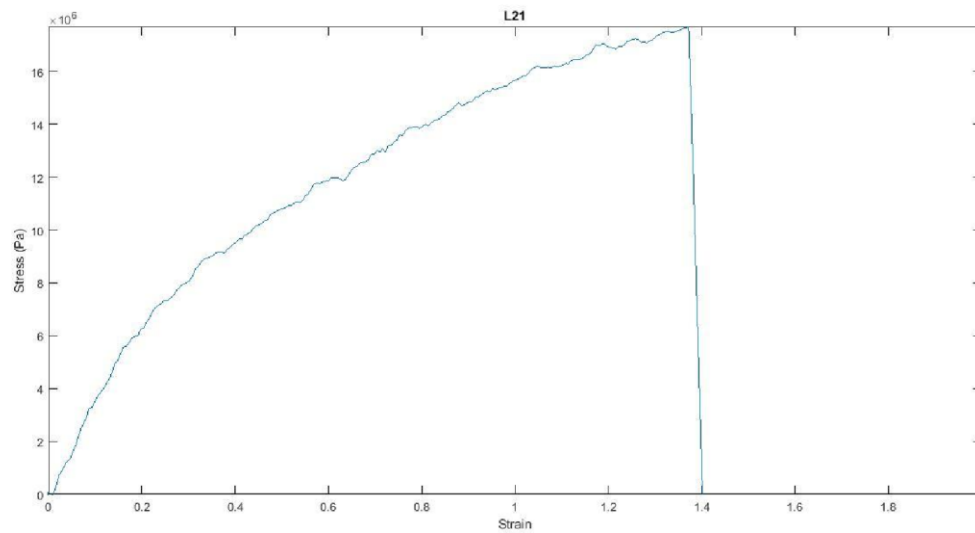
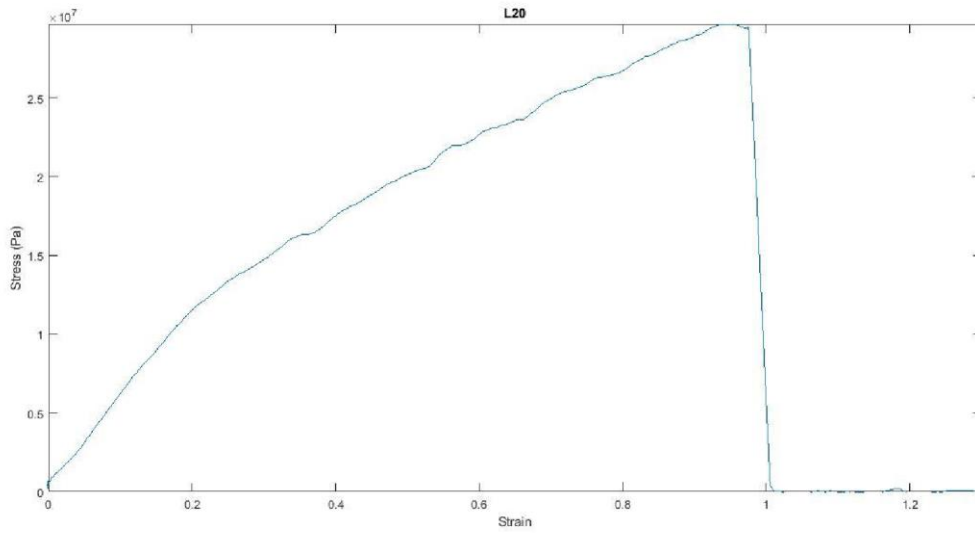


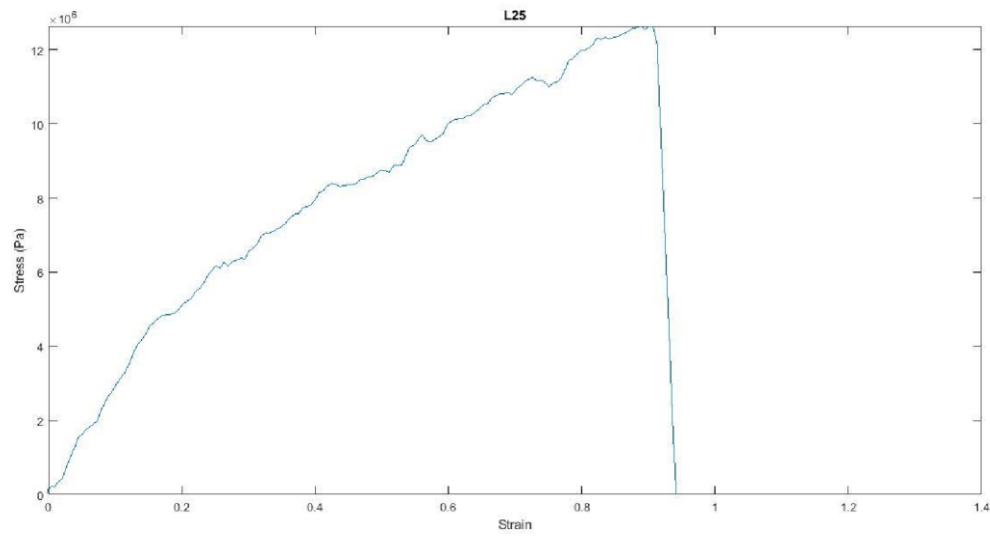
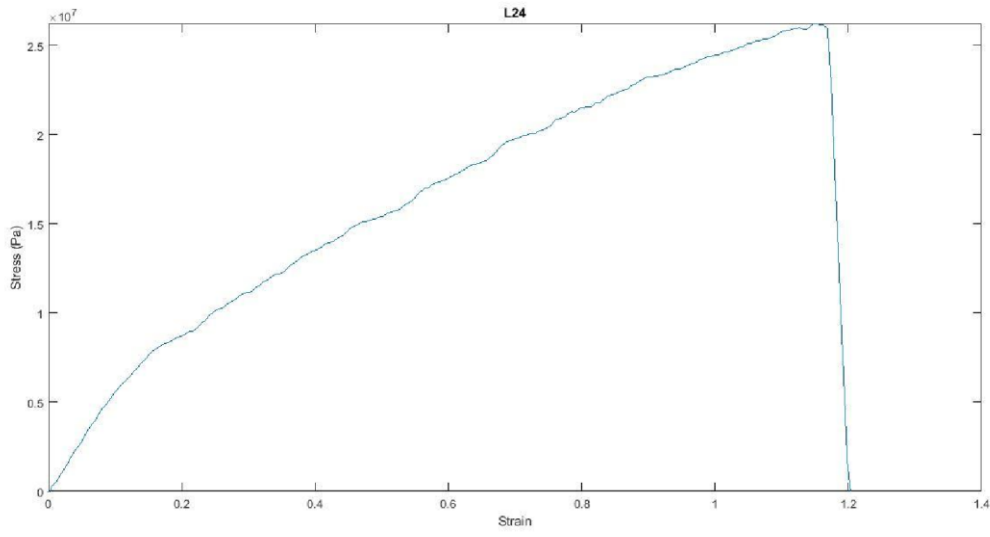
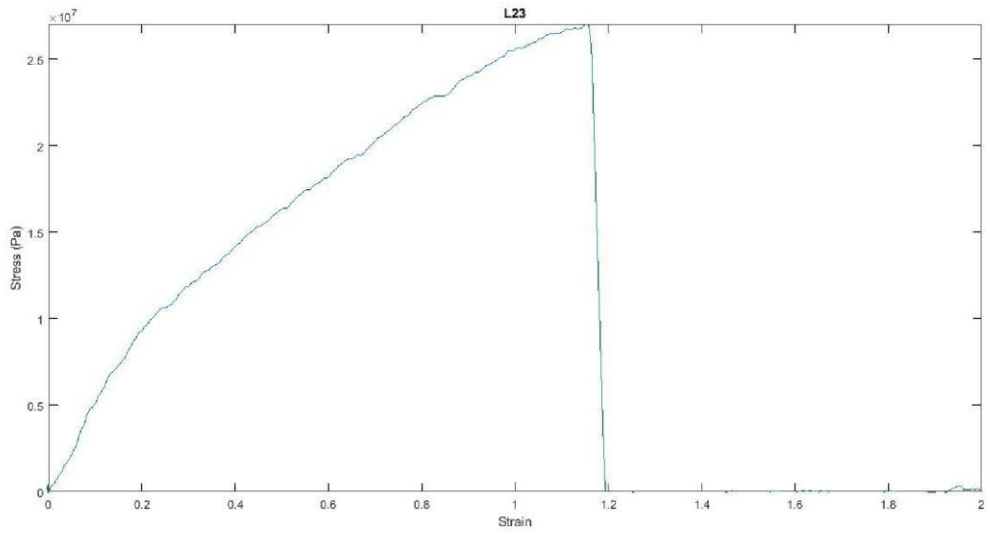


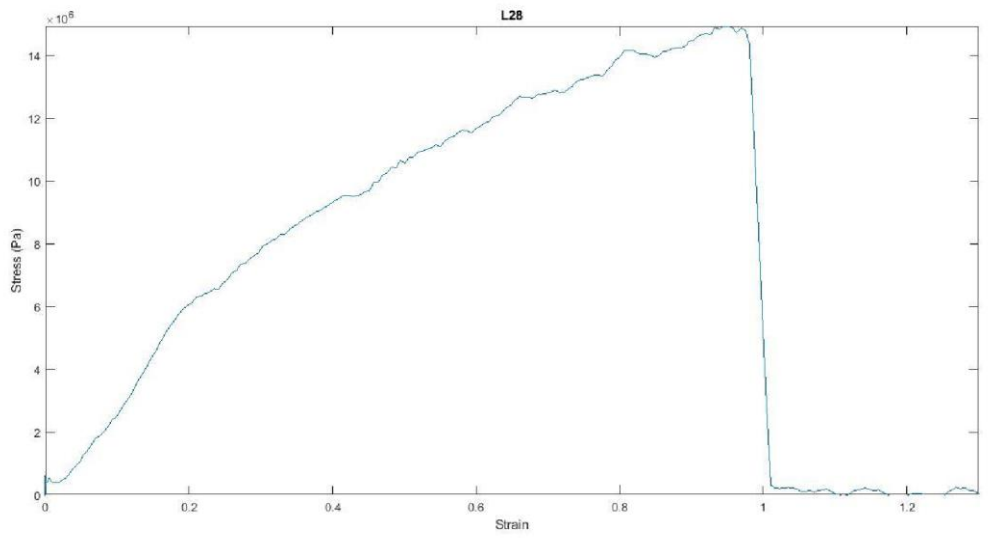
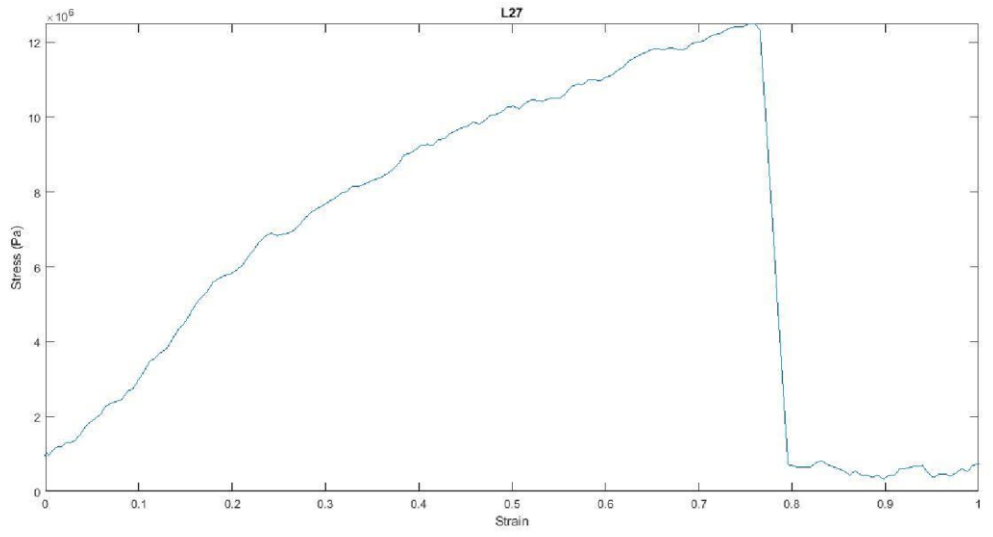
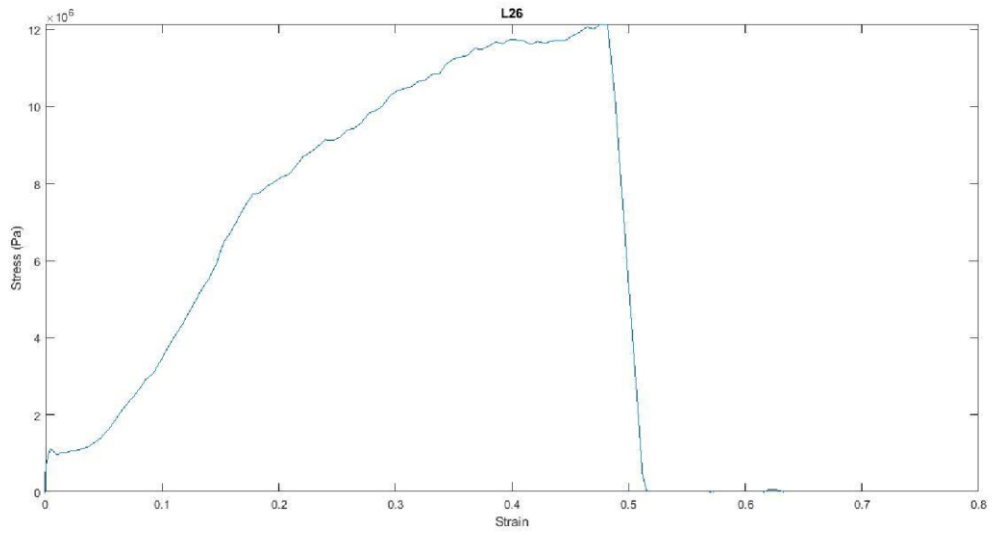


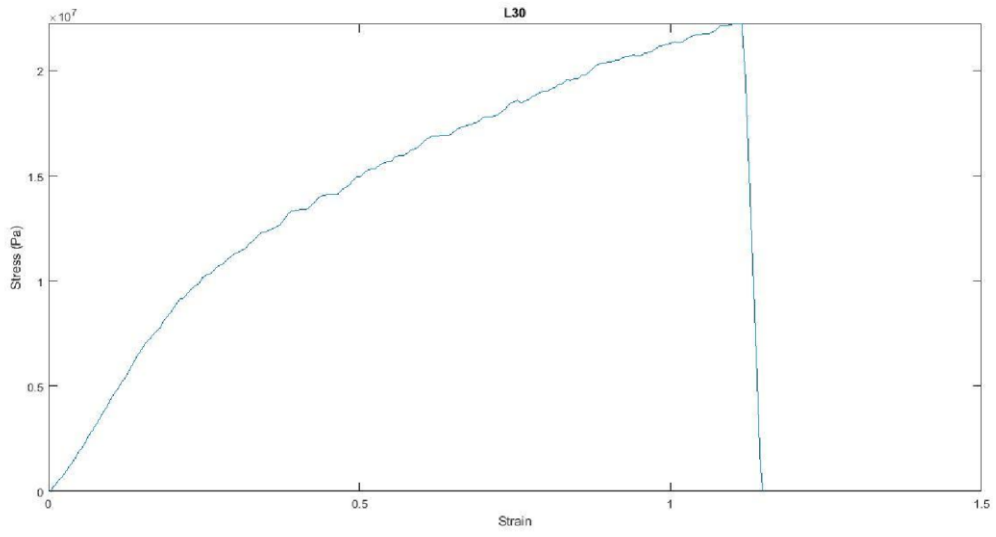
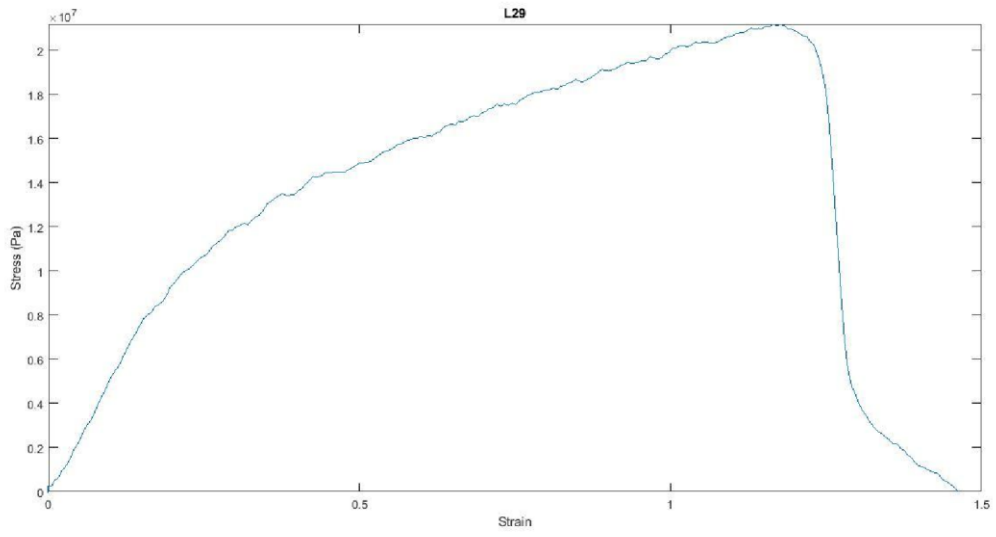
Appendix B - Round Two Stress-Strain Graph



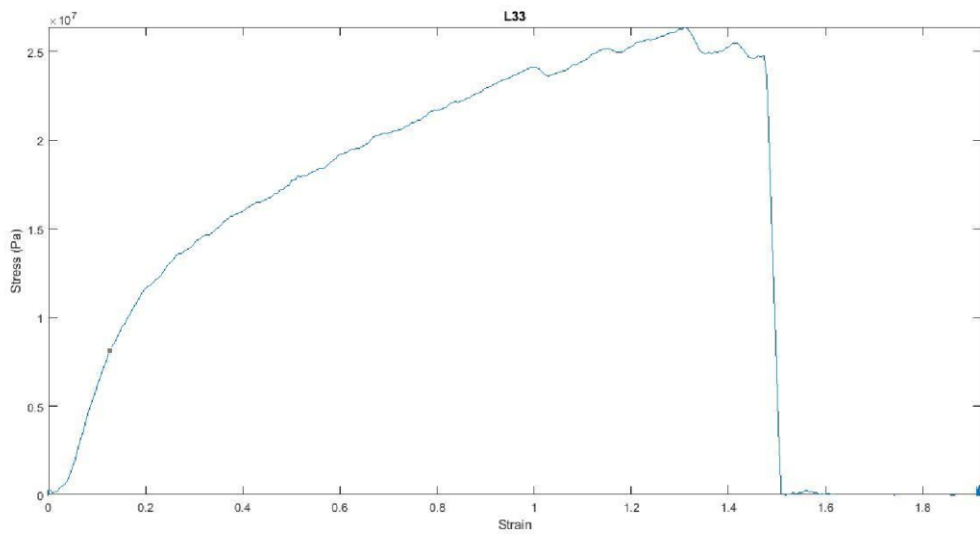
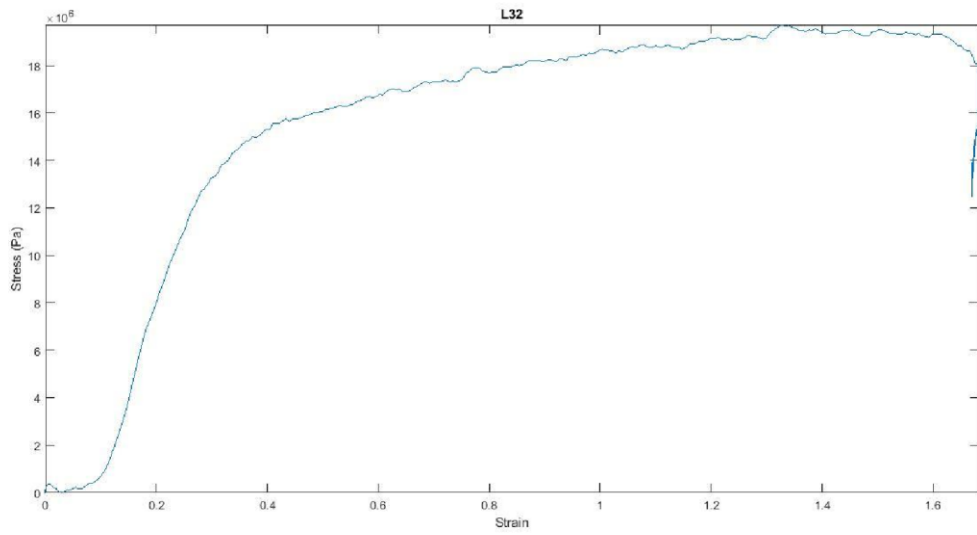
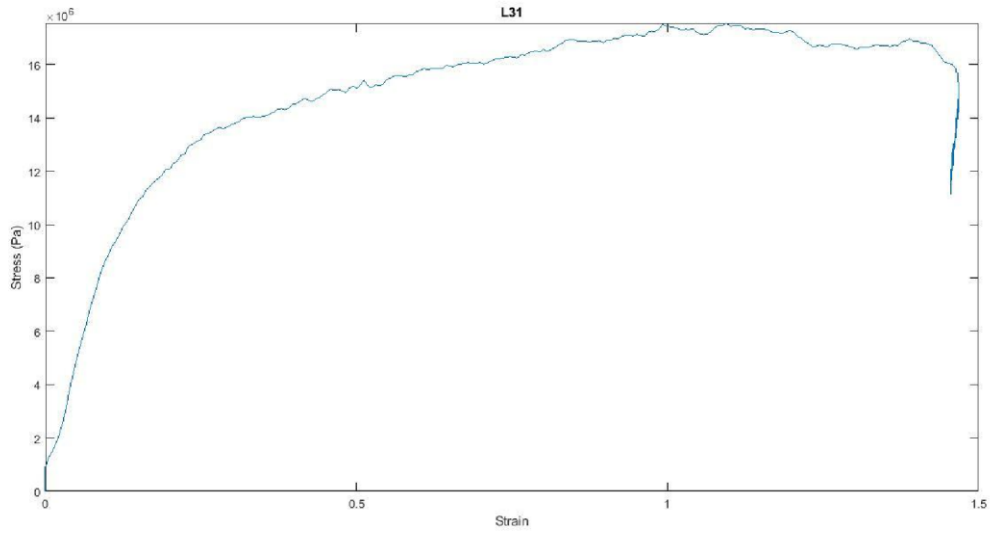


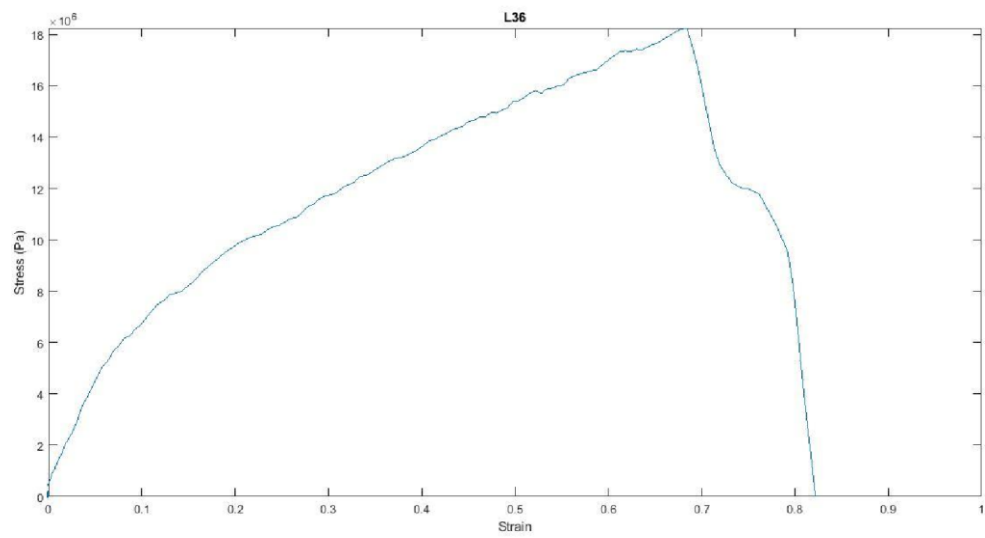
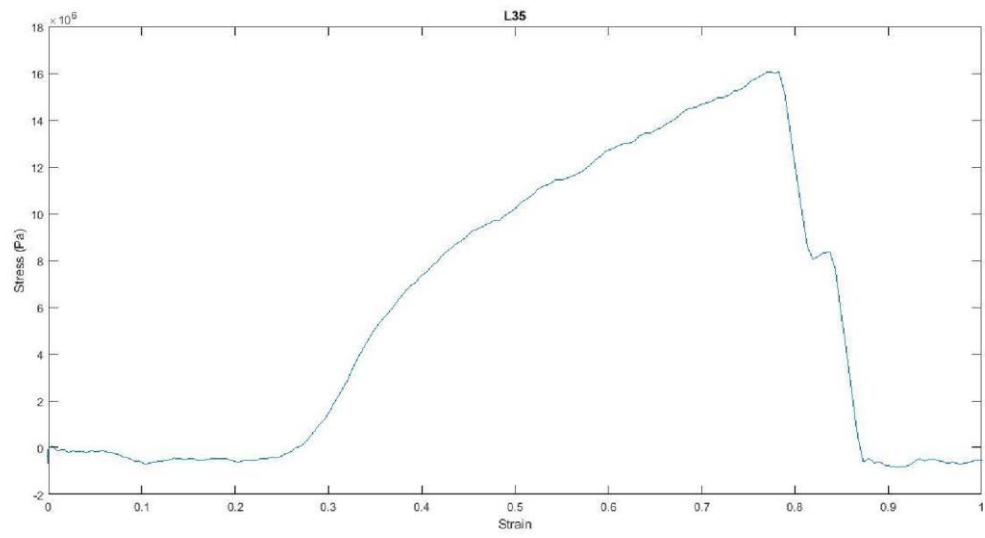
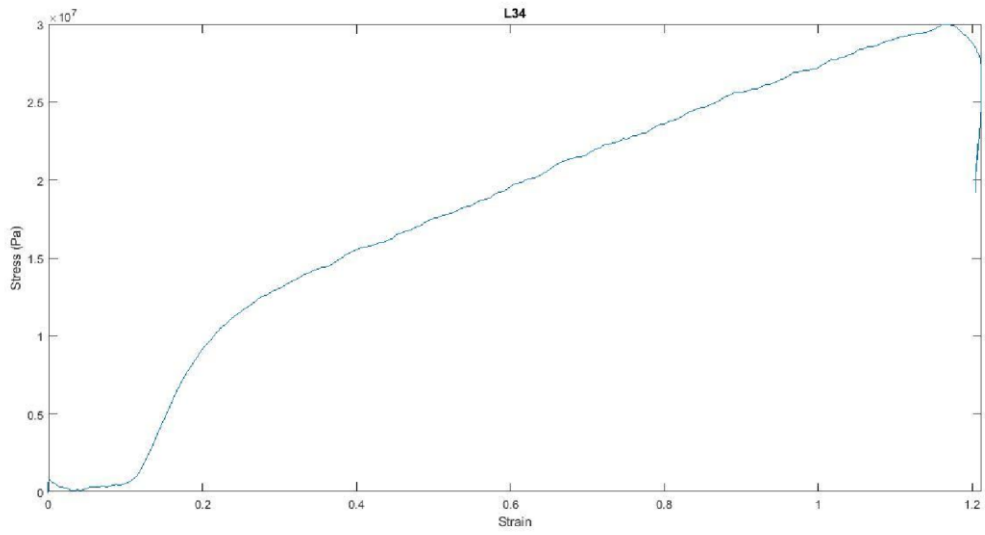


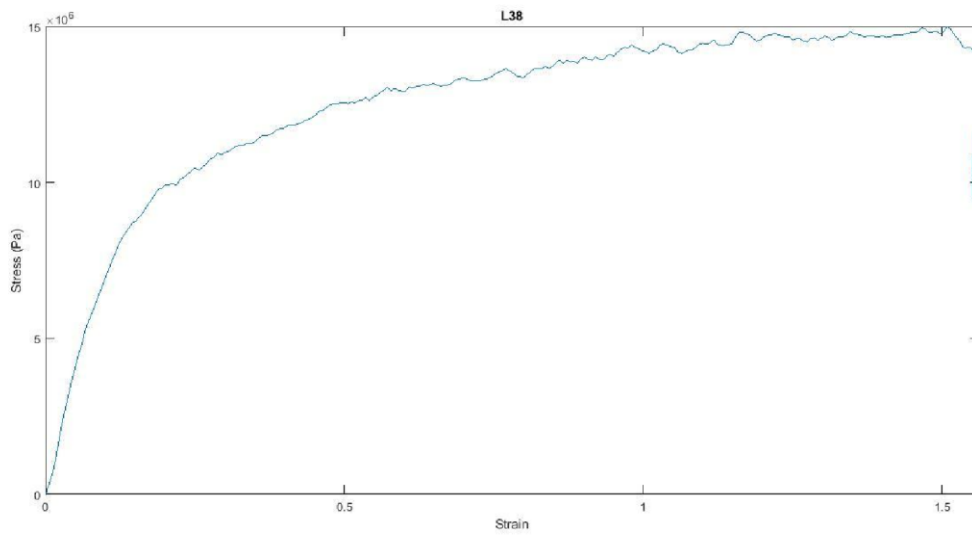
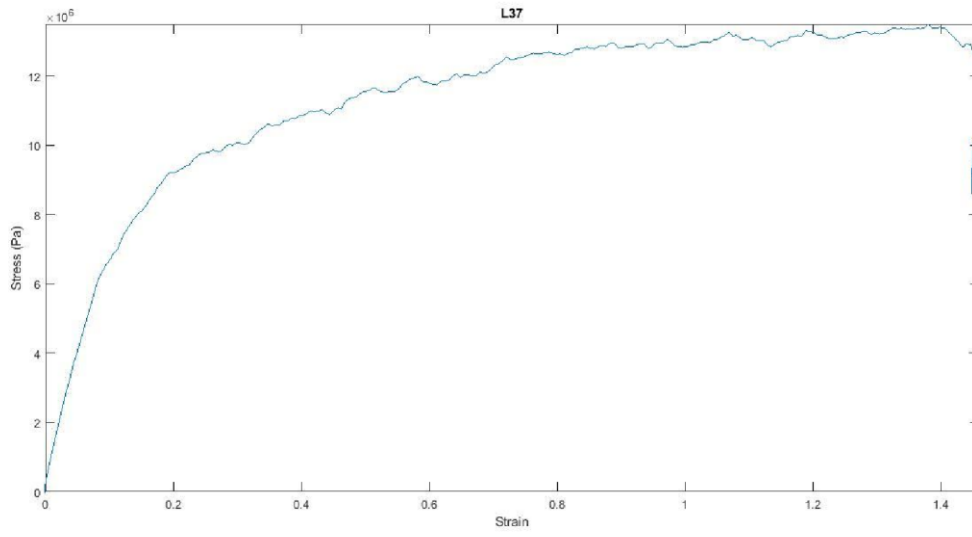




Appendix C - Round Three Stress-Strain Graphs







Appendix D – MATLAB Code for Graph Generation

```
clear all;
close all;
    data =
xlsread('L1.xlsx');

xs = data(:,5); %strain ys
= data(:,4); %stress ts =
data(:,1); %time

%find index where time > 0 ind = 0;
for i=1:length(ts) if ts(i) == 0
&& isnumeric(ts(i)) ind =
ind + 1; end end
xs_strain = smooth(xs(ind:end)); ys_stress
= smooth(ys(ind:end));

plot(xs_strain,ys_stress), xlabel('Strain'),ylabel('Stress (Pa)'),
xlim([0,inf]), ylim([0,inf])
```

Appendix E – MATLAB Code for Correlation Graphs

```
clear all;
close all;

%10% with 50:50 solvents conc
= [10 13 15 18 21];
modulus = [46.1 82.7 188.5 153.1 140.3]; err
= [9.5 11.4 53.9 26.6 18.9];
    figure(1) errorbar(conc, modulus, err), xlabel('Concentration (%)'),
ylabel('Elastic Modulus (MPa)') axis([8 22 0 270])

voltage = [21 21.45 22.5
modulus = [46.1 188.5 82.7 153.1 140.3]; err
= [9.5 53.9 11.4 26.6 18.9];
    figure(2) errorbar(conc, modulus, err), xlabel('Concentration (%)'),
ylabel('Elastic Modulus (MPa)') axis([8 22 0 270])

%10% with 27:75 solvents
diam = [198 221]; err =
[47 63]; voltage =
[20.02 23.03]; rpm =
[1080 1032];
    figure(3)
hold on;
errorbar(voltage, diam, err) xlim([19.5 23.5])
xlabel('Voltage (kV)'),ylabel('Fibre Diameter (nm)')
    figure(4)
errorbar(rpm, diam, err, 'r' ) xlabel('Rotational Speed
(rpm)'),ylabel('Fibre Diameter (nm)') xlim([1030 1085])

%13% with 50:50 solvents diam =
[169 195 277 366]; err = [19 28
81 131]; voltage = [25.5 25.1
20.02 20.05]; rpm = [1047 1088
```

```

1050 1080 ]; voltage = [20.0
20.06 25 25.5]; diam = [277 366
195 169]; err = [81 131 28 19];

figure(5)
hold on;
errorbar(voltage, diam, err) xlim([19.5
25.7]),ylim([140 inf])
xlabel('Voltage (kV)'),ylabel('Fibre Diameter (nm)')
title('Fibre Diameter and Voltage Correlation for 10% 50:50 solutions')

diam = [169 277 366 195]; err =
[19 81 131 28]; voltage = [25.5
20.02 20.05 25.1]; rpm = [1047
1050 1080 1088];
figure(6)
errorbar(rpm, diam, err,'r' ) xlabel('Rotational Speed
(rpm)'),ylabel('Fibre Diameter (nm)') xlim([1045
1090]),ylim([148 501]) title('Fibre Diameter and Collector RPM
Correlation for 10% 50:50 solutions')

```